ORNL-4653
UC-80 – Reactor Technology

HEAVY-SECTION STEEL TECHNOLOGY PROGRAM
SEMIANNUAL PROGRESS REPORT
FOR PERIOD ENDING AUGUST 31, 1970

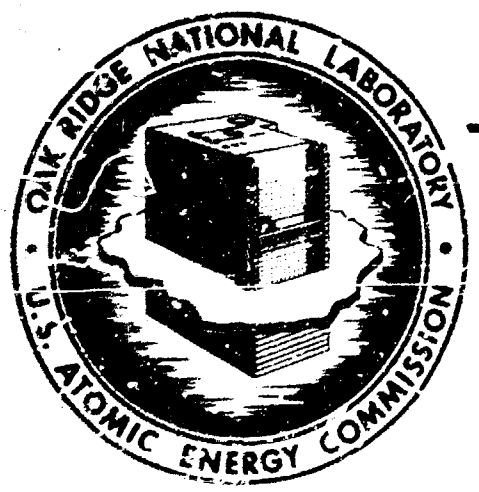

OAK RIDGE NATIONAL LABORATORY
operated by
UNION CARBIDE CORPORATION
for the
U.S. ATOMIC ENERGY COMMISSION

BLANK PAGE

Printed in the United States of America. Available from
National Technical Information Service
U.S. Department of Commerce, Springfield, Virginia 22161
Price: Printed Copy $3.00; Microfiche $0.65

BLANK PAGE

ORNL-4653
UC-80 – Reactor Technology

Contract No. W-7405-eng-26

HEAVY-SECTION STEEL TECHNOLOGY PROGRAM

SEMIANNUAL PROGRESS REPORT

For Period Ending August 31, 1970

F. J. Witt, Program Director

APRIL 1971

OAK RIDGE NATIONAL LABORATORY
Oak Ridge, Tennessee
operated by
UNION CARBIDE CORPORATION
for the
U. S. ATOMIC ENERGY COMMISSION

Contents

Foreword

The Heavy-Section Steel Technology (HSST) Program is a USAEC-sponsored effort for investigating the effects of flaws, variations of properties, stress raisers, and residual stress on the structural reliability of present and contemplated water-cooled reactor pressure vessels. The cognizant engineer for USAEC is J. R. Hunter. At ORNL the program is under the Pressure Vessel Technology Program of which G. D. Whitman is Director. The HSST program is being carried out in very close cooperation with the nuclear power industry. Prior reports in this series are ORNL-4176, ORNL-4315, ORNL-4377, ORNL-4463, ORNL-4512, and ORNL-4590.

Summary

The Heavy-Section Steel Technology (HSST) Program is an AEC-sponsored engineering effort that is coordinated with efforts by the manufacturing and utility sectors of the nuclear power industry to assess the in-service structural safety of the massive pressure vessels typical of those used in boiling-water and pressurized-water reactor systems. Particular emphasis is placed on the effects of flaws in such vessels. However, the scope of the activity covers metallurgy, chemistry, materials properties, inspection, analytical and experimental stress and strain analyses, environmental effects, fracture mechanics, and the general areas of fracture behavior. Through the culmination of this effort, as well as that of the nuclear industry, a technology should be developed for making reliable engineering estimates of margins of safety against fracture during the service life of the plants. The results of these programs will assist the USAEC regulatory bodies, the professional code-writing bodies, and the nuclear power industry in providing the safety standards necessary to maintain a vigorous economical industry with proper regard to public health and welfare.

There are 12 tasks of the HSST program. In this report the activities under these tasks are grouped under administration and procurement, unirradiated materials, irradiated materials, and pressure vessel investigations.

Unirradiated Materials

Dynamic fracture toughness tests were conducted by Westinghouse Electric Corporation on 1-, 2-, 4-, and 8-in.-thick specimens of HSST plate 02 material. The results of these tests are compared with those of previous static tests. As for the static tests the K_{Ic} data indicate a rapid increase in toughness with temperature. Below ambient temperature, where a direct comparison with the K_{Ic} fracture toughness obtained in the static tests is possible, a decrease in the toughness curve with temperature was noted in the dynamic tests. Accordingly it was possible to measure the dynamic toughness at ambient temperature. The results of tests of the 2-, 4-, and 8-in.-thick compact tension specimens indicated the dynamic fracture toughness properties of A 533, grade B, steel plate at room temperature to be above 100 ksi $\sqrt{\text{in.}}$ at loading rates exceeding $K = 10^4$ ksi $\sqrt{\text{in.}}$/sec. A final report covering these tests is in preparation.

TRW is investigating the gross strain crack tolerance of pressure vessel steels in the presence of flaws. TRW's approach is to measure critical gross strains in a surface-cracked tension specimen of rectangular cross section as a function of crack size, temperature, and constraint. Scaleup to heavy sections requires a size-effect study, preceded by investigation of the effects of specimen shape and size relative to crack size, to permit knowledgeable extrapolation.

At TRW the tensile properties of the material furnished from plate 02 were measured in some detail. Natural flaws in the form of slag inclusions were encountered. A better system of strain measurements was developed, and studies were begun on the effects of shape on specimen cross section and the ratio of crack area to gross area on critical gross strain in the presence of a 0.10-in.-deep crack. These studies are prerequisites to the size-effect study that is the basic part of this work.

Previous work on the strain rate and crack arrest studies by Materials Research Laboratory showed that the crack-initiation toughness could be varied by changing loading rate, fatigue precracking procedures, etc. Variations in the initiation conditions influenced the length of crack jump, but the value of the arrest toughness was the same within a tight scatter band, independent of the preceding initiation level. Recent work has been directed toward measuring crack-arrest toughness at higher temperatures.

BLANK PAGE

Tests of initiation and crack-arrest toughness were run with contoured double-cantilever beam specimens on which a temperature gradient in the direction of crack arrest was imposed so that fracture was initiated at a low temperature and arrested at a higher temperature. All the initiation values were obtained in the temperature range where the toughness increases rapidly with temperature, with the higher initiation toughness values being obtained on specimens that experienced some plastic bending of the arms prior to fracture. All the crack-arrest toughness values fell distinctly below the corresponding initiation toughness values.

The arrest toughness values seem to fall into two groups. A large number of tests, representing crack arrest at temperatures ranging from 75 to 115°F, gave arrest toughness values clustering around 110 ksi $\sqrt{\text{in.}}$ A significant number of tests gave lower values, suggesting that the low end of the scatter band of arrest toughness may define a rather gradual linear increase in the crack-arrest toughness with increasing temperature. Examination of the fracture surfaces showed that in the specimens that gave the higher crack-arrest toughness values the plane of the crack wandered from the minimum section far enough to give some shear lip in the vicinity of the crack-arrest position. The specimens that gave lower arrest toughness values invariably had fracture surfaces that were more flat. Hence it is suggested that the lowest values of the arrest toughness are the most significant.

The primary activities of Brown University on the three-dimensional elastic-plastic analysis were the preparation of a topical report covering the work completed to date and the accomplishment of some internal improvements in the computer program being developed. The main improvement in the computer program was the introduction of a direct method of solution for the system of equations generated by the elastic part of the problem. This improvement reduces by a factor of approximately 2 the time required to accomplish the elastic solution and therefore makes the program significantly more efficient.

Brown University's topical report covers the development of an elastic-plastic finite-element analysis for three-dimensional specimens with flaws. Particular attention was paid to the analysis of a semielliptical crack and a through crack in a plate of finite thickness. Three-dimensional polar, cubic, and cubic-distorted elements were developed for this purpose. In addition, programs to generate the mesh of elements and nodal points for a given problem size and specimen geometry were written and tested.

Two final reports covering fracture toughness characterization of A 533, grade B, class 1 steel and notch preparation in compact tension specimens were prepared by Westinghouse Electric Corporation and distributed. Westinghouse also continued the testing of compact tension specimens from approximately −50 to 550°F. An equivalent-energy procedure was used to determine the fracture toughness parameter K_{Icd}. The experimental study has indicated that K_{Icd} values determined from small compact tension specimens may be almost numerically equal to the K_{Ic} values determined from much larger specimens. Compact tension specimens $^1/_2$ and 1 in. thick were tested, but only the evaluation of the results for the 1-in.-thick specimens are presented in this report.

A fatigue-crack growth experiment in high-temperature pressurized water was initiated by Westinghouse Electri Corporation. Three 2-in.-thick WOL specimens were evaluated. Examination of the fracture surfaces of the specimens revealed that the starter crack (fatigue precrack) did not remain in the side notch plane during crack growth. It was concluded that because of the constraint of the chamber head, the stress intensity K_I at the crack tip was not well defined. The constraint occurred from fixing the test specimen to the test chamber head. This technique of testing was required to utilize the ultrasonic crack-monitoring system to follow crack growth. Various solutions to the problem were considered, and it was concluded that the desired crack growth experiment could be performed if the test specimen was not fixed to the chamber head. This modification will require the use of compliance calibration to experimentally measure rates of crack propagation.

Irradiated Materials

The irradiation at 550°F of two capsules containing 2-in.-thick compact tension specimens was completed by Westinghouse Electric Corporation. The fracture toughness K_{Ic} properties were generated for A 533, grade B, class 1 steel plate and submerged-arc weldment material in the postirradiation condition [2×10^{19} to 6×10^{19} neutrons/cm^2 ($E > 1$ MeV)]. Tensile properties were also obtained for the plate material following neutron exposure under the same conditions. In addition, the postirradiation fracture toughness from one test performed on A 508, class 2, steel was obtained. The results indicate the postirradiation fracture toughness properties to be highly temperature dependent; that is, they exhibit the same transition temperature

shift as the 30 ft-lb-fix Charpy transition temperature. In particular, a valid fracture toughness K_{Ic} value of around 70 ksi $\sqrt{in.}$ was obtained at 150°F following irradiation. A final report was prepared on this activity.

Specimen irradiations are under way on plate and weld material at Hanford Engineering Development Laboratory to fluences between 2×10^{19} and 8×10^{19} neutrons/cm^2 ($E > 1$ MeV). Charpy V-notch, tensile, and compact tension specimens are being irradiated. The irradiation temperature is about 550°F.

One-inch-thick irradiated compact tension specimens were tested between −125 and 175°F. The results at the higher temperatures indicated that rapid transition behavior initiates at somewhat over 100°F. The temperature shift of the 40 to 60 ksi $\sqrt{in.}$ toughness level appears to be over 200°F for the irradiation conditions given above.

A feasibility study for using the Advanced Tests Reactor (ATR) and the Experimental Test Reactor (ETR) to irradiate 4-in.-thick compact tension specimens was completed. Neither reactor was found to be ideally suited for the desired irradiations. The ATR was shown to require about seven years to accomplish the fluence levels, while gamma heating presents a problem in the ETR. The ETR could be used to achieve the irradiation, however, if methods currently under investigation for controlling the temperature prove feasible.

A fractographic examination was performed on irradiated steels. This study confirmed that irradiation embrittlement results primarily from a loss of the metallurgical ability of the steel to undergo the cleavage-to-plastic dimpling transition rather than low-energy ductile fracture.

At ORNL, impact and tensile data were obtained for irradiated samples of weld metal from a submerged-arc weldment and an electroslag weld. The tensile properties of the submerged-arc weldment showed a greater sensitivity to radiation damage than either base plate or electroslag weld following comparable irradiation at 150 and 550°F. Similar results were shown to hold for impact data from Charpy V-notch specimens.

Pressure Vessel Investigations

A procedure was developed at ORNL for fatiguing a machined notch by local pressurization of the notch. The method was successfully applied to a 6-in.-thick tensile specimen that contained a machined flaw 2 in. deep and 8 in. long. The flaws grew in fatigue about ½ in. uniformly around the machined tip of the notch.

The second, large, flawed tensile specimen tested by Southwest Research Institute was instrumented with acoustic emission devices. The results indicated yielding and crack extension at loads below those at which these behaviors were observed experimentally and tended to support the predictive capabilities of the method.

A third 6-in.-thick flawed tensile specimen was tested at Southwest Research Institute. The test temperature was 50°F and the flaw (segment of a circle, 2 in. deep, 8 in. long) was fatigue sharpened in three-point loading. A flat fast fracture occurred at a load of slightly over 5.3×10^6 lb. Only a slight amount of yielding occurred in the specimen. This behavior was not unexpected, since the test conditions and flaw size were chosen to produce the behavior exhibited.

A parametric study was completed on a series of specimens to elicit the true tensile behavior of the specimen configuration used for the large flawed tensile specimens. The results confirm that a near uniform tensile load is exhibited over a sufficient length of the test section.

The fabrication of the 6-in.-thick 39-in.-OD intermediate test vessels is well along. Six vessels are on order. Most of the various components are nearing completion and will be assembled by welding.

1. Program Administration and Procurement

The civilian nuclear power industry has progressed rapidly in the last few years, as attested to by the some 100 nuclear power stations now in operation, under construction, or on order. Capacities of plants under construction are exceeding 1100 MW(e). The walls of the primary pressure vessels are approaching 12 in., with design pressures up to 2500 psi. The design temperature ranges up to 650°F.

As a result of this growth of the nuclear power industry and the limited operating experience with nuclear power systems, the United States Atomic Energy Commission is sponsoring extensive research to assess the safety of these plants. One of the larger research programs is the Heavy-Section Steel Technology (HSST) Program, which is being carried out under the direction of Oak Ridge National Laboratory (ORNL). The emphasis in the HSST program is on the structural behavior of the thick reactor pressure vessels, particularly in the presence of flaws. The material of interest is the ASTM A 533, grade B, class 1 steel and welds typical for this material that are currently used in the fabrication of reactor pressure vessels. The program is being carried out in close cooperation with the materials, fabrication, and design interests of the United States nuclear power industry.

Since all steel vessels are assumed to contain flaws (inhomogeneities or discontinuities) of some size, the effects of such flaws on the fracture behavior of pressure vessels are of primary interest. The development of a quantitative technology to make the necessary safety assessments, together with an understanding of the factors (including irradiation) that degrade or change the anticipated behavior of the steel, is a primary objective of the HSST program. However, the broad spectrum of investigations of the HSST program covers metallurgy, chemistry, materials properties, inspection, analytical and experimental stress and strain analyses, and environmental effects, with emphasis on irradiation, fracture mechanics, and the general area of fracture behavior.

The work of the HSST program is carried out under 12 separate tasks. In addition to the administrative and procurement task, which is discussed in this chapter, the remaining task activities are grouped under investigations of unirradiated materials, investigations of irradiated materials, and pressure vessel investigations.

No new research subcontracts were initiated during this reporting period; however, two minor extensions were negotiated, as well as one second-year extension. Four technical reports were distributed, bringing the total to nine.[1-9] Three more were reviewed and

---

1. S. Yukawa, *Evaluation of Periodic Proof Testing and Warm Prestressing Procedures for Nuclear Reactor Vessels*, Report HSSTP-TR-1, General Electric Company, Schenectady, New York, July 1, 1969.

2. L. W. Loechel, *The Effect of Testing Variables on the Transition Temperature in Steel*, Report MCR-69-189, Martin-Marietta Company, Nov. 20, 1969.

3. P. N. Randall, *Gross Strain Measure of Fracture Toughness of Steels*, Report HSSTP-TR-3, TRW Systems Group, Nov. 1, 1969.

4. C. Visser, S. E. Gabrielse, and W. Van Buren, *A Two-Dimensional Elastic-Plastic Analysis of Fracture Test Specimens*, Report WCAP-7368, Westinghouse Electric Corporation, PWR Systems Division, August 1969.

5. T. R. Mager, F. O. Thomas, and W. S. Hazelton, *Evaluation by Linear Elastic Fracture Mechanics of Radiation Damage to Pressure Vessel Steels*, Report WCAP-7328, Rev., Westinghouse Electric Corporation, PWR Systems Division, October 1969.

6. W. O. Shabbits, W. H. Pryle, and E. T. Wessel, *Heavy Section Fracture Toughness Properties of A 533, Grade B, Class 1 Steel Plate and Submerged Arc Weldment*, Report WCAP-7414, Westinghouse Electric Corporation, PWR Systems Division, December 1969.

7. F. J. Loss, *Dynamic Tear Test Investigations of Fracture Toughness of Thick-Section Steel*, NRL Report 7056, U.S. Naval Research Laboratory, May 14, 1970.

BLANK PAGE

approved for publication. Three technical or programmatic manuscripts were published, bringing the total to four.[10-12] Four such reports were approved for publication.

The fourth annual information meeting was held on March 31–April 1 at ORNL. Some 150 persons registered to attend the presentation of 34 papers. Some highlights of the meeting are depicted in Fig. 1.1.

The current major procurement effort evolves around the fabrication of the intermediate test vessels; this activity is discussed in Chapter 4.

---

8. P. B. Crosley and E. J. Ripling, *Crack Arrest Fracture Toughness of A533 Grade B Class 1 Pressure Vessel Steel*, Report HSSTP-TR-8, Materials Research Laboratory, March 1970.

9. T. R. Mager, *Post-Irradiation Testing of 2T Compact Tension Specimens*, Report WCAP-7561, Westinghouse Electric Corporation, PWR Systems Division, August 1970.

10. Teledyne Materials Research Company, *HSST Intermediate Vessel Closure Analysis*, Report E-1253 (b), Mar. 25, 1970.

11. C. L. Segaser, *Conceptual System Design Description of the Intermediate Vessel Tests for the Heavy Section Steel Technology Program*, USAEC Report ORNL-TM-2849, Oak Ridge National Laboratory, June 1970.

12. F. J. Witt and R. G. Berggren, *Size Effects and Energy Disposition in Impact Testing of ASTM A533 Grade B Steel*, USAEC Report ORNL-TM-3030, Oak Ridge National Laboratory, August 1970.

PHOTO 77786

Fig. 1.1. Photographic highlights of 4th annual information meeting.

2. Investigation of Unirradiated Materials

The material investigations under the Heavy-Section Steel Technology Program are divided, in general, into studies of unirradiated materials and studies of irradiation effects. The studies of unirradiated material include inspection, characterization, variability determinations, transition temperature investigations, fracture mechanics studies, and fatigue-crack propagation tests. The current work in these areas is discussed in this section. Additional results for unirradiated material are presented in discussions of preirradiation studies in the section on irradiated materials in Chapter 3.

In this particular report the inspection and variability activities are reported in Chapters 4 and 3, respectively. No work was carried out under the characterization and transition temperature activities.

FRACTURE MECHANICS INVESTIGATIONS

J. G. Merkle

The objectives of the fracture mechanics investigations are (1) to establish the applicability of fracture mechanics methods as currently understood to the low-alloy steels being used in reactor pressure vessels, (2) to extend the applicability of this body of knowledge to cover the tougher behavior at higher temperatures, and (3) to develop new methods specifically applicable for predicting the fracture behavior of steels that undergo gross plastic strains before fracture. These objectives are being pursued through a series of five subcontracts, with related tasks (described elsewhere) contributing significantly to the developments. The activities under the subcontracts are discussed on the following pages.

Effect of loading rate on dynamic toughness of A 533, grade B, class 1 steel[1] (W. O. Shabbits, L. J. Ceschini, E. T. Wessel, and T. R. Mager, Westinghouse Electric Corporation)

Unlike the measurement of static toughness (K_{Ic}) properties, for which a standard procedure[2] has been adopted by the ASTM E-24 Committee on the Fracture Toughness of Metals, dynamic toughness testing required the development of experimental techniques. In the interests of uniformity, the static toughness testing procedures were adhered to wherever possible. The two major problems encountered in dynamic testing were the design of a loading system and fixtures that would provide uniform, rapid, vibration-free specimen loading and the measurement of loads and displacements on the specimen with sufficient accuracy and resolution.

A loading system capable of 60-in./sec ram velocities and 150-kip capacity was designed specifically for this test program. Gripping fixtures similar to those recommended by ASTM were used. The system provided for static preloading of the specimen and pretravel of the actuator loading rod, and also permitted the placement of damping materials between the actuator rod and the loading clevis. Damping was found necessary to permit gradual acceleration of the system and avoid the shock

1. This program is part of an overall Westinghouse Electric Corporation, Empire State Atomic Development Associates, Inc., and Oak Ridge National Laboratory (under UCCND Subcontract 3078) cooperative program.

2. ASTM Standard E399-70T, "Tentative Methods of Test for Plane-Strain Fracture of Metallic Materials," *ASTM Standards*, pt. 31, 1970.

waves associated with direct impact. The measurement of specimen loads and displacements required instrumentation with adequate frequency response and linearity characteristics. Electrical strain-gage instrumentation was used to measure loads, and the displacement-measurement transducers included linear variable transformers, plastic film potentiometers, and electrical clip gages. The outputs were recorded on a frequency-modulated magnetic-tape recorder.

The 8-in.-thick compact tension specimens were tested with a gas-driven extrusion machine. Special fixtures were designed to attain constant acceleration on the specimen to avoid shock and vibration. The basic design consisted of parabolic machined wedges separating standard-sized (4-in.-diam) pins that were free to roll on a flat surface.

Tests were conducted on 1-, 2-, 4-, and 8-in.-thick specimens of HSST plate 02 material. Interpretation of the results was based on standard ASTM static procedures for testing metallic materials.[2] The limitation of 3% linearity imposed by the oscilloscope made it difficult to resolve a 5% secant intercept. Since the data appeared linear to within the linearity requirements, fracture loads were used to compute the measured fracture toughness. The results of these tests are compared with the previously generated static data in Figs. 2.1, 2.2, and 2.3 and are summarized in Table 2.1.

As with the static (K_{Ic}) data the results indicate a rapid increase in toughness with temperature. Below ambient temperature, where a direct comparison with the static (K_{Ic}) fracture toughness is possible, a decrease in toughness is observed. The apparent overall effect is a shift in the ambient temperature. The results for the 2-, 4-, and 8-in.-thick compact-tension specimens indicated the dynamic fracture toughness of A 533, grade B, class 1 steel plate to be above 100 ksi $\sqrt{\text{in.}}$ at room temperature.

Crack-arrest toughness studies[3] (P. B. Crosley and E. J. Ripling, Materials Research Laboratory)

Previous work showed that the crack-initiation toughness could be varied by changing loading rate, fatigue precracking procedures, etc. Variations in the initiation conditions influenced the length of crack jump, but the value of the arrest toughness was the same within a

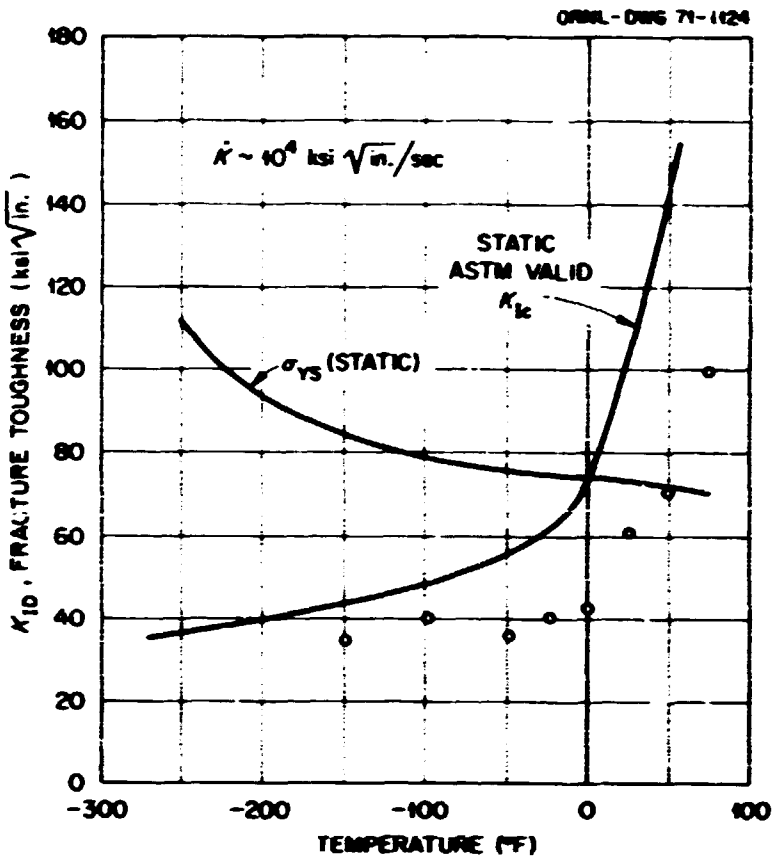

Fig. 2.1. Compact tension dynamic toughness data for 2-in.-thick specimens of A 533, grade B, class 1 steel from 12-in.-thick HSST plate 02.

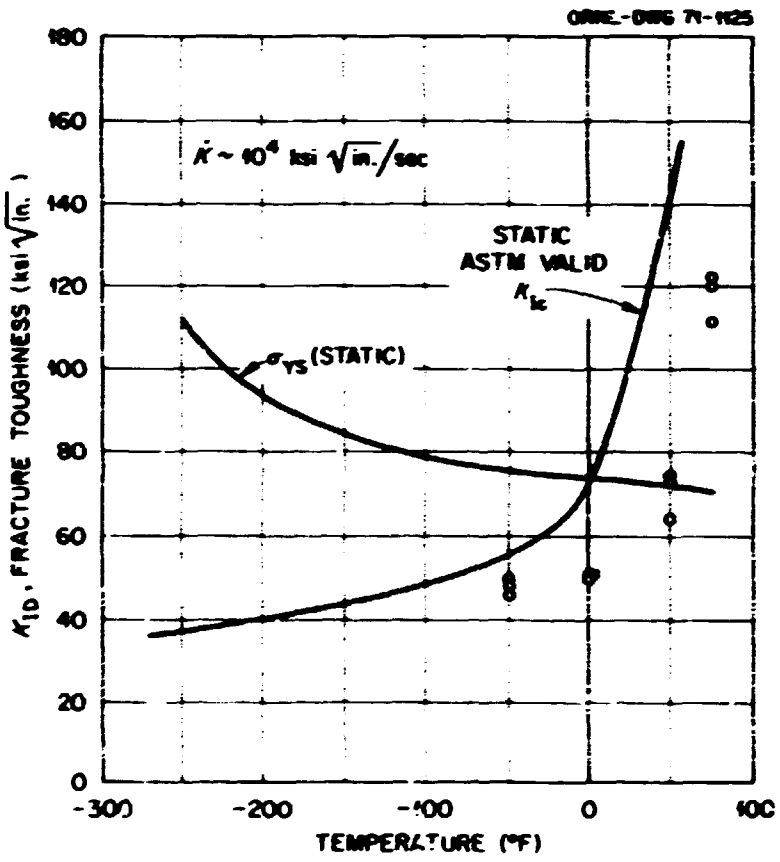

Fig. 2.2. Compact tension dynamic toughness data for 4-in.-thick specimens of A 533, grade B, class 1 steel from 12-in.-thick HSST plate 02.

3. Work performed under UCCND Subcontract No. 3152 between Union Carbide Corporation and Materials Research Laboratory.

Table 2.1. Compact tension dynamic fracture toughness (K_{ID}) data for HSST plate 02

Specimen identification	Test temperature (°F)	Yield stress (ksi)	B, Width (in.)	W, Depth (in.)	K_f, Fatigue (ksi $\sqrt{\text{in.}}$)	Average crack length (in.)	Ultimate load (kips)	K_Q or K_{ID}, Toughness (ksi $\sqrt{\text{in.}}$)	K, Loading rate (ksi $\sqrt{\text{in.}}$/sec)	β_c [a] (a)
HS21-4	-50	74.0	1.003	2.000	15.5	1.0288	5.22	35.9	62,000	0.234
HS21-3	-50	74.0	1.003	2.000	15.6	1.0337	7.65	54.5	46,200	0.542
HS21-2	-50	74.0	1.003	2.000	15.6	1.0309	6.0	42.7	68,100	0.332
HS21-1	-50	74.0	1.003	2.000	15.5	1.0292	6.64	46.9	10.900	0.402
HS21-6	-50	74.0	1.003	2.000	15.4	1.0249	5 8	40.4	61,300	0.298
HS21-5	-50	74.0	1.003	2.000	14.8	0.9966	4.9	32.8	50,500	0.196
HS22-4	75	69.0	2.004	3.999	21.4	2.0801	39.1	99.6	19,500	1.04
HS22-6	50	71.0	2.004	3.999	21.3	2.0745	27.5	69 7	17,400	0.482
HS22-5	25	72.0	2.004	3.999	21.3	2.0753	24.0	60.9	19,000	0.357
HS22-1	0	73.0	2.004	3.999	21.5	2.0863	16.5	42.4	13,900	0.167
HS22-3	-25	74.0	2.004	3.999	21.1	2.0630	16.0	40.2	13,400	0.148
HS22-8	-100	79.0	2.004	3.999	21.7	2.1015	15.7	40.7	12,700	0.133
HS22-7	-150	84.0	2.004	3.999	21.9	2.1088	13.0	33.8	10,900	0.0812
HS22-2	-50	74.0	2.004	3.999	21.2	2.0731	13.8	34.9	13,500	0.112
HS26-8	-50	74.0	2.004	3.999	21.4	2.0794	21.6	55.0	48.6	0.276
HS26-7	-50	74.0	2.004	3.999	21.4	2.0805	19.1	48.5	123	0.245
HS26-5	-50	74.0	2.004	3.999	21.1	2.0639	14.1	35.5	31,600	0.115
HS26-2	-50	74.0	2.004	3.999	21.2	2.0726	14.3	36.3	33,200	0.126
HS26-3	-50	74.0	2.004	3.999	22.3	2.1339	15.3	40.7	8,480	0.151
HS2112	-50	74.0	2.003	3.999	16.1	2.0994	22.0	56.9	6.22	0.296
HS2111	-50	74.0	2.003	3.999	15.9	2.0771	16.0	40.7	1,660	0.151
HS27-1	-50	74.0	2.003	3.999	16.1	2.0971	20.7	53.5	1,130	0.261
HS212-2	-50	74.0	2.003	3.999	15.2	2.0219	18.3	44.6	2.62	0.182
HS218-1	-50	74.0	2.003	3.999	15.3	2.0341	16.2	39.4	92.8	0.142
HS227-1	-50	74.0	2.003	3.999	15.3	2.0256	19.6	47.9	479	0.209
HS227-2	-50	74.0	2.003	3.999	15.4	2.0321	23.1	56.8	6.31	0.295
HS218-2	-50	74.0	2.003	3.999	15.4	2.1131	18.4	47.6	173	0.207
HS2183	75	69.0	4.015	8.011	15.6	4.1130	138.0	121	23,400	0.772
HS2-24	0	73.0	4.002	8.001	21.5	4.1762	56.8	51	12,300	0.125

[a] $\beta_c = \frac{1}{B}\left(\frac{K_Q}{\sigma_{ys}}\right)$, where σ_{ys} is the 0.2% offset static yield strength.

Table 2.1 (continued)

Specimen identification	Test temperature (°F)	Yield stress (ksi)	B, Width (in.)	W, Depth (in.)	K_f, Fatigue (ksi $\sqrt{in.}$)	Average crack length (in.)	Ultimate load (kips)	K_Q or K_{ID}, Toughness (ksi $\sqrt{in.}$)	$\dot{K}$, Loading rate (ksi $\sqrt{in.}$/sec)	β_c (a)
HS2-23	0	73.0	4.002	8.002	21.1	4.1339	56.4	50	14,000	0.119
HS2113	-50	74.0	4.013	8.015	16.0	4.1797	54.2	48	34,900	0.109
HS2-26	0	73.0	4.002	7.999	21.3	4.1547	73.5	66	25,400	0.205
HS27-3	-50	74.0	4.012	8.007	15.8	4.1463	54.0	48	482	0.106
HS2283	75	69.0	4.002	7.999	15.8	4.1045	122.0	107	16,300	0.609
HS2273	-50	74.0	4.002	8.000	15.7	4.0937	51.5	45	11,900	0.093
HS2124	75	69.0	4.002	7.999	15.7	4.0862	140.0	122	15,700	0.791
HS2D13	50	71.0	4.003	7.999	16.4	4.1970	126.0	115	462	0.702
HS2D15	50	71.0	4.003	7.999	16.3	4.1737	117.0	106	3,720	0.592
HS2D17	50	71.0	4.003	7.999	16.3	4.1757	134.0	121	73.6	0.773
HS2D10	50	71.0	4.003	7.999	16.1	4.1467	131.0	117	30.5	0.726
HS2D16	50	71.0	4.002	8.000	16.6	4.2200	149.0	136	12.2	0.981
HS2D8	50	71.0	4.002	8.000	16.3	4.1720	85.6	77.6	6,160	0.636
HS2-13-3	50	71.0	4.008	8.01	15.4	4.0833	71.5	62.3	13,000	0.203
HS2-7-4	50	71.0	4.002	8.000	15.3	4.0570	81.4	70.6	13,100	0.265
HS2-28-4	0	73.0	4.002	7.998	15.3	4.0538	55.5	48.1	11,400	0.108
HS2-11-4	50	71.0	4.002	8.000	15.4	4.0715	80.3	70.0	13,500	0.257
HS2-21	75	69.0	4.001	7.998	15.4	4.1000	120.0	105	5,250	0.573
HS2D4	125	65.1	8.005	16.001	36.6	8.135	594	182	87,000	0.975
HS2D2	125	65.1	8.004	15.999	37.0	8.193	466	145	98,000	0.615
HS2D1	100	67.4	8.005	15.998	36.8	8.165	416	128	61,300	0.452
HS2D3	75	69.0	8.002	16.002	37.0	8.189	308	95.8	63,800	0.241
HS2D6	75	69.0	8.004	16.001	36.8	8.164	304	94.1	75,200	0.233
HS2D5	150	62.9	8.001	16.002	36.0	8.165	650	>200		

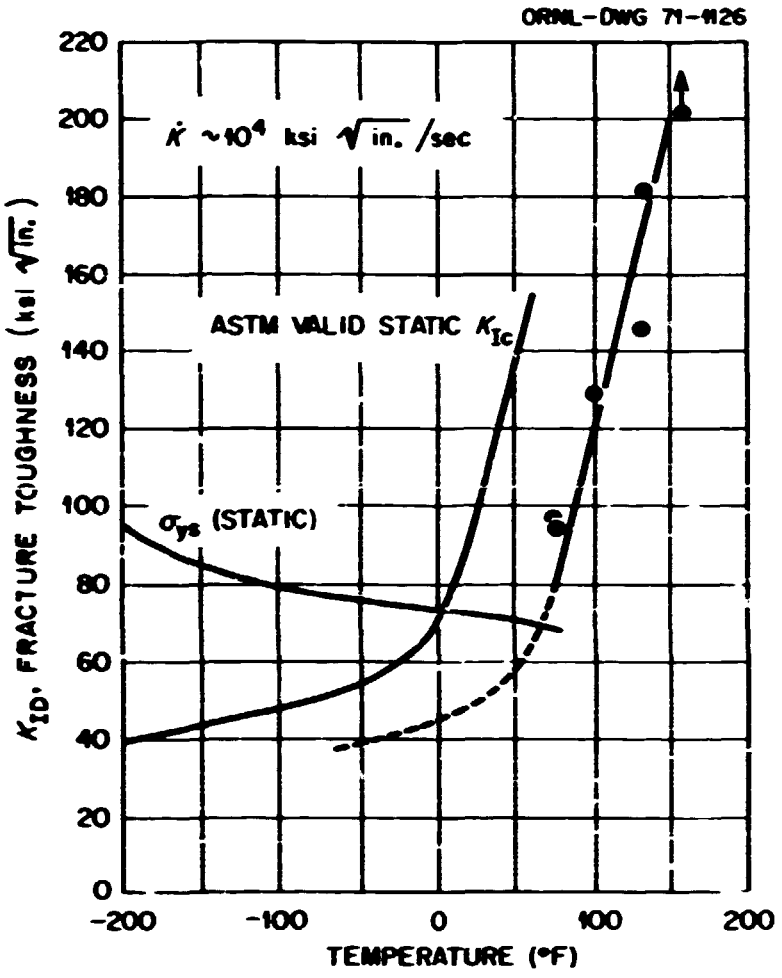

Fig. 2.3. Compact tension dynamic toughness data for 2-in.-thick specimens of A 533, grade B, class 1 steel from 12-in.-thick HSST plate 02.

tight scatter band independent of the preceding initiation level. It was also found that at low temperatures the initiation toughness showed only a modest rate sensitivity, and the crack-arrest toughness was essentially equal to the initiation toughness. With increasing temperature, greater rate effects appeared, and static initiation and crack-arrest toughness values were more widely separated. Since the crack-arrest toughness increases less rapidly with increasing temperature than the initiation toughness, it should be possible to measure the crack-arrest toughness at higher temperatures than the initiation toughness with reasonably sized specimens. Therefore recent work has been directed toward measuring crack-arrest toughness at higher temperatures.

Experimental procedure. In order to measure crack-arrest toughness it is first necessary, of course, to initiate a flat fracture that runs at a high velocity. Because the crack-arrest toughness value is independent of the preceding crack-initiation value, attention was focused on a method of artificially lowering the initiation value so that a running crack could be obtained at the higher temperatures of interest for crack-arrest measurements. The method selected was to test specimens with a temperature gradient in the direction of the crack propagation so that fracture was initiated at a low temperature and arrested at a higher temperature.

The tests were run with contoured DCB (double-cantilever-beam) specimens loaded dynamically in a closed-loop servo-hydraulic machine following procedures described in previous reports.[4-6] The temperature gradient was established by cooling the front end of the specimen with dry ice. Then, with the specimen placed in the test machine, the back end was heated with an oxyacetylene torch. The temperature was monitored with six Chromel-Alumel thermocouples spot welded to the specimen. The thermocouples were spaced $\frac{3}{4}$ in. apart adjacent to the crack line. With this procedure, temperature gradients of 15 to 20°F/in. were established over a region including the crack jump distance. After testing, the crack-arrest position was marked by extending the crack a short distance in fatigue prior to breaking the specimen completely at a low temperature. Typical jump distances were of the order of $\frac{1}{2}$ to 1 in., although in some cases the distance was as much as 2 in.

Results. Initiation and arrest toughness measurements obtained for specimens with a temperature gradient are shown in Fig. 2.4. The initiation values are denoted by squares (for 2-in.-thick specimens) and triangles (for 3-in.-thick specimens). The arrest toughness values are denoted by *X*'s. Lines connecting the initiation and arrest values indicate an initiation and an arrest from a single pop. As is obvious in Fig. 2.4, the initiation values were obtained in the temperature range where the toughness increases rapidly with temperature. The higher initiation toughness values were obtained on specimens that experienced some plastic bending of the arms prior to fracture. This slowed down the straining rate as the crack-initiation load was approached. Nevertheless, in all the tests the load corresponding to crack initiation was clearly defined, and unstable crack extension occurred with an abrupt drop in load. As may

---

4. F. J. Witt, *Heavy-Section Steel Technology Program Semiann. Progr. Rept. Feb. 28, 1969*, USAEC Report ORNL-4463, Oak Ridge National Laboratory.

5. F. J. Witt, *Heavy-Section Steel Technology Program Semiann. Progr. Rept. Aug. 31, 1969*, USAEC Report ORNL-4512, Oak Ridge National Laboratory.

6. F. J. Witt, *Heavy-Section Steel Technology Program Semiann. Progr. Rept. Feb. 28, 1970*, USAEC Report ORNL-4590, Oak Ridge National Laboratory.

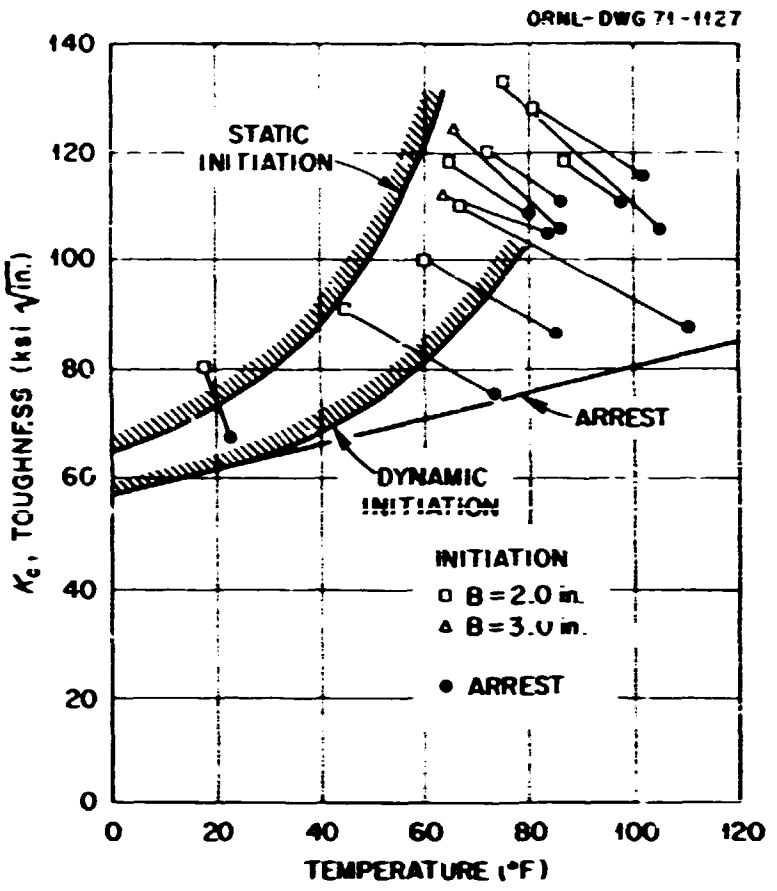

Fig. 2.4. Initiation and arrest toughness data from tests of contoured DCB specimens with a temperature gradient imposed. Specimens from RW direction of plate 02.

be seen in Fig. 2.4, all the crack-arrest toughness values are distinctly below the corresponding initiation toughness values. The arrest toughness values seem to fall into two groups. A large number of tests representing crack arrest at temperatures ranging from 75 to 115°F gave arrest toughness values clustering around 110 ksi $\sqrt{in.}$ A significant number of tests gave lower values, which suggested that the low end of the scatter band of arrest toughness may define a rather gradual linear increase in the crack-arrest toughness with increasing temperature. Examination of the fracture surfaces showed that in the specimens that gave the higher crack-arrest toughness values the plane of the crack wandered from the minimum section far enough to give some shear lip in the vicinity of the crack-arrest position. The specimens that gave lower arrest toughness values invariably had fracture surfaces that were more flat. Hence it is suggested that the lowest values of the arrest toughness are the more significant.

Discussion. In the temperature range 80 to 100°F, crack-arrest toughness values are distinctly below the crack-initiation values. It is not yet possible, however, to project the behavior of crack-arrest toughness with further increases in temperature. Some data suggest that the arrest toughness may begin to increase rapidly with temperature in a temperature range somewhat higher than that at which crack-initiation toughness behaves in the same manner. Other measurements are consistent with the possibility that the arrest may continue to show a gradual increase with temperature at temperatures still higher than those at which measurements have yet been made. An immediate goal of the present work is to measure the crack-arrest toughness at higher temperatures in order to answer this question.

Gross strain as a measure of crack tolerance of steels[7]
(P. N. Randall, TRW Systems Group of TRW, Inc.)

In common with the other HSST projects, the basic objective of this study is to predict the fracture behavior of full-scale hardware from tests of a practical specimen of the material. The approach is to measure critical gross strains in a surface-cracked tension specimen of rectangular cross section as a function of crack size, temperature, and constraint. Scaleup to heavy sections requires a size-effect study, preceded by investigation of the effects of specimen shape and size relative to crack size to permit knowledgeable extrapolation. Some of these variables were studied in the first year's work, which was reported previously.[6] A full statement of the problem and an explanation of the gross strain measurement approach were also given and will not be repeated here.

Progress during this first six months of the second year's contract is discussed here. The tensile properties of the material furnished (from plate 02) were measured in some detail, and effects of natural flaws in the form of slag inclusions were encountered. An improved system of strain measurements was developed, and studies were begun on the effects of shape of specimen cross section and the ratio of crack area to gross area on critical gross strain in the presence of a 0.10-in.-deep crack. These were preliminary steps in the size-effect study.

Material. The material furnished at the beginning of the program was from the lower end of plate 02 – pieces 02G*X*, *Y*, and *Z*, as shown in Fig. 2.5. To avoid the inhomogeneity in yield properties that was found previously and which required classification of specimens as either midplate or bottom-block material, these pieces were cut 3.5 in. from either plate surface. To check for variability at the yield-point loading through the thickness of the block and along the length, several

7. Work performed under UCCND Subcontract No. 3134 between Union Carbide Corporation and TRW, Inc.

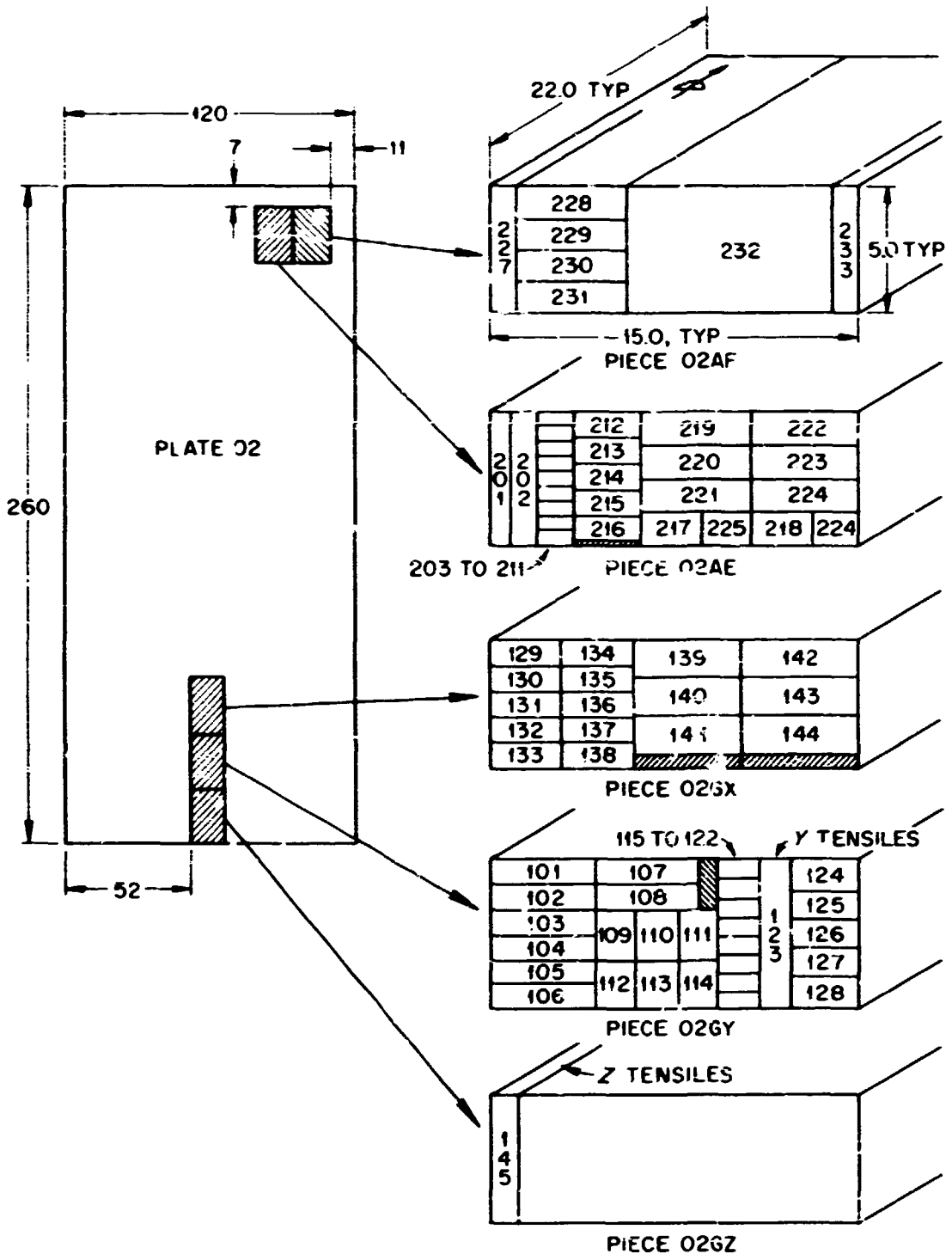

Fig. 2.5. Layout of specimens showing their locations in plate 02. All blocks were cut with 5-in. thickness centered on the plate midplane.

0.505-in.-diam tensile specimens were prepared from locations shown in Fig. 2.5. They were tested at −20°F because most of the tests of gross strain crack tolerance were expected to be made at subzero temperatures. The results for individual specimens are listed in Table 2.2. There was little variation of yield or ultimate strength with position in the block. The range of ultimate strength values was about 2 ksi, and that of lower yield point values was less than 4 ksi. The shape of the stress-strain curves in the yield region was uniform for all locations in the block -- the yield plateau extended to about 1.4% total (elastic plus plastic) strain. Strain to maximum load was about 12% (±1%), which means that the upper limit of ε_{gnc}, critical gross strain in the net section, is about 12% for this material at −20°F.

Elongation and reduction-of-area values were reduced in some specimens by the presence of slag inclusions and by another form of inhomogeneity that produced "fisheyes" in the fracture surface. The inclusions were most evident in the central part of the block; that is, in

Table 2.2. Results from tensile tests at −20°F on specimens from HSST plate 02

Specimen No.	Ultimate strength (ksi)	Upper yield stress (ksi)	Lower yield stress (%)	Elongation at yield point (%)	Strain to maximum load (%)	Elongation (%)	Reduction of area (%)
Z2	93.3	72.0	70.0	1.4	12.4	27.0	60.5
Z3	93.7	70.5	69.8	1.4	11.7	27.0	61.1
Z6	91.6	69.8	68.2	1.3	12.2	28.0	58.3
Z7	90.1	71.4	69.0	1.3	9.3[a]	17.5[a]	46.3[a]
Z8	91.5	69.5	68.5	1.4	12.8	22.5	42.7
Z9	91.0	68.7	68.3	1.5	11.4	20.0	40.9
Z10	90.7	70.4	68.9	1.4	12.8	25.0	50.1
Z11	90.6	70.0	68.4	1.4	12.3	28.5	62.0
Z14	89.2	70.1	66.6	1.2	13.4	28.0	59.3
Z15	89.4	67.7	66.9	1.4	12.6	28.5	56.9
Y2	66.5[a]	63.1[a]	62.3[a]	0.4[a]	1.2[a]	5.5[a]	20.8[a]
Y3	88.8	69.4	67.1	1.5	10.8	14.0[a]	27.3[a]
Y6	91.2	69.3	68.5	1.4	12.3	27.5	56.4
Y7	90.9	70.3	68.7	1.4	12.1	27.0	54.6
Y8	89.3	69.7	67.5	1.4	11.5	16.0[a]	23.9[a]
Y9	91.1	70.7	67.5	1.2	12.8	25.0	48.8
Y10	91.7	69.3	68.9	1.3	13.9	28.0	59.0
Y11	92.3	72.6	69.4	1.3	12.3	28.5	59.4
Y15	90.5	71.5	67.6	1.3	12.0	23.5	44.0
Y16	91.0	68.8	68.8	1.4	12.1	22.5	47.7

[a]Test data affected by the presence of slag inclusions or "fisheyes."

the middle third of the plate. Figure 2.6 shows the failure surfaces from three of the tensile specimens, the behaviors of which were noticeably affected by the presence of inhomogeneities, as indicated in footnote *a* in Table 2.2. The photos in Fig. 2.6 represent the worst fractures in the tensile specimens. All three specimens were tested at −20°F, and all three had a "spongy" or "woody" patch, which in specimen Y-2 occupied about 40% of the cross section. In addition, specimen Y-3 had a large "fisheye." Many specimens had fisheyes 0.020 to 0.050 in. in diameter, and they failed by formation of a cup-and-cone fracture, with the fisheye forming the bottom of the cup. The fractures on specimens from the top and bottom block were nearly normal.

The data of Table 2.2 indicate that all but one or two specimens developed 90% of the median value of strain to maximum load; hence, the flaws did not generally produce failure by crack propagation prior to normal tensile instability. Only one specimen (Y-2) showed a reduction in ultimate strength. Ten of the 20 specimens tested at −20°F showed reduced values of elongation and reduction of area.

The trend in tensile properties with temperature was also measured by testing one pair of specimens at +75°F and another pair at −100°F, as shown in Table 2.3. The instability at yield-point loading was more pronounced at the low temperature. Tensile instability strain also increased slightly at the low temperature. Trends in elongation and reduction of area values are hard to detect, because many of the values were reduced by the presence of slag in the vicinity of the fracture. By comparing the higher values at each temperature and assuming that they were least affected by inclusions, it may be concluded that the effect of temperature on these ductility values was small.

Radiographs of the largest inclusions in the machined gross strain specimens, taken normal to the plate surface, showed the inclusions to have the appearance of clouds of low-density particles. The largest dimension of the largest cloud was between 0.5 and 1.0 in. Figure 2.7 shows a print of the radiograph of the inclusion in specimen 103 and of the fracture that originated at that point in a room-temperature test. The inclusion was more severe than the 0.100-in.-deep surface crack, although the latter showed almost the expected crack-opening displacement, and the gross strain values were nearly equal to the tensile instability strain. Hence the test result was included in the data discussed later (see Table 2.6).

PHOTO 0019-71

(a) SPECIMEN Y-2

(b) SPECIMEN Y-3

(c) SPECIMEN Z-7

Fig. 2.6. Failure surfaces in three tensile specimens containing inhomogeneities.

PHOTO 0020-71

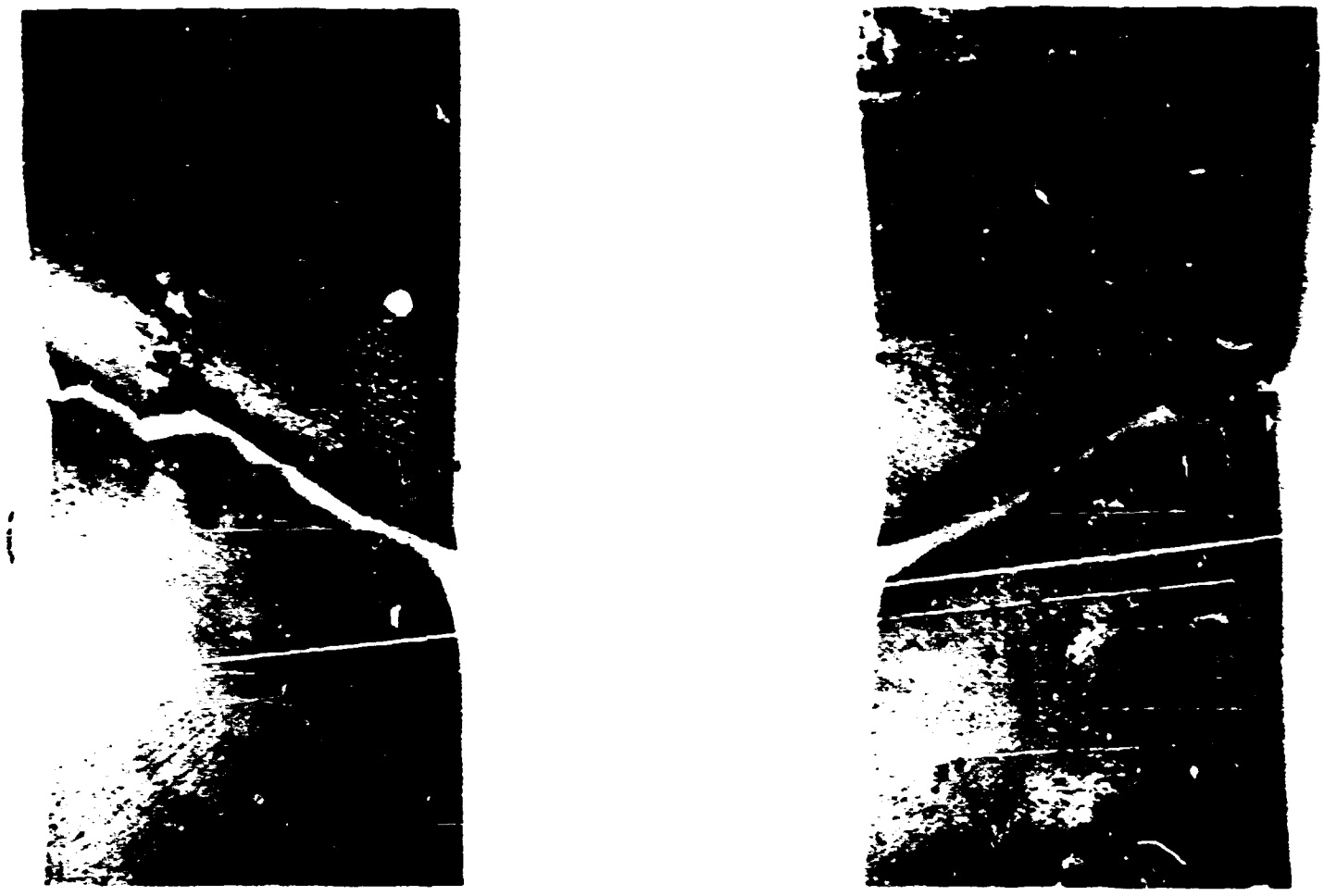

Fig. 2.7. Radiograph of slag inclusion in specimen 103 (bottom) that became the fracture origin (top left) supplanting the 0.100-in.-deep fatigue crack (top right).

Table 2.3. Effects of temperature on tensile properties

	Specimens tested at 75°F			Averaged results of tests[a] at −20°F	Specimens tested at −100°F		
	Y13	Y14	Average		Y17	Y18	Average
Ultimate strength, ksi	85.9	84.9	85.4	90.9	99.2	99.8	99.5
Yield stress, ksi							
Upper	65.7	65.0	65.4	70.1	77.4	76.6	77.0
Lower	65.7	64.8	65.2	68.3	76.8	75.8	76.3
Elongation at yield point, %	1.2	1.2	1.2	1.4	1.8	1.8	1.8
Strain to maximum load, %	10.8	11.4	11.1	12.3	13.4	13.5	13.4
Elongation, %	27.0	26.5	26.8	(b)	26.0	27.5	26.8
Reduction of area, %	64.6	55.7	60.2	(b)	46.0	53.2	49.6

[a]Data from Table 2.2; data affected by presence of slag inclusions or "fisheyes" not included.
[b]Average not computed because spread in values caused by presence of slag inclusion was so large.

A study of the radiographs that were made as a result of the findings from the tensile tests led to the conclusion that as many as one-third of the test results for individual gross strain specimens might be affected by the slag inclusions. For example, (1) the specimen might fail at the inclusion instead of at the fatigue crack, (2) the size of the fracture origin might be put in doubt by the presence of fisheyes adjacent to the fatigue crack, (3) delamination might reduce constraint below the crack, or (4) gross strain values might be affected by local strain around an inclusion. Consequently, replacement material, pieces 02AE and 02AF (see Fig. 2.5), was furnished by ORNL from the upper end of plate 02. The use of this material is described after the presentation of the test plan.

Strain measurement. One result of the first year's work was the conclusion that critical values of gross strain should be measured in the gross section above and below the crack (ϵ_{ggc}), as well as in the net section spanning the crack (ϵ_{gnc}). The ϵ_{ggc} values can be obtained after a test from micrometer readings that give the reduction in width and thickness by using the technique described in HSST Technical Report No. 3.[8] For small strains, extensometers are more accurate.

Records of load versus displacement provide for measurement of energy values and for fuller observation of the deformation process, and hence pairs of extensometers (back to back) were provided for measurement of average values of ϵ_{gg}, as well as ϵ_{gn}, and a single extensometer for measuring the crack-opening displacement (COD). In the initial adjustment for axiality of loading, the difference in the output of two units of a pair of extensometers was read to measure bending.

The seven extensometers shown in Fig. 2.8 utilize the conventional strain-gaged flexure principle and have special fingers to contact the specimen. Many gage lengths are required in a size-effect study of this kind, but for reasons of economy and survival when the specimen breaks, all extensometers are of one size – as small as possible. The gage points on the specimen are spot welds that hold adapters made of wire and threaded rod, the length of which can be adjusted fairly easily to fit the extensometer to any gage length. Typical configurations are shown in Fig. 2.8.

For size-effect studies, gage lengths must be scaled the same as other dimensions. Figure 2.9 shows the dimensional requirements for the placement of gage points. Exceptions to this pattern for other studies are noted where those tests are discussed.

A typical set of records is shown in Fig. 2.10. The curves in Fig. 2.10 were traced from charts obtained from *X-Y* plotters. The dip in load in the curve for ϵ_{gn} was caused by sudden yielding in the lower part of the specimen. While not evident in this record, the *X-Y* recorder pens traverse the yield plateau at different times during the test. In the ideal case, the net section yields first, but when the ratio of crack area to gross area is very small, this may not be true. In these tests, yielding frequently occurred first at the fillets at either end of the reduced section. Figure 2.15, discussed later, illustrates this condition.

Test plan. Two features of this work are a study of net section effects and a study of crack size effects. Superimposed on both is the problem of how gross strain is to be measured – what gage length, what

8. P. N. Randall, "Gross Strain Measure of Fracture Toughness of Steels," *Heavy Section Steel Technology Program Technical Report No. 3*, TRW Systems Group, p. 7, Nov. 1, 1969.

PHOTO 0021-71

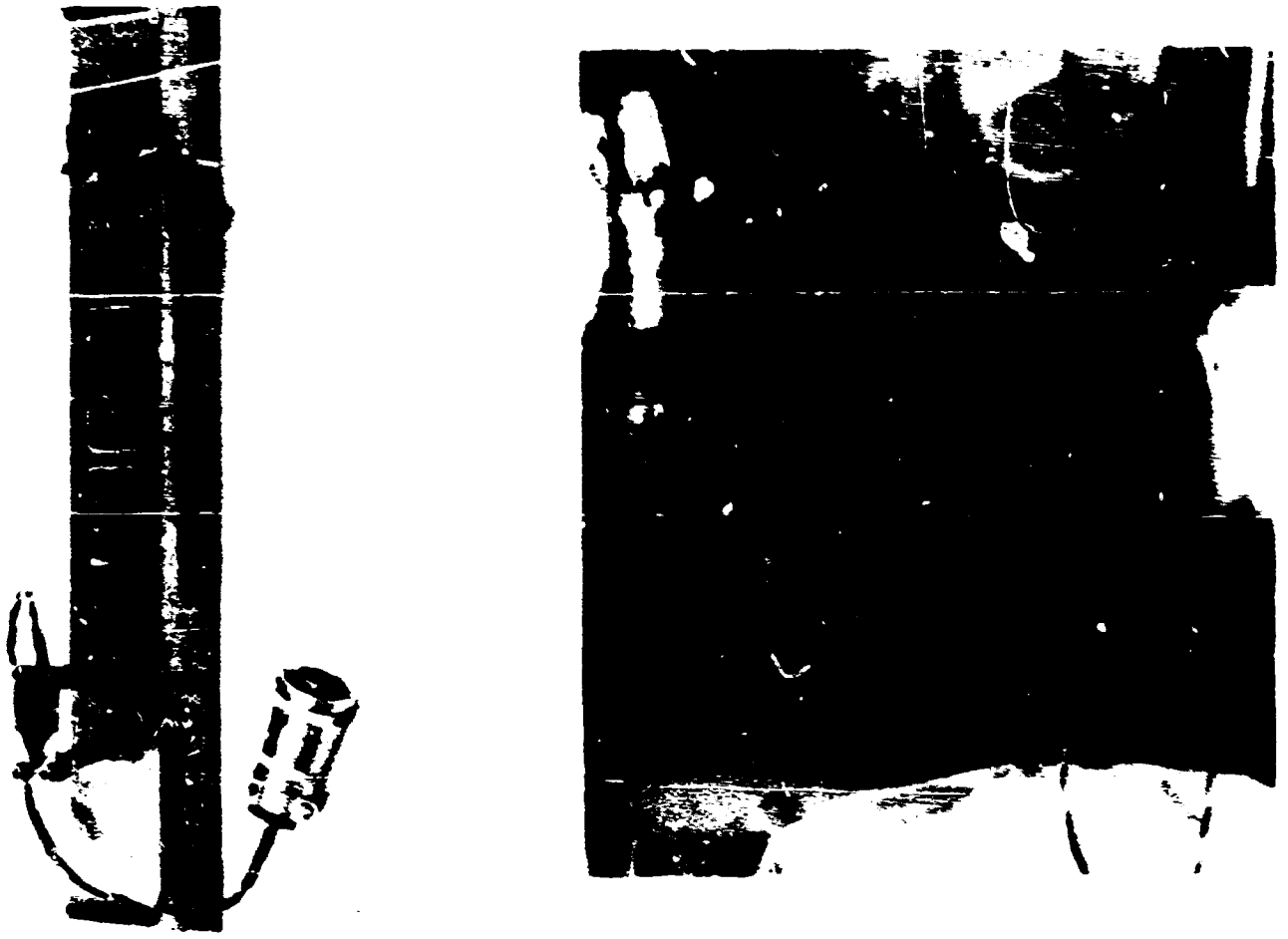

Fig. 2.8. Extensometer and gage-length adapters (top left), assembled specimen in grips (top right), and cold-box plus tubes for liquid nitrogen (bottom).

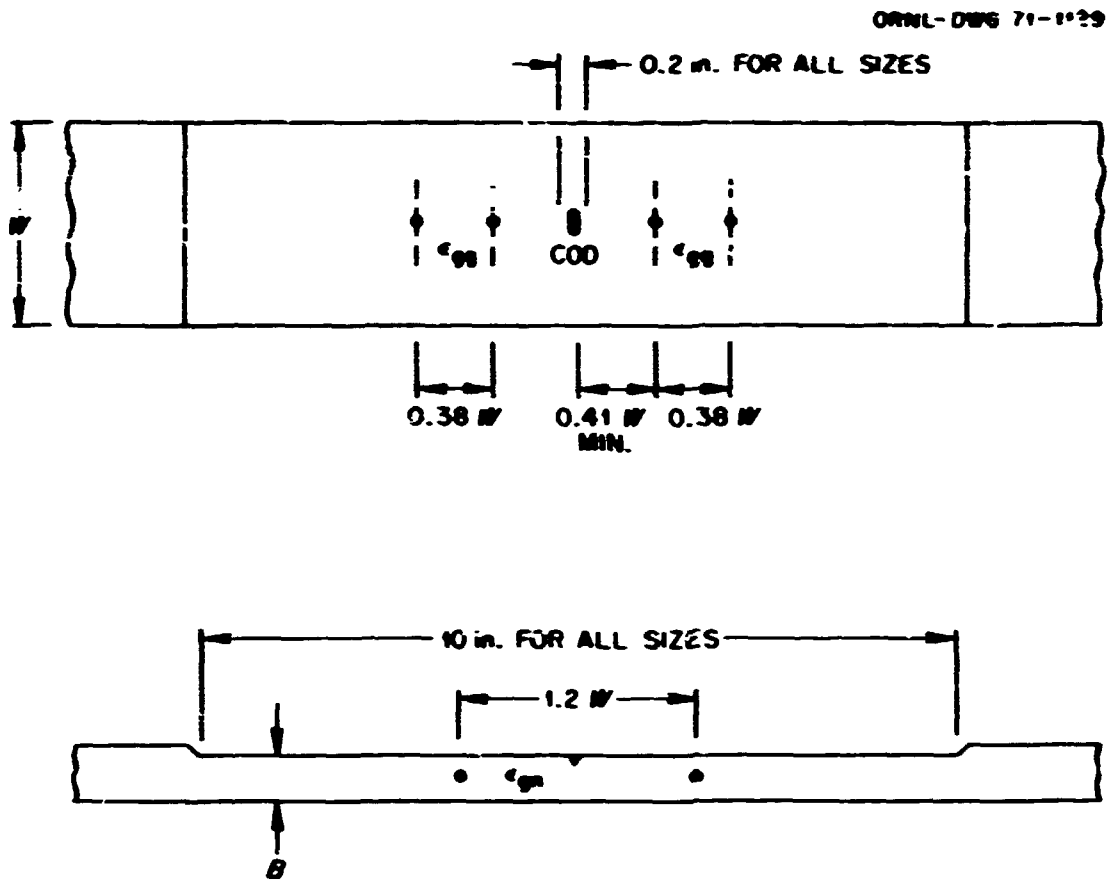

Fig. 2.9. Sketch showing location of displacement measurements.

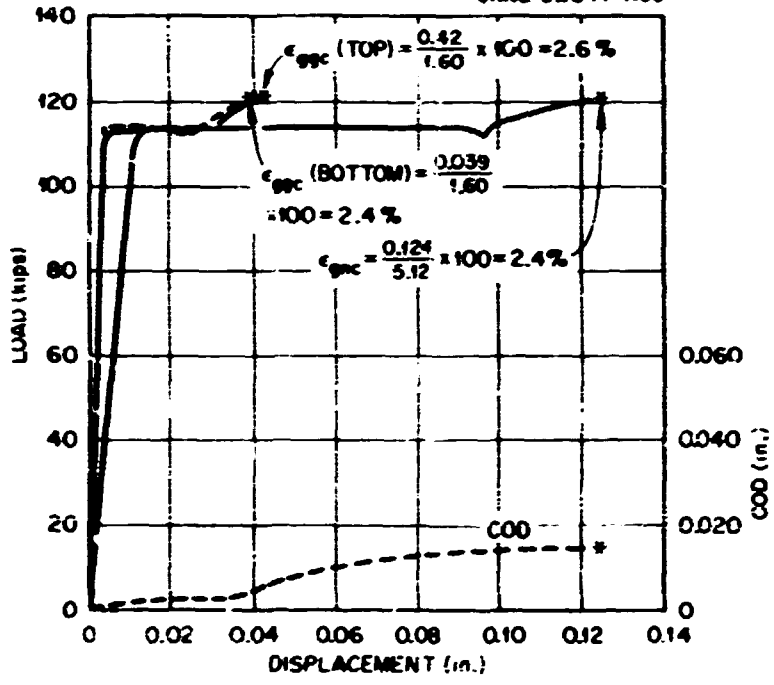

Fig. 2.10. Typical records traced from test results for specimen 112.

location, etc.? – with the purpose being to obtain results from a practical test specimen that can be applied to full scale hardware.

The importance of net-section effects was realized when previous results showed that the transition temperature was the temperature at which the material in a given specimen configuration could tolerate the local (crack tip) strain that was present at the load level that caused gross-section yielding. It appeared that a specimen having a very small crack area relative to the gross area would exhibit a lower transition. This aspect of specimen design is to be investigated by tests of the three specimens with the cross sections shown in Fig. 2.11. All have a semielliptical surface crack grown in fatigue to a nominal size of 0.10 in. deep by 0.30 in. long. The ratio of crack area to gross area is about 1.5% in the first two groups of specimens and about 6.0% in the third. The purpose in testing both wide specimens and narrow ones was to check the hypothesis that the shape of the specimen cross section is unimportant provided the crack tip region is embedded sufficiently to provide all the restraint possible for that particular crack size.

The importance of a crack size-effect study in the HSST program is fairly obvious. The approach is simply to test a range of cracks of various sizes embedded in geometrically similar cross sections and measure the critical displacements over geometrically similar gage lengths. Extrapolation to the crack size expected in full-scale hardware will be in terms of critical strain both below and at the transition temperature. The specimens to be tested are shown in Fig. 2.12. All these

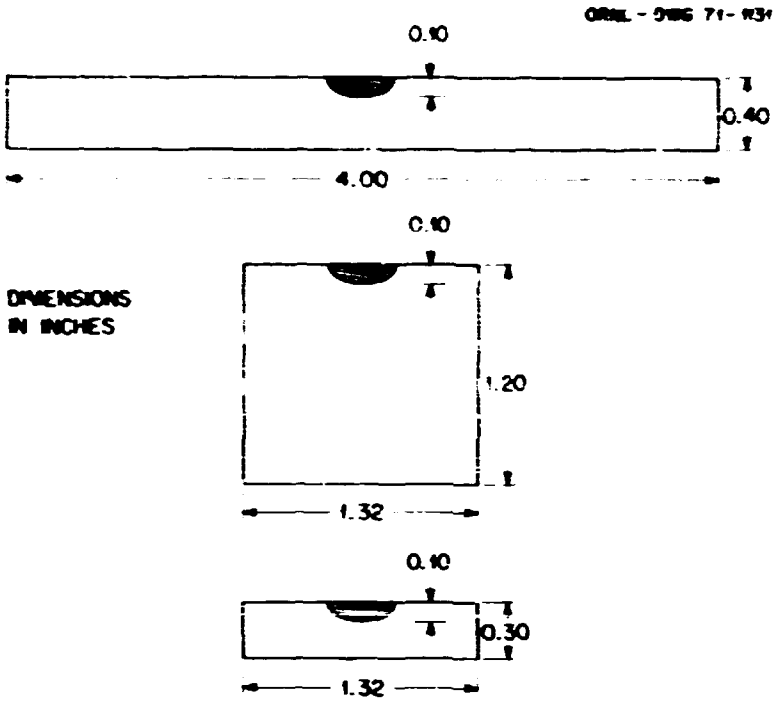

Fig. 2.11. Specimen cross sections to be tested to study effects of shape of cross section and of the ratio of the crack area to the gross area.

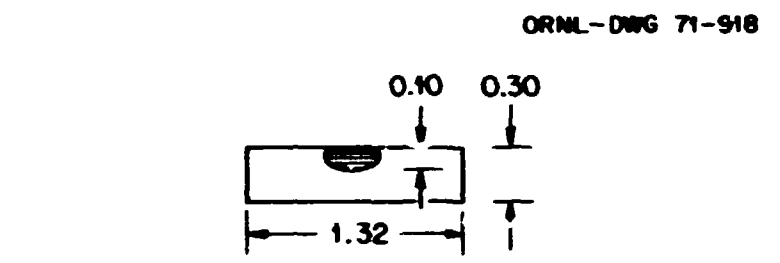

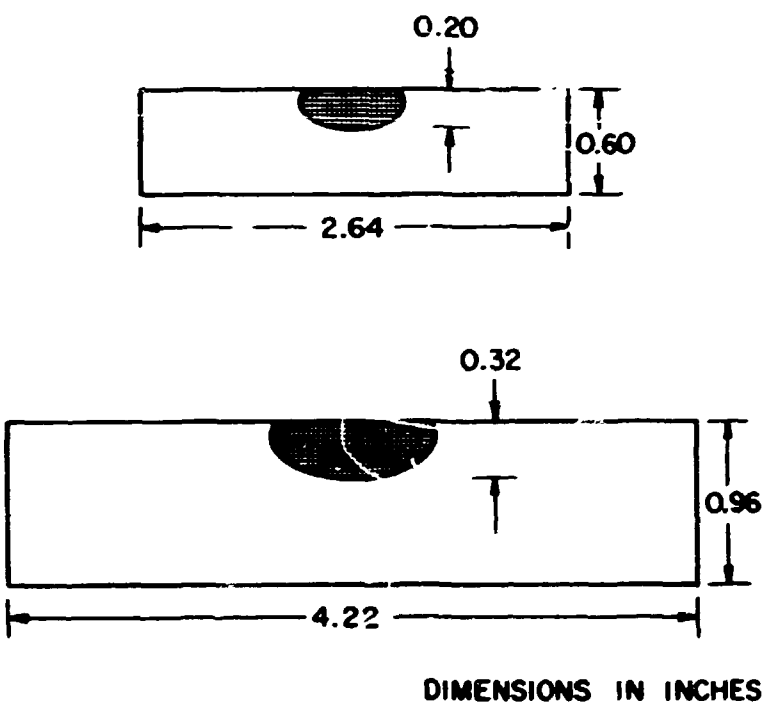

Fig. 2.12. Specimen cross sections to be studied in size-effect tests.

have a ratio of crack area to gross area of about 6.0%. The smallest specimen was also shown in Fig. 2.11, and the sketch was repeated here for completeness.

One other task planned is the preliminary study of strain-gradient effects. The objective is to decide on a suitable test specimen and means of loading and to get a first indication of the magnitude of the effects. There are two kinds of strain gradients to be studied: a transverse gradient, such as that produced by testing cracked specimens in bending, and a combined axial and transverse gradient, such as that produced by a tension test of a specimen having a very short reduced section so that the surface crack is located in a fillet. The transverse gradient will be tested first because it poses the simpler question; namely, what critical strain value in bending correlates with those measured in tension for the same crack size? This year's effort should provide a basis for planning the testing required to include the treatment of strain gradients in the gross strain approach.

Test results. Only the test results relative to the effects of shape of cross section are available for this report (see the two top sketches in Fig. 2.11). Table 2.4 lists the actual specimen dimensions and Table 2.5 gives results in terms of loads and displacements, as well as stresses and strains. Gage lengths were the same for both tests: 5.12 in. for ϵ_{gn} and 1.60 in. for ϵ_{gg}.

The transition temperature for 0.10-in.-deep cracks in this material appears to be at about -90 ± 10°F for the foot of the transition in values of ϵ_{gnc}, ϵ_{ggc}, and COD. Figure 2.13 presents the data for specimens 4 X 0.4 in., and Fig. 2.14 shows the data for specimens 1.32 X 1.2 in. The trend for ϵ_{ggc} values is less clear because these specimens, which had a net-section stress only 1.5 to 2.0% greater than the stress on the gross section, often yielded first at the fillet at one end of the specimen. The Luder's bands spread toward the crack and caused the extensometer in the gross section to indicate higher strain than that in the net section or in the other gross-section gage length until the yielded region covered the entire reduced section. Figure 2.15 illustrates this condition.

Some difference possibly exists between the two specimen shapes, but it is masked by the scatter in crack sizes plus the fact that crack depth was greater for the thicker specimens. The ratio of crack depth to crack length was 0.33 for the 0.4-in.-thick specimens and 0.41 for the 1.2-in. ones. This difference was to be expected and should have been compensated for by growing longer cracks in the thinner bars, but through an oversight it was not. As a matter of side interest,

Table 2.4. Specimen dimensions for determination of critical gross strains and displacements

Specimen No.	Test temperature (°F)	Specimen dimensions			Crack size			Specimen net area ($in.^2$)	Ratio crack area to gross area (%)
		Width (in.)	Thickness (in.)	Gross area ($in.^2$)	Length (in.)	Depth (in.)	Area ($in.^2$)		
103	+75	4.005	0.403	1.612	0.300	0.160	0.0235	1.588	1.46
102	−40	4.002	0.397	1.588	0.302	0.102	0.0241	1.564	1.52
104	−60	4.001	0.400	1.601	0.302	0.101	0.0239	1.577	1.49
106	−83	4.003	0.402	1.610	0.347	0.105	0.0285	1.582	1.77
101	−90	4.002	0.398	1.594	0.300	0.103	0.0242	1.570	1.52
105	−112	4.000	0.396	1.583	0.304	0.096	0.0229	1.560	1.45
109	−50	1.328	1.200	1.593	0.300	0.128	0.0301	1.563	1.89
112	−72	1.328	1.199	1.592	0.304	0.130	0.0310	1.561	1.95
110	−83	1.328	1.201	1.593	0.321	0.153	0.0386	1.554	2.42
111	−84	1.328	1.201	1.594	0.304	0.123	0.0294	1.565	1.84
114	−104	1.327	1.200	1.592	0.304	0.114	0.0272	1.565	1.71
113	−118	1.328	1.201	1.594	0.311	0.130	0.0317	1.562	1.99

Table 2.5. Results of tests for determining critical gross strains and displacements

Nominal specimen size (in.)	Specimen No.	Test temperature (°F)	Maximum load (kips)	Gross stress (ksi)	Net stress (ksi)	Critical gross strains and displacements				
						ϵ_{ggc} at top (%)	ϵ_{ggc} at bottom (%)	ϵ_{gnc} (%)	Displacement in ϵ_{gn} gage length spanning crack (mils)	COD (mils)
4 x 0.4	103	+75[a]	132.0	81.9	83.1	12.4	9.8	>5.2[b]	>370	70
	102	−40	141.8	89.3	90.7	13.1	12.9	>6.8[b]	>350	
	104	−60	128.2	80.0	81.2		4.1	3.8	192	16
	106	−83	117.5	73.0	74.3	2.5	0.25	1.0	52	4
	101	−90	120.3	75.5	76.7	0.24	0.25	0.33	17	7
	105	−112	119.8	75.7	76.8	0.29	0.30	1.3	68	6
1.23 x 1.2	109	−50	143.1	89.8	91.5	13.6	11.8	12.8	658	89
	112	−72	120.7	75.8	77.3	2.6	2.4	2.4	124	15
	110	−83	112.8	70.8	72.5	0.69	0.37	0.66	34	10
	111	−84	128.8	80.0	82.2	3.6	2.6	3.70	189	16
	114	−104	118.8	74.6	75.9	2.2	0.23	1.1	57	9
	113	−118	123.5	77.5	79.0	0.32	0.29	0.44	22	6

[a]Broke at slag inclusion rather than at crack.
[b]Ran out of extensometer travel.

specimen 106, which had a ratio of 0.30, was grown completely in reversed bending (inadvertently).

The relationship of gross stress to temperature, plotted in Fig. 2.16, shows a transition at the same temperature (−90°F) as that for the strain values. The data for yield and ultimate strengths are from Table 2.3. As expected from the previous work, the transition occurred at the temperature at which gross-section yielding preceded the onset of fast fracture.

Figure 2.17 is a replot of a set of the load displacement records from which ϵ_{gnc} values were computed for the bars of 1.32 X 1.20-in. cross section. They show how elongation and maximum stress values drop off at the transition. Obviously the area under these curves is the energy to maximum load consumed in deformation within the gage length (5.12 in.). From Fig. 2.10, it is evident that the strain was fairly uniform along this length once the yield plateau was passed at all points along the gage length.

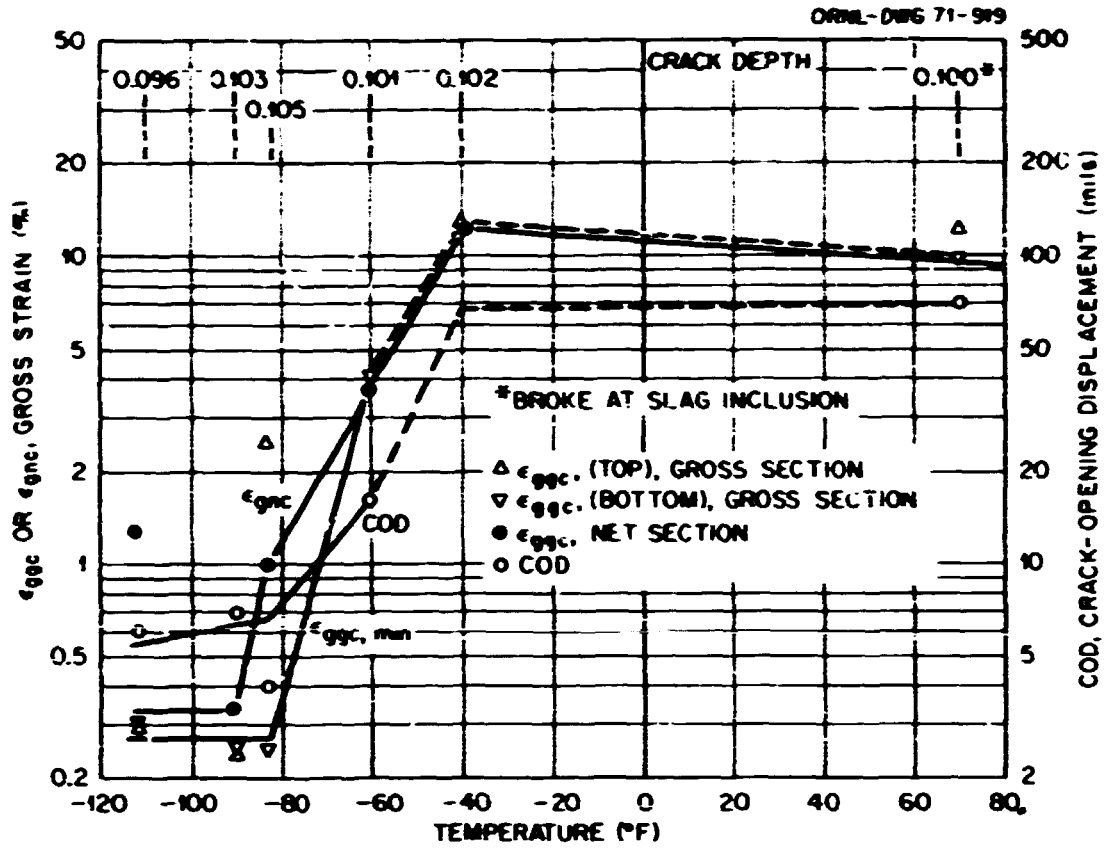

Fig. 2.13. Effect of temperature on gross-strain crack tolerance for 0.100-in.-deep surface cracks in specimens 4 in. wide by 0.4 in. thick.

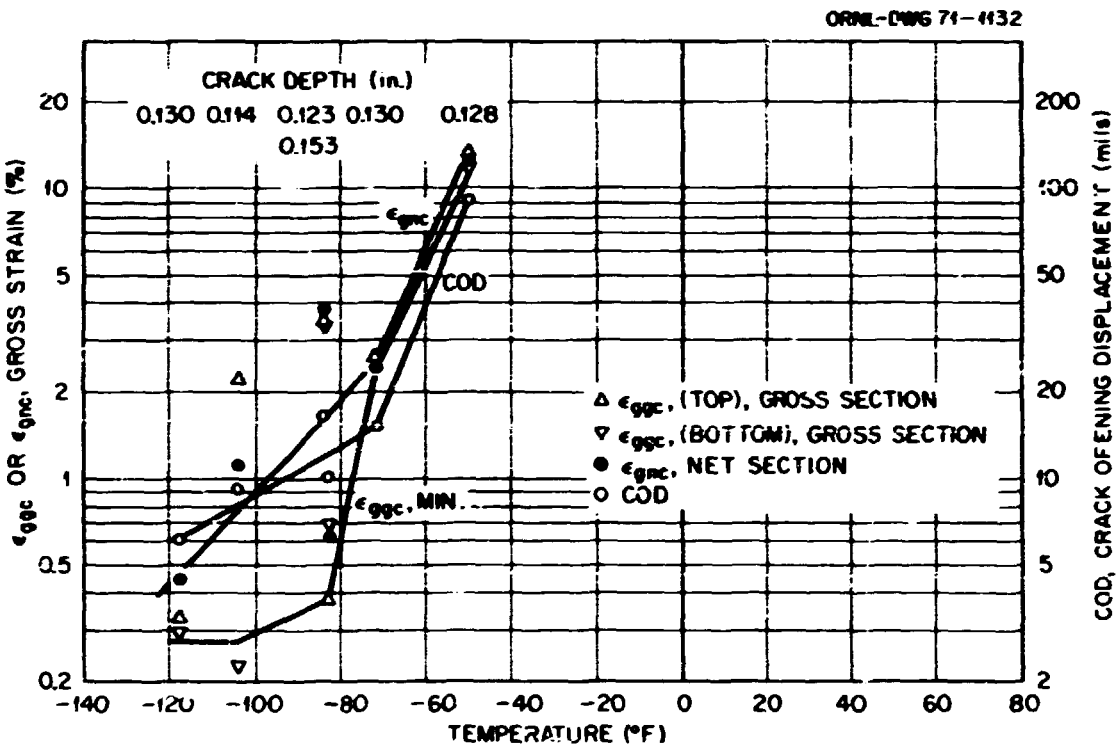

Fig. 2.14. Effect of temperature on gross-strain crack tolerance for 0.100-in.-deep surface cracks in specimens 1.32 in. wide by 1.2 in. thick.

Fig. 2.15. Luders' bands spreading downward from fillet at end of gage length. These bands caused plastic strain to occur first in the gross section. Ratio of crack area to gross area was 1.5%.

Plans for completion of work. When it was discovered that the presence of slag inclusions in pieces 02G*X*, *Y*, and *Z* might interfere with the interpretation of test results, additional material was provided by ORNL. Pieces 02AE and 02AF were from the upper end of plate 02, as shown in Fig. 2.5. Tensile specimens (0.505 in. in diameter) are currently being machined. They will be tested to check homogeneity of yield properties, primarily. The size-effect study described in Fig. 2.12 will be done on this material. The tests of the smallest specimens (0.10-in.-deep crack) will repeat those on specimens from block 02*GY* to provide correlation with the other work done to date.

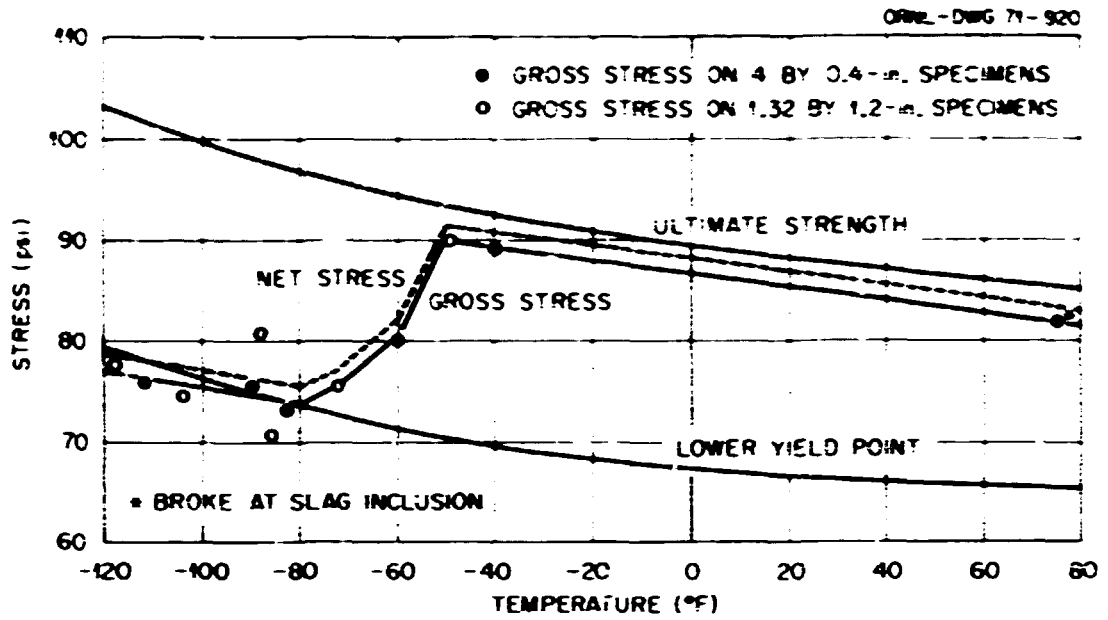

Fig. 2.16. Effect of temperature on relationship of maximum stress sustained by specimens containing a 0.100-in.-deep crack to the yield and ultimate strengths of the material.

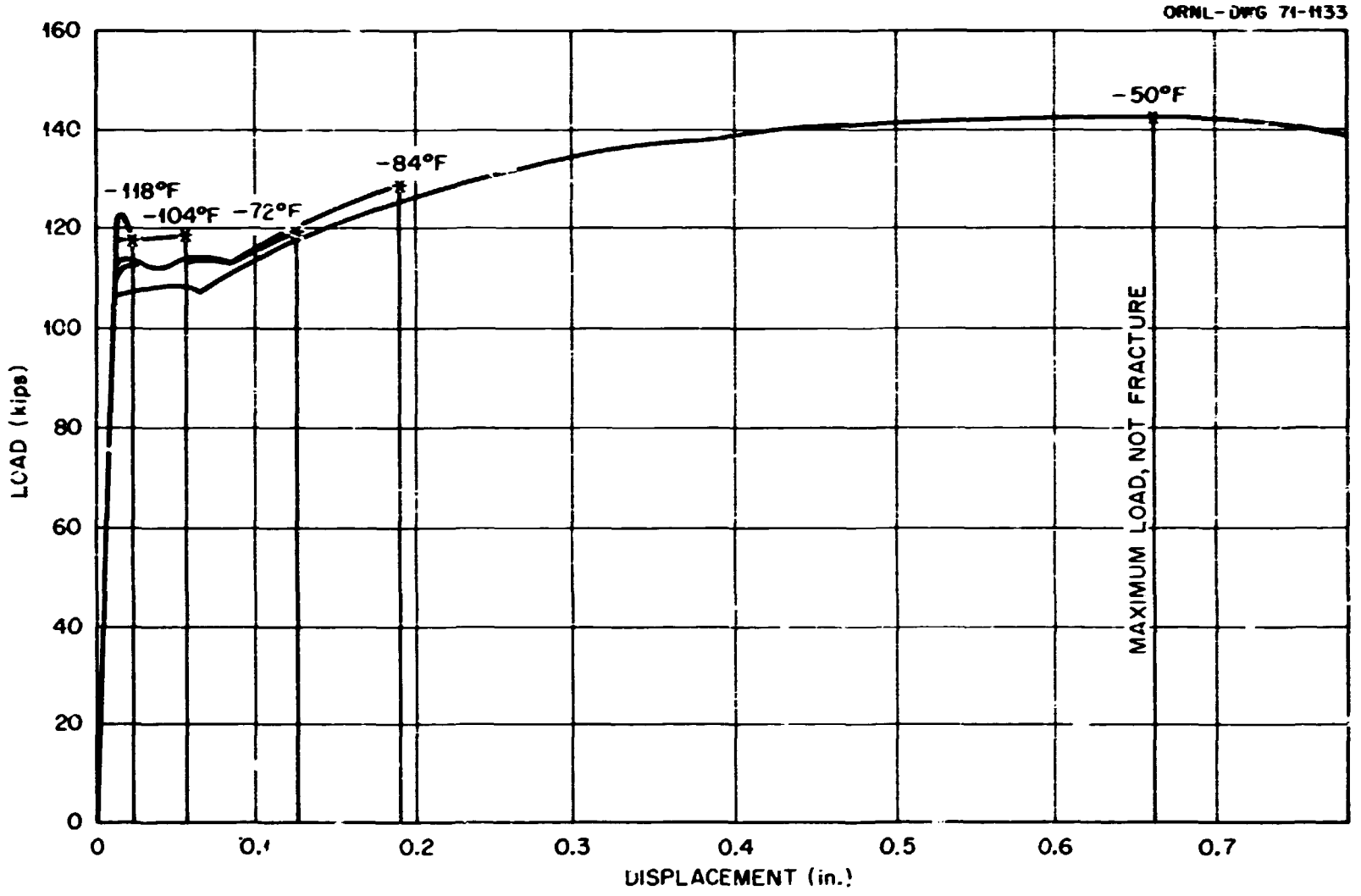

Fig. 2.17. Effects of temperature on record of load versus displacement on a 5.12-in. gage spanning the crack in bars 1.32 in. wide by 1.2 in. thick.

Three-dimensional elastic-plastic stress and strain analysis for fracture mechanics[9] (N. J. Levy, P. V. Marcal, and J. R. Rice, Brown University)

The primary activities during the current reporting period were the preparation of a topical report covering the work completed to date and the accomplishment of some internal improvements in the computer program being developed. The main improvement in the computer program was the introduction of a direct method of solution for the system of equations generated by the elastic part of the problem. This improvement reduces the time required to accomplish the elastic solution by a factor of approximately 2 and therefore makes the program significantly more efficient.

The topical report covers the development of an elastic-plastic finite-element analysis for three-dimensional specimens with flaws. Particular attention was paid to the analysis of a semielliptic crack and a through crack in a plate of finite thickness. Three-dimensional polar, cubic, and cubic-distorted elements were developed for the analysis. In addition, programs to generate the mesh of elements and nodal points for a given problem size and specimen geometry were written and tested. The finite-element analysis was implemented by a computer program developed to handle problems with up to 10,000 degrees of freedom. As is well known, such large problems are frequently encountered in three-dimensional analysis. This capability was also required for analysis of the stress and strain field near cracks. The results of analysis for a through crack with 4500 degrees of freedom and for a semielliptic crack with 2700 degrees of freedom are also reported. The problems discussed were studied mainly to test the finite-element program, the mesh-generating programs, and the suitability of the elements developed.

With respect to the three-dimensional crack problem – case study (a) – the elastic solution obtained reproduced closely the features of the approximate solution suggested by Hartranft and Sih.[10] The main result shown by the elastic solution is that at the crack tip the plane-strain regime prevails across the specimen thickness, except perhaps at the free surface or in a thin layer – called the boundary layer in ref. 10 – near the free surface. It should be noted that the three-dimensional polar element is a generalization of the two-dimensional polar element reported in ref. 11 and used in the plane-strain crack problem. As shown in ref. 11, the two-dimensional element reproduces quite well the displacement singularity at the crack tip in the plastic regime. It is therefore believed that the three-dimensional polar element developed here will be excellent for the study of the stress and strain field in the three-dimensional through-crack problem, especially at the proximity of the crack tip in the elastic as well as in the plastic domain.

As to the elastic-plastic analysis of the semielliptic crack, there are no analytic or approximate solutions with which to compare the results of the finite-element analysis. However, a qualitative study of the stress and strain distribution based on equilibrium in the large shows that the finite-element results are qualitatively correct. The main result of the analysis is that the limit load of the specimen with the flaw is the same as the limit load of a specimen of the same dimensions but without a flaw. In addition the stress and strain field disturbance due to the presence of the flaw fades away almost completely at a distance equal to three times the thickness of the specimen.

Finally, it would be very interesting and instructive to compare these findings with the experimental results when these are available.

Fracture mechanics characterization and crack-preparation studies of HSST program materials[12] (T. R. Mager, Westinghouse Electric Corporation)

Two final reports covering fracture toughness characterization of A 533, grade B, class 1 steel and notch preparation in compact tension specimens were prepared.[13,14]

Testing of compact tension specimens from approximately −50°F to approximately 550°F continued. An

---

9. Work performed under UCCND Subcontract 3153 between Union Carbide Corporation and Brown University.

10. R. J. Hartranft and G. C. Sih, *An Approximate Three-Dimensional Theory of Plates with Application to Crack Problems*, Lehigh University, Technical Report No. 7 May 1969.

11. N. Levy, P. V. Marcal, W. J. Ostegren, and J. R. Rice, "Small Scale Yielding Near a Crack in Plane Strain: A Finite Element Analysis," *Int. J. Fracture Mechanics* (in press).

12. This program was performed under UCCND Subcontract No. 3196 between the Oak Ridge National Laboratory and Westinghouse Electric Corporation.

13. T. R. Mager, "Fracture Toughness Characterization of A533, Grade B, Class 1 Steel," *Heavy Section Steel Technology Program Technical Report No. 10*, Report WCAP-7578, Westinghouse Electric Corporation.

14. T. R. Mager, "Notch Preparation in Compact Tension Specimens," *Heavy Section Steel Technology Program Technical Report No. 11*, Report WCAP-7579, Westinghouse Electric Corporation.

equivalent-energy procedure was used to determine the fracture toughness parameter K_{Icd}. The experimental studies indicated that K_{Icd} values determined from small compact tension specimens may be almost numerically equal to K_{Ic} values determined from much larger specimens. Compact tension specimens ½ and 1 in. thick were tested.

Witt[15] proposed an equivalent-energy method for relating crack size, temperature, and stress levels at maximum load to fracture and outlined a procedure for obtaining the fracture toughness value, K_{Icd}, which is not to be confused with the dynamic fracture toughness K_{ID}.

The procedure for obtaining K_{Icd} values from standard fracture toughness tests consists of the following:

1. Measure the area under the load-deflection curve up to maximum load of a specimen of width d.

2. Select any point on the linear portion of the load-deflection curve. Measure the area up to this point, and divide this area into the area up to maximum load: call this ratio b. Scale the dimensions of the specimen tested by the factor b and the load by b^2. Using this load as P_Q, determine K_Q for the scaled-up specimen. The value determined is unique regardless of the point selected on the linear portion of the curve. This number is K_{Icd}.

Experimental test procedure. Twenty 1-in.-thick and twenty ½-in.-thick compact tension specimens were machined from HSST plate 02. The specimens were prefatigue cracked according to the ASTM recommended procedure,[2] and a clip gage was placed on the front face of each specimen. In addition to the front-face clip gage, a deflection gage was placed on one side across the machined crack and ¼ in. from the top of the prefatigue crack on the surface of some of the 1-in.-thick specimens. This clip gage measured surface crack opening displacement (surface COD). The clevises and specimen were placed in a temperature-controlled chamber for testing.

For temperatures below ambient, liquid nitrogen vapor was used to cool the test specimen; above ambient, an electrically heated chamber was utilized. The load-displacement readings were read out on standard x-y plotters. After the test, the crack lengths at crack initiation were read at five equally spaced intervals. These were averaged to give the crack length for the test. A time-load behavior was also recorded.

Results. The specimens were tested at 15 temperatures from −50 to +550°F. Then, using the method previously outlined,[15] K_{Ic1} (that is, K_{Icd} from a 1-in.-thick specimen) values were calculated at each test temperature. At temperatures where the specimen maintained a maximum load over considerable displacement, the point where the maximum load was first reached was chosen as the maximum load to fracture. Data for the ½-in.-thick specimens are still being evaluated.

The K_{Ic1} data are summarized in Table 2.6, and Fig. 2.18 is a plot of all the K_{Ic1} data obtained from testing 1-in.-thick compact tension specimens between −50 and 550°F. These data indicate a very high resistance to fracture at elevated temperatures, even though a slight degradation is noted at 550°F.

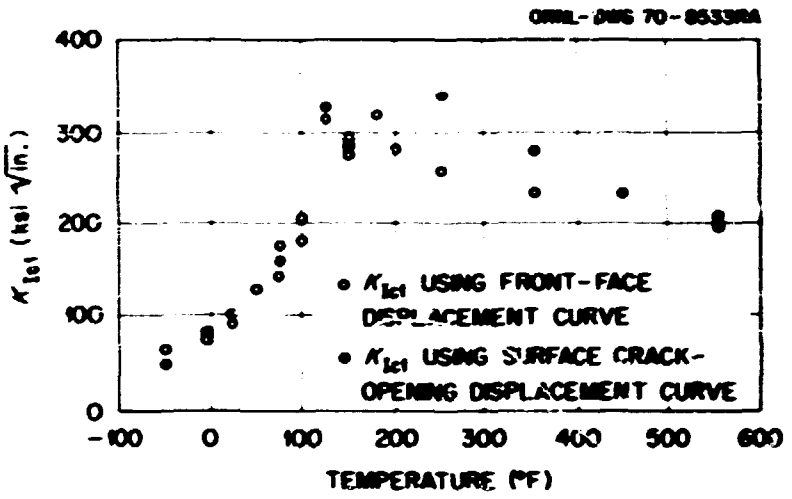

Fig. 2.18. Variation of K_{Ic1} as a function of temperature for longitudinally oriented 1-in.-thick compact tension specimens of ASTM A 533, grade B, class 1 steel (nonsurface specimens).

Future work will include evaluating 4-, 6-, and 10-in.-thick specimens at temperatures corresponding to the upper-shelf Charpy V-notch range (200 to 550°F).

15. F. J. Witt, Equivalent Energy Procedures for Predicting Gross Plastic Fracture, paper presented at Fourth National Symposium on Fracture Mechanics, Carnegie-Mellon University, August 24–26, 1970 (in publication); see also USAEC Report ORNL-TM-3172 (in publication).

Table 2.6. Fracture toughness results determined from testing 1-in.-thick compact tension specimens up to 550°F

Specimen designation	Test temperature (°F)	Crack length (in.)	Some fracture toughness parameters (ksi $\sqrt{in.}$)				K_{Icd} from front-face displacement (ksi $\sqrt{in.}$)	K_{Icd} from surface COD (ksi $\sqrt{in.}$)
			KD^a	KQ^b	KU^c	KF^d		
HS2-7-C10	−50	1.022	43.1	58.2	63.6	7.2	61.0	
HS2-7-C8	0	1.010	37.0	46.9	73.9	7.1	76.0	80.6
HS2-7-C7	25	1.016	41.4	63.6	84.7	7.1	96.0	102.0
HS2-7-C3	50	1.010	61.6	91.7	97.6	7.0	128.0	
HS2-7-C12	75	1.032	67.5	93.1	103.8	7.3	176.5	194.0
HS2-28-C5	75	1.029	49.2	61.5	99.5	16.6	143.5	
HS2-28-C10	90	1.027	55.5	66.5	100.5	17.0	203.0	
HS2-28-C2	103	1.024	35.9	56.0	103.4	16.5	184.0	
HS2-7-C5	125	1.034	54.8	89.7	107.5	7.4	312.0	331.0
HS2-7-C2	150	1.026	55.1	87.1	106.3	7.3	276.0	283.0
HS2-28-C4	150	1.020	39.0	52.4	106.3	16.3	293.0	
HS2-7-C9	180	1.024	42.0	81.3	105.7	7.3	321.0	
HS2-28-C9	200	1.025	46.3	57.9	104.2	16.6	283.0	
HS2-7-C4	250	1.018	42.4	82.0	105.4	7.1	282.0	338.0
HS2-7-C11	250	1.016	60.5	85.8	105.8	7.0	269.0	341.0
HS2-7-C1	350	1.016	62.5	79.6	99.6	7.1	237.0	287.0
HS2-28-C1	448	1.019	57.0	59.0	104.1	16.5	234.0	
HS2-7-C6	550	1.022	63.5	80.1	96.4	7.2	204.0	212.0
HS2-28-C8	550	1.014	51.8	69.0	102.5	16.3	206.0	

[a]Fracture toughness at deviation from linearity in load-displacement curve.
[b]Fracture toughness at secant offset load.
[c]Fracture toughness at ultimate load.
[d]Fracture toughness intensity during fatigue precracking.

FATIGUE AND CRACK-PROPAGATION INVESTIGATIONS

L. F. Kooistra

The effects of environment and stress state on crack growth rates are being studied. Currently crack growth rates are being measured in an environment of high-temperature water (without irradiation). All combinations of two water conditions (typical of pressurized-water and boiling-water reactors), four materials (plate, submerged-arc weld, electroslag weld, and shielded-metal-arc weld), and two locations (surface and center for plate, weld metal and heat-affected zones for welds) are being investigated at 550°F with the use of 2-in.-thick compact tension specimens. Some characterization studies will also be made at room temperature.

Fatigue-crack growth characteristics[16]
(T. R. Mager, Westinghouse Electric Corporation)

The fracture mechanics approach is being used to study the effect of high-temperature reactor-grade primary water on the fatigue-crack growth characteristics of materials of nuclear pressure-vessel grade. The 2-in.-thick WOL (wedge opening loading) specimen is being utilized to measure the fatigue-crack growth at 550°F in an environment (excluding irradiation) typical of pressurized-water reactors and boiling-water reactors. The crack growth rate, da/dN, of pressure vessel materials is being measured as a function of ΔK_I, the change in the stress intensity factor at the tip of the crack.

Applications of the ultrasonic technique for measuring crack growth of the WOL specimen was found in prior work to have many advantages. Ultrasonic crack detection can be used over a wide range of temperatures (−200 to 600°F) without instrument recalibration, and the equipment can be automated to produce a continuous record of crack length versus elapsed cycles. The test chamber was designed for exposure of the

16. Work sponsored by HSST program under UCCND Subcontract No. 3290 between Union Carbide Corporation and Westinghouse Electric Corporation.

WOL specimens in primary reactor coolant water at pressures up to 2000 psi. Obviously, if the ultrasonic crack-growth monitoring technique was to be used, access to the specimen surface was necessary. This was accomplished by clamping the specimen to the lid of the test chamber and having an access slot in the chamber lid to permit the ultrasonic transducer to contact the specimen. An O-ring in a groove around the slot and between the chamber lid and specimen surface provide the seal.

When the chamber initially reached 550°F and 2000 psi, a leak developed at the interface between the chamber lid and the test specimen. This was corrected by proper selection of the O-ring. Next, a problem developed when the ultrasonic transducer overheated at the test specimen temperature of 550°F. This was corrected by circulating a coupling fluid.

Experimental results. Three 2-in.-thick WOL specimens were evaluated; a specimen from the top surface and center thickness of HSST plate 02 and a specimen from the submerged-arc weldment of A 533, grade B, class 1 steel. The results are presented in Figs. 2.19, 2.20, and 2.21. Examination of the fracture surfaces of

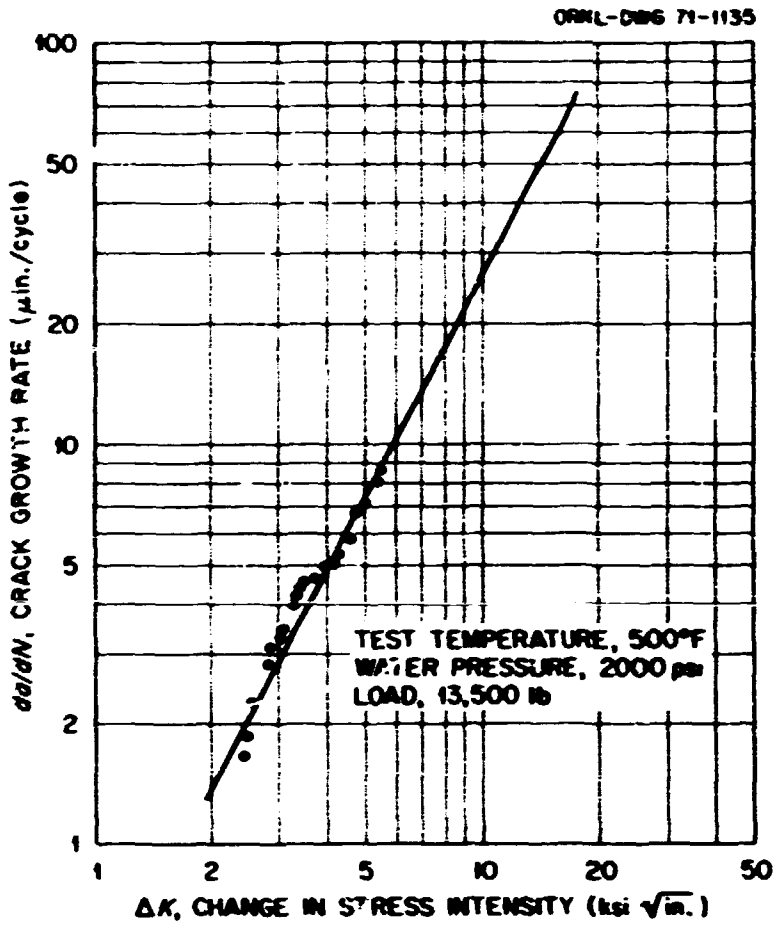

Fig. 2.20. Crack growth rate as a function of change in stress intensity at center thickness of A 533, grade B, class 1 steel specimen 2C-10.

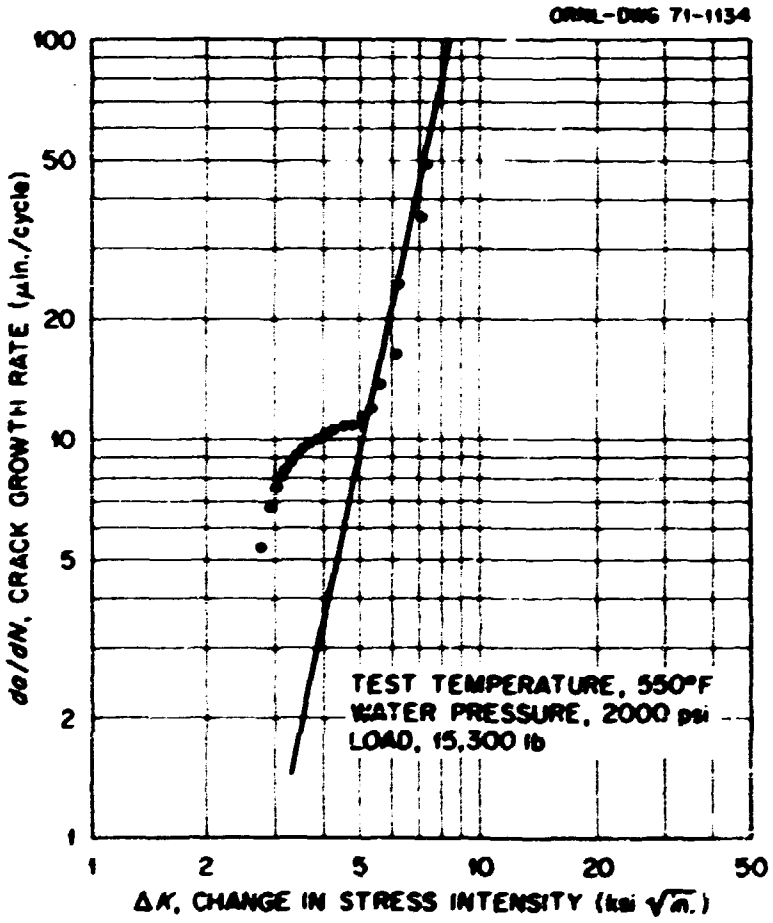

Fig. 2.19. Crack growth rate as a function of change in stress intensity at top surface of A 533, grade B, class 1 steel specimen 2T-4.

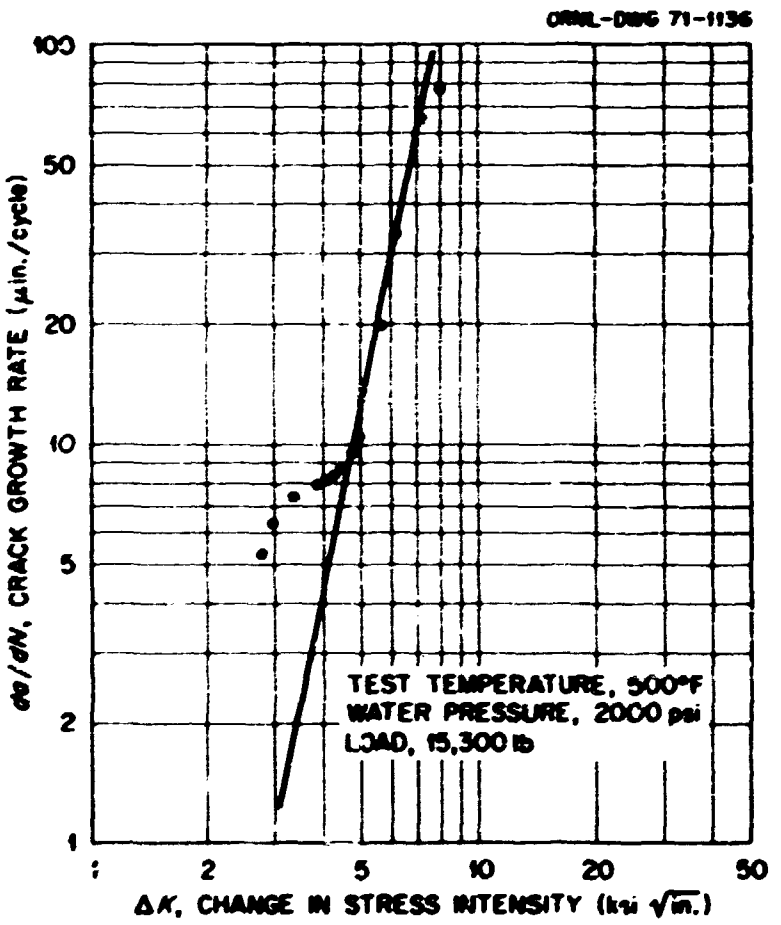

Fig. 2.21. Crack growth rate as a function of change in stress intensity on submerged-arc weldment specimen WD-2.

the specimens revealed that the starter crack (fatigue precrack) did not remain in the plane of the side notch during crack growth. It was concluded that because of the constraint of the chamber lid, the stress intensity K_I (mode I fracture) at the crack tip was not well defined.

In order to verify the conclusion that the loading arrangement influenced the compliance characteristics of the specimen and ultimately, the stress intensity calibration, a series of compliance tests was conducted both in and out of the test chamber. The difference in compliance (deflection across the machined notch at the front of the specimen per unit load) measured in and out of the test chamber was approximately 26%. The lower compliance values were measured in the test chamber.

The crack-tip stress-intensity factor, K, is related to the crack-tip energy release rate, G, which in turn is related to the specimen compliance. The factor K is given by

$$K = \left(\frac{GE}{1-\nu^2}\right)^{1/2},$$

where E is modulus of elasticity and ν is Poisson's ratio. From this relationship it can be concluded that a 26% decrease in compliance represents approximately a 5% decrease in the stress intensity.

It was also concluded that a component of K_{II} loading (mode II fracture) was also present during the fatigue-crack growth tests.

Future work. Three methods of obtaining interpretable data were considered:

1. Devise an analytical solution for the stress intensity at the crack tip that takes into consideration the decrease in K_I and the presence of mixed mode loading (K_I and K_{II}).
2. Redesign the chamber with bellows on the bottom to provide a flexible seal between the chamber and the lower loading stud.
3. Redesign the experiment to utilize compliance (LVDT gage) to measure the crack growth rather than the ultrasonic crack-monitoring technique.

It was concluded that compliance measurements were the most feasible. At present, a new chamber head is being fabricated to accommodate the LVDT gage. Compliance calibration is being performed at 600°F to insure the accuracy of the crack-growth measurements.

3. Investigations of Irradiated Materials

Irradiation is one of the environmental factors that must be considered in safety evaluations of reactor pressure vessels, since the mechanical properties of metals may be modified thereby to a degree that is of considerable engineering significance. Investigations of irradiation effects are being carried on by Hanford Engineering Development Laboratory (HEDL), Westinghouse Electric Corporation, Naval Research Laboratory (NRL), and Oak Ridge National Laboratory. The areas of primary interest to the HSST program are the temperature range 450 to 600°F and the fast-neutron ($E > 1$ MeV) fluence range 1×10^{19} to 8×10^{19} neutrons/cm^2.

The projected work at NRL, Westinghouse, and ORNL has essentially been completed, and final reports are being prepared. Results not previously reported, in addition to those from HEDL, are reported here.

Irradiation Effects on Pressure Vessel Materials[1]

T. R. Mager
Westinghouse Electric Corporation

Background

Experimental tests of a group of reactor vessel steels were performed to investigate the application of the fracture mechanics approach to these materials in the postirradiation condition. Materials investigated included the center material from a 12-in.-thick quenched-and-tempered ASTM A 533, grade B, class 1 steel plate (HSST plate 02), a heat of A 508, class 2, forging-grade steel, and the weld metal from a heavy-section weldment of A 533, grade B class 1 steel produced by the submerged-arc process.

To generate the fracture toughness data, compact tension[2] specimens were used. Five 2-in.-thick compact tension specimens were selected from HSST plate 02, one was fabricated from the heat of forging-grade steel, and two were selected from the weld metal. The five specimens fabricated from the plate 02 were oriented in the longitudinal (RW) direction. The notch direction was coplanar to the direction of the weld beads for the two specimens from the weldment. The notch was oriented in the tangential direction for the forging-grade specimen.

Tensile specimens were also included in the experimental program to satisfy the validity requirements (yield strength), as well as to provide correlation data. The design, fabrication, and irradiation of the capsule assemblies were performed by Babcock & Wilcox at the Babcock & Wilcox Test Reactor (BAWTR). The BAWTR is a pool-type experimental reactor with an output of 6 MW. The capsules were designed so that the specimens could be maintained at 540 ± 15°F through a combination of gamma heating and externally applied electric heat. Typical temperature readings for each capsule are given in Table 3.1.

Results

The postirradiation tensile properties of the A 533, grade B, class 1 steel (HSST plate 02) are listed in Table 3.2 and plotted on Fig. 3.1. The curves in Fig. 3.1 are the postirradiation (~4×10^{19} neutrons/cm^2) tensile properties of HSST plate 02 (quarter thickness) reported in ref. 3 (see Fig. 14, p. 34, of ref. 3 for correct

1. Work sponsored by the HSST program under UCCND Subcontract No. 3209 between Union Carbide Corporation and Westinghouse Electric Corporation.

2. ASTM Standard E399-70T, "Tentative Methods for Test of Plane-Strain Fracture of Metallic Materials," *ASTM Standards*, Pt. 31, May 1970.

3. T. R. Mager and F. O. Thomas, *Evaluation of Linear Elastic Fracture Mechanics of Radiation Damage to Pressure Vessel Steels*, Report WCAP-7328, Rev., Westinghouse Electric Corporation, October 1969.

Table 3.1. Typical temperature reading for capsules irradiated in BAW-1R

Thermocouple number and location	Temperature (°F)	
	Capsule 7	Capsule 8
1, front	Open	545
2, front	575	520
3, front	Open	535
1, back	Open	555
2, back	555	560
3, back	Open	565
4, back	Open	Open
5, back	525	550
Frame, top	575	Open
Frame, bottom	Open	515

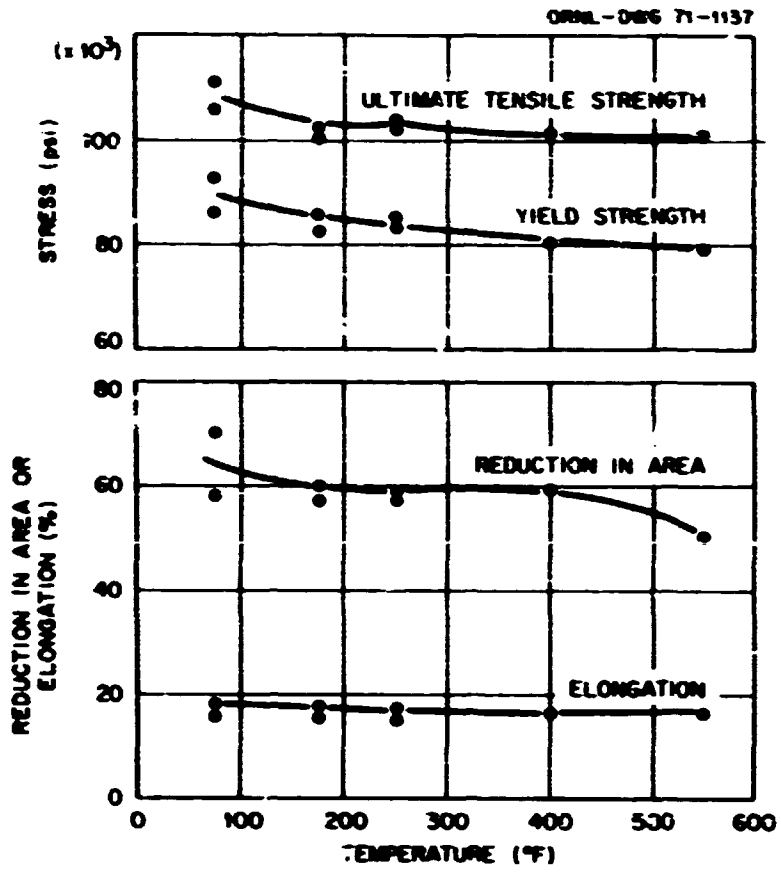

Fig. 3.1. Postirradiation tensile properties of A 533, grade B, class 1 steel from HSST plate 02.

prior data). The good correlation between the two sets of tensile data indicates that conditions of irradiation were similar for both the 1-in.-thick[3] and 2-in.-thick fracture mechanics specimens.

Fracture toughness testing was performed with the techniques and specimens discussed in ref. 3. The requirements of the type of fracture toughness testing employed are unusual in that it is necessary to compare posttest data with specimen pretest dimensions to determine validity of the test data.

The postirradiation fracture toughness results are given in Table 3.3 and Figs. 3.2 and 3.3. For comparison, preirradiation data, as well as previously obtained[3] postirradiation data, are also illustrated in Figs. 3.2 and 3.3.

It is interesting to note that the higher exposure received by capsule 7 in comparison with capsule 8 (5.7 X 10^{19} versus 2.8 X 10^{19} neutrons/cm^2) did not influence the postirradiation fracture toughness of the material (specimen 18-6 versus 11-5, 18-5 versus 27-6, A1 versus A2). This tends to indicate that irradiation damage saturates at approximately 2 X 10^{19} neutrons/cm^2 when fracture toughness K_{Ic} is used as the criterion for evaluating the effect of high-energy neutron bombardment.

The ASTM recommended method[2] for establishing validity of fracture toughness (K_{Ic}) data obtained with

Table 3.2. Postirradiation tensile properties of A 533, grade B, class 1 steel from center section of HSST plate 02

Specimen	Test temperature (°F)	0.2%-Offset yield strength (psi)	Ultimate tensile strength (psi)	Elongation (%)	Reduction in area (%)
21Q4	Room	86,838	106,362	18.0	70.0
21Q5	Room	93,155	111,993	17.0	58.0
21Q3	+175	82,822	100,657	18.0	60.0
21Q6	+175	85,008	102,651	16.0	57.0
21Q1	+250	84,707	103,086	16.0	58.0
21Q7	+250	84,878	103,269	16.0	59.0
21Q8	+400	80,056	100,837	16.0	59.0
21Q2	+550	78,649	103,702	16.0	50.0

Table 3.3. Fracture toughness of irradiated 2-in.-thick compact tension specimens

Specimen	Temperature (°F)	Yield Strength (ksi)	a, Crack length (in.)	a/w, Ratio of crack length to specimen width	Plastic zone size (in.)		K_{Ic} or K_Q, Stress-intensity factor (ksi $\sqrt{\text{in.}}$)	Validity[a]	Capsule No.	Fluence (neutrons/cm^2)
					Test	Precracking				
ASTM A 533, grade B, class 1 steel from HSST plate 02										
										$\times 10^{19}$
11-6	Room	90.0	2.099	0.525	0.014	0.0036	47.7	1	7	5.3 5.7
18-6	150	85.5	2.092	0.523	0.040	0.0027	75.1	1	7	5.3 5.7
11-5	150	85.5	2.081	0.520	0.029	0.0026	63.5	1	8	2.3 2.8
18-5	170	83.9	2.087	0.522	0.055	0.0070	86.1	2	8	2.3 2.8
27-6	173	83.9	2.070	0.517	0.049	0.0034	80.9	2	7	5.3 5.7
A 533, grade B, class 1 steel weld										
A2	Room	110.0	2.057	0.514	0.011	0.0030	51.7	1	8	2.3 2.8
A1	148	100.0	2.040	0.510	0.043	0.0029	91.0	2	7	5.3 5.7
A 508, class 2, forging-grade steel										
C8	125	87.0	2.157	0.539	0.051	0.0039	85.7	2	8	2.3 2.8

[a] 1. Meets both criteria: a and B greater than 2.5 $(K_{Ic}/\sigma_{ys})^2$ and secant offset, where a is crack width and B is specimen thickness.
2. Fails a and B greater than 2.5 $(K_{Ic}/\sigma_{ys})^2$; meets secant offset criterion.

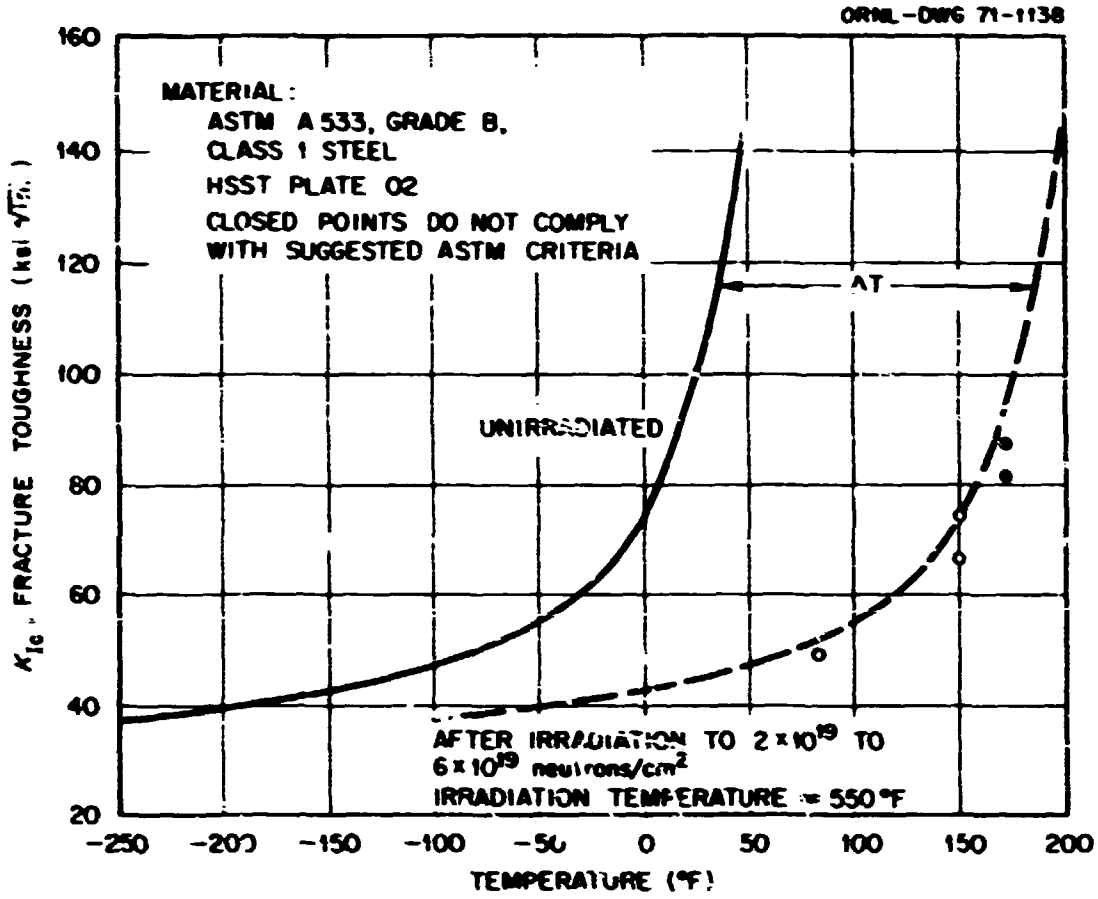

Fig. 3.2. Pre- and postirradiation temperature dependence of the fracture toughness K_{Ic} of A 533, grade B, class 1 steel from HSST plate 02.

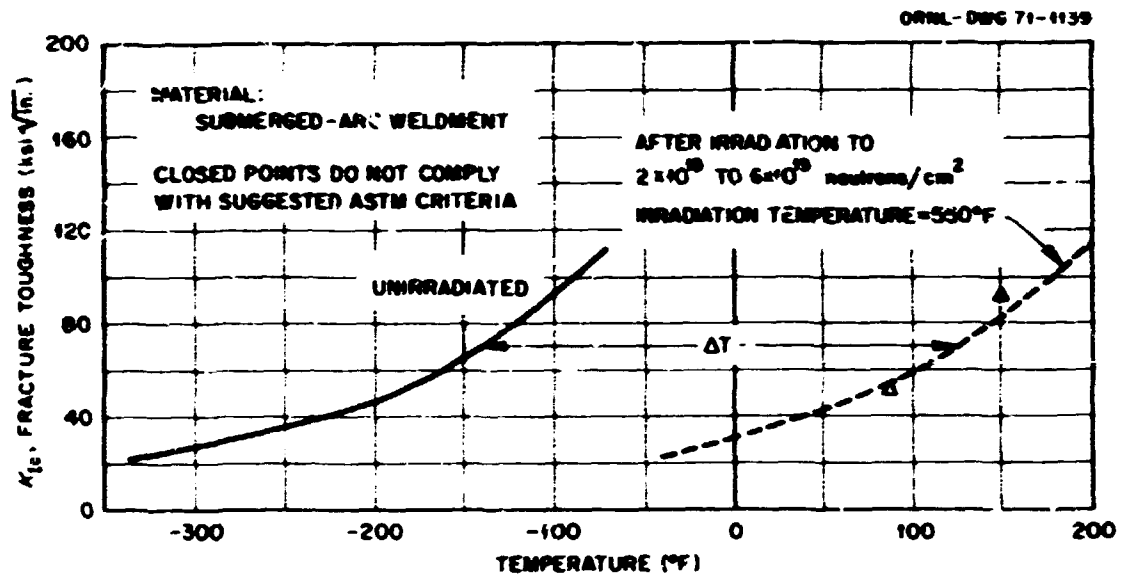

Fig. 3.3. Pre- and postirradiation temperature dependence of submerged-arc weldment in A 533, grade B, class 1 steel.

compact tension specimens is based on specimen thickness B and crack length a. ASTM recommends that both B and a be equal to or greater than $2.5\,(K_{Ic}/\sigma_{ys})^2$. As the test temperature is increased, the yield strength, σ_{ys}, of the material decreases; thus the specimen thickness B and the crack length a must be increased to meet the recommended validity criterion.

As shown in Fig. 3.2, fracture toughness data obtained for unirradiated A 533, grade B, class 1 steel specimens up to 12 in. in thickness indicated a sharp upswing in K_{Ic} values somewhere near the nil-ductility transition (NDT) temperature. Similar data were obtained for forging-grade material and weldments. There are no inherent reasons for these materials not to

Table 3.4. K_{Ic} Measuring capacity of compact tension specimens

Specimen thickness (in.)	Measurement capacity, K_{Ic}/σ_{ys} ($\sqrt{\text{in.}}$)	K_{Ic} (ksi $\sqrt{\text{in.}}$)				
		Measuring[a] capacity at 75°F	Measuring[a] capacity at 100°F	Measuring[a] capacity at 150°F	Measuring[a] capacity at 250°F	Measuring[a] capacity at 400°F
1	0.63	56.7	56.0	55.4	54.1	51.6
2	0.90	81.0	80.1	79.2	77.4	73.8
4	1.30	117.0	115.7	114.4	111.8	106.6
6	1.60	144.0	142.4	140.8	137.6	131.2

[a]Based on postirradiation (4×10^{19} neutrons/cm^2) yield strength.

exhibit the same behavior in the postirradiation condition. Data for A 533, grade B, class 1 steel suggest that the shift in fracture toughness of nuclear vessel-grade materials after high-energy neutron exposure is approximately the same as the 30 ft-lb fix Charpy transition temperature shift, ΔT. Therefore, the postirradiation fracture toughness could be projected if ΔT applied over the complete curve. The projected curves for A 533, grade B, class 1 steel and A 533, grade B, class 1 weldment material are also shown in Figs. 3.2 and 3.3, respectively. Based on the previously reported postirradiation (4×10^{19} neutrons/cm^2) yield strength[3] and the measuring capacity of the various specimens, the maximum K_{Ic} values that can be obtained with compact tension specimens are summarized in Table 3.4.

From Table 3.4 and Figs. 3.2 and 3.3, it could be predicted that valid K_{Ic} data would be obtained at +150°F and that invalid data would be obtained at +175°F. The test results (Table 3.3) verify these predictions. This is a good indication that the postirradiation fracture toughness exhibits an increase or a transition with temperature, as was the case with the preirradiated material. To exceed a K_{Ic} value of 100 ksi $\sqrt{\text{in.}}$ would require testing a 4-in.-thick compact tension specimen at 175 to 200°F.

A final report was prepared on this activity.[4]

4. T. R. Mager, *Post-Irradiation Testing of 2T Compact Tension Specimen*, Report WCAP-7561, Westinghouse Electric Corporation, August 1970.

Irradiation Effect on Fracture of Heavy-Section Pressure Vessel Steels

C. W. Hunter J. A. Williams
Hanford Engineering Development Laboratory

Specimen irradiation

Specimen irradiations were resumed in the M-3 hot-water loop of the ETR at the beginning of reactor cycle 108 after the completion of heater installation for water temperature control of the loop. The addition of loop heaters constituted a major loop modification to allow for the temperature control of the M-3 specimen assembly over the temperature range 125 to 600°F. The heater installation included the addition of heater loop piping and necessary valving for use with the M-3 piping system. Twenty heaters, each of 6-kW capacity, are mounted on the heater loop piping and are powered by a three-phase solid-state power supply. Power to the heaters is controlled in a proportional manner to avoid undue thermal shock to the heaters and to supply a reasonable response to changing reactor power.

Two specimen tubes of the M-3 irradiation capsule were modified for the irradiation of Charpy V-notch specimens. The capsule charged during cycle 108 contained twelve 1-in. compact tension specimens, 24 Charpy V-notch specimens, and 21 tensile specimens. Of the compact tension specimens, eight were WR orientation A 533, grade B, HSST plate 02, with goal exposures being 2×10^{19} and 8×10^{19} neutrons/cm^2 ($E > 1$ MeV) for two groups of four, respectively. The balance of four compact tension specimens are weld center material of A 533, grade B, class 1 submerged-arc weld metal with a goal exposure of 8×10^{19} neutrons/cm^2 ($E > 1$ MeV). The Charpy V-notch specimens include five WR and five RW specimens of A

533, grade B, class 1 steel, with a goal exposure of 2×10^{19} neutrons/cm^2 ($E > 1$ MeV), and seven WR and seven RW specimens, with a goal exposure of 8×10^{19} neutrons/cm^2 ($E > 1$ MeV). Nine A 533, grade B, class 1 steel transverse tensile specimens are to be irradiated to 2×10^{19} neutrons/cm^2 ($E > 1$ MeV) and eight to 8×10^{19} neutrons/cm^2. Four weld center tensile specimens were inserted for a goal fluence of 2×10^{19} neutrons/cm^2 ($E > 1$ MeV).

A dosimeter pin with monitor sets selected to provide the energy-dependent absolute integrated flux (10^{-10} to 18 MeV) at three axial positions in the M-3 capsule was included for irradiation during cycle 108. Previously flux determinations were made with iron and Al–0.1% Co wire dosimeters and a calculated spectrum. Determination of the actual spectrum will provide a basis for assessing the degree of confidence to be placed on previous flux determinations or the necessary correction factors.

Irradiation of 4-in.-thick specimens

Thicker irradiated specimens are necessary to obtain higher valid K_{Ic} values. Based upon the irradiated yield strength and the fracture toughness behavior of 1-in.-thick specimens, a 4-in.-thick compact tension specimen would yield a K_{Ic} of 110 ksi $\sqrt{\text{in.}}$ at approximately 200°F. The intended large-specimen irradiation facility was a capsule containing four 4-in.-thick compact tension specimens in the ATR north reflector. The anticipated values of gamma heating and neutron flux previously reported[5] were based on low-power measurements in the ATR and measurements in the ATRC.[6,7] To verify or refine these values, experiments were run in the ATR north reflector during cycles 1 and 2. These gamma heating values obtained were comparable to the previously reported values, but the fluxes were only 10% of those anticipated. Subsequent additional flux measurements with spectral compensation during cycle 3 revealed a higher flux of 4.5×10^{11} neutrons/cm^2·sec ($E > 1$ MeV); however, this flux is still only 23% of the value anticipated. Based on neutron flux attenuation and reactor operating efficiency, an unacceptably long irradiation period of seven years would be required to achieve a fluence of 5×10^{19} neutrons/cm^2.

A high ratio of fast flux to gamma heating is required to produce meaningful irradiation of a thick specimen in a reasonable time. High gamma heating results in too large temperature gradients in the specimen, and low flux, of course, leads to long reactor tenure. For both the ETR and ATR reflector positions the values of gamma heating and flux that would exist through a 4-in.-thick specimen are plotted in Fig. 3.4. The markers on each line indicate the front and back faces of the 4-in. specimen, with the higher values of heating and flux being nearest the core. The general relation of heating and flux is quite evident, and probably these values for any water-cooled test reactor would fall on nearly the same line. The arrows on the lines in Fig. 3.4 indicate the values of heating and flux that may be obtained by moving the 4-in. specimen in the reflector.

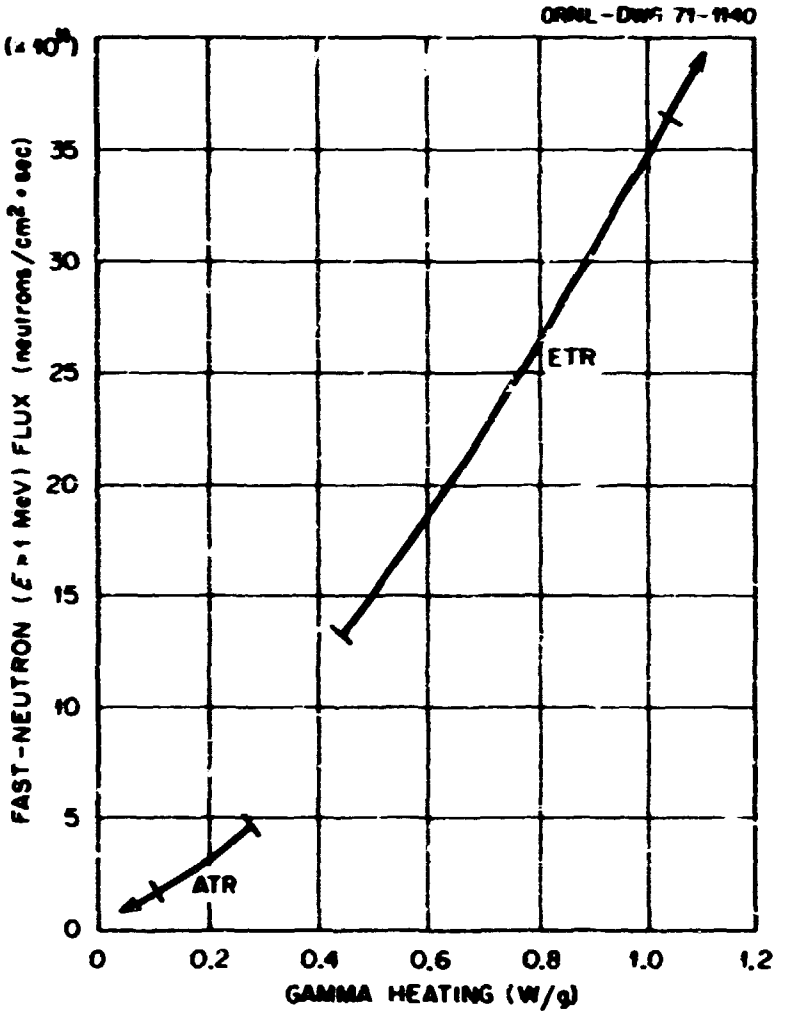

Fig. 3.4. Fast-neutron flux and gamma heating in ATR and ETR reflectors considered for the irradiation of 4-in.-thick compact tension fracture mechanics specimens. The marks on each curve correspond to the condition on the specimen face at the crack line.

---

5. C. W. Hunter and J. A. Williams, "Irradiation Effect on Fracture of Heavy-Section Pressure Vessel Steels," pp. 102–121, *Heavy-Section Steel Technology Program Seminar. Progr. Rept. Feb. 28, 1970*, USAEC Report ORNL-4590, Oak Ridge National Laboratory.

6. F. L. McMillan, *Pricing Schedules for TRA Test Reactors*, USAEC Report IN-1213, Idaho Nuclear Corporation, July 1968.

7. N. C. Kaufman and J. L. Durney, *Reactor Physics Results from Low Power Measurements in the ATR*, USAEC Report IN-1260, Idaho Nuclear Corporation, February 1969.

In the ETR, the vessel wall prevents movement of the specimen away from the core, while in the ATR the reflector construction precludes movement of the specimen closer to the core. Thus the ATR is too "cool" for a high-fluence irradiation, the ETR is too "hot," and a more favorable heating and flux range is not covered by either. Therefore the following three alternative methods of irradiating a 4-in. specimen are being considered:

1. Achieve a uniform crack-tip temperature in a high gamma-heating position, such as the ETR reflector, by controlling the heat flow in the specimen with appropriately located insulating patches.

2. Produce a higher ratio of flux to heating in the ETR reflector with shielding materials that preferentially reduce gamma heat generation.

3. Use a reactor with more favorable gamma heating and flux ranges.

Capsules considered for large-specimen irradiation until recently were of the type in which specimens are completely encapsulated and the temperature of the specimen is controlled by varying the conductivity of a fixed gas gap by varying the composition of the helium-argon mixture in the gap. In such a capsule the heat flow is out the two large parallel surfaces of the specimen, and since the crack line (region of interest in a fracture initiation test) is perpendicular to these surfaces and intersects their centers, the largest temperature gradient in the specimen exists along the crack line. Instead, by insulating only a small area at the ends of the crack line, heat flow parallel along the crack line would be greatly reduced, and thus the temperature gradient along the crack line would be reduced. In a fracture initiation test the material outside the plastic zone along the crack tip would be strained only elastically, and since irradiation temperature does not affect the elastic properties, the proper irradiation temperature is essential only within the plastic zone. In the ETR reflector a 4-in.-thick compact tension specimen with insulated areas of 16 $in.^2$ centered on the ends of the crack line would have a maximum temperature differential of about 25°F in the plastic zone from the face of the specimen nearest the reactor core to two-thirds through the thickness of the specimen. During the irradiation, the back one-third of the specimen would receive less than 25% of the neutron exposure and would be maintained at a cooler temperature than the front two-thirds of the specimen. As described previously, the specimen would be rotated halfway through the irradiation period to achieve a symmetrical exposure through the specimen thickness. Two specimens could be irradiated simultaneously in one reflector of the ETR to a fluence of 5×10^{19} neutrons/cm^2 in less than one year. The principal disadvantage to such an irradiation experiment is that the periphery of the specimen would have been irradiated at a cooler temperature and therefore would be of questionable value as a source of irradiated material for machining smaller specimens. This insulation concept is of course applicable to irradiation in any other reactor, but it is of decreased significance at lower gamma heating and flux values and longer irradiation times.

It is possible to preferentially decrease gamma heating with respect to flux with suitable shielding and adsorber materials. Heating results from specimen adsorption of gamma rays generated outside the specimen and from gamma rays generated by capture of low-energy neutrons in the specimen. This latter source is probably the dominant one and may be greatly reduced by lithium, which captures low-energy neutrons without generating gamma rays. Also the externally generated gamma rays may be reduced, without appreciably disturbing the fast-neutron flux, by a heavy-metal shield, such as lead or tungsten. The potential of such shielding is being evaluated with 31-group neutron diffusion calculations to determine the spatial and spectral distributions of neutrons and gamma rays in the ETR, and the influences caused by lithium, lead, and tungsten shielding. If such shielding is effective and practical, it will enable the meaningful irradiation of thick specimens afforded by no other means.

The heating and flux relations indicated in Fig. 3.4 for the ATR and ETR reactors are quite similar to those in all water-cooled reactor reflector positions, and thus it is not reasonable to expect that a very favorable ratio of flux to gamma heating will exist in another reactor. Nevertheless, the flux and gamma heating conditions in several other reactor reflector positions are being determined or evaluated. The reactors being considered are the BAWTR, ORR, and GETR. Hopefully the information obtained will reveal reactor positions that will fill the gap in flux and heating values between the ETR and ATR and the reactor that has the most favorable ratio of flux to gamma heating.

Base material studies of ASTM A 533, grade B, class 1 steel

Irradiated 1-in.-thick compact tension specimens from 12-in. ASTM A 533, grade B, class 1 HSST plate 02 were tested at temperatures as high as 175°F and as low as −125°F. The specimens were of RW orientation and had been irradiated to approximately 2×10^{19}

neutrons/cm² ($E > 1$ MeV) at 540°F. The results of irradiated fracture toughness studies completed to date are given in Table 3.5. The fracture toughness for irradiated A 533, grade B, class 1 steel, as shown in Fig. 3.5, exhibits considerable sensitivity to irradiation embrittlement. In terms of arbitrary toughness levels of 40 and 60 ksi the shifts in the transition temperatures are at approximately 240 and 210°F, respectively. The start of transitional behavior is indicated only through the use of invalid fracture toughness, K_Q, data. The unirradiated K_Q data shown closely represent the fracture behavior of A 533, grade B, class 1 steel when compared with the data of Shabbits, Pryle, and Wessel[8] for the same material, and it is surmised that the irradiated K_Q values represent, at least, a temperature

8. W. O. Shabbits, W. H. Pryle, and E. T. Wessel, *Heavy Section Steel Technology Program Technical Report No. 6, Heavy Section Fracture Toughness Properties of A533 Grade B, Class 1, Steel Plate and Submerged Arc Weldment*, Report WCAP-7414, Westinghouse Electric Corporation, December 1969.

Table 3.5. Fracture toughness of irradiated ASTM A 533, grade B, class 1 steel from RW orientation of HSST plate 02

Specimen	Test temperature (°F)	a, Crack length (in.)	Yield strength (psi)	Fast-neutron ($E > 1$ MeV) fluence (neutrons/cm²)	K_Q (ksi $\sqrt{\text{in.}}$)	$2.5(K_Q/\sigma_{ys})^2$	K_{Ic} (ksi $\sqrt{\text{in.}}$)
			$\times 10^3$	$\times 10^{19}$			
02GA10	−120	1.026	115	1.85	27.6	0.145	27.6
02GA24	−100	1.119	107	2.26	40.5	0.358	40.5
02GA23	−25	1.063	101	2.10	32.8	0.264	32.8
02GA22	26	0.971	97	1.82	41.8	0.458	41.8
02GA1	85	0.973	94	1.85	43.1	0.525	43.1
02GA4	120	0.924	92	1.83	47.0	0.654	47.0
02GA9	125	0.994	92	1.7	82.3	1.98	
02GA3	145	0.991	91	1.85	69.7	1.47	
02GA2	175	1.014	89	1.92	79.6	2.0	

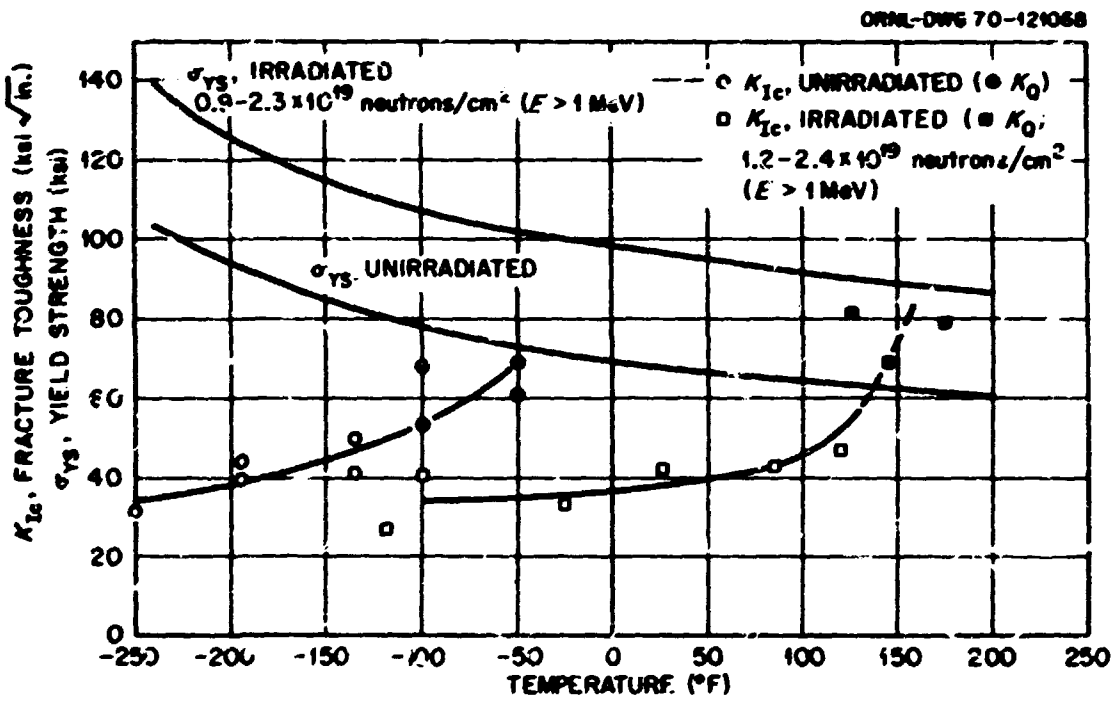

Fig. 3.5. Fracture toughness and yield strength of irradiated and unirradiated A 533, grade B, class 1 steel as a function of temperature. The properties are for the RW orientation of HSST plate 02.

range in which an increase in toughness would actually be observed. Eventual verification of transitional behavior will depend on the results of valid fracture toughness measurement.

An analysis incorporating the combined effects of irradiation, stress, and temperature on a simple structure of A 533, grade B, class 1 steel is shown in Fig. 3.6 for a plate 6 in. thick with a crack depth a and unit plane strain length.[9] The critical flaw depth under conditions of yield loading was calculated from fracture toughness data. Temperatures above which significant flaw sizes can be tolerated may readily be seen in Fig. 3.6. The temperature shift in this type of analysis is of significance because the effect of irradiation on both the yield strength and decrease in the fracture toughness are accounted for.

The fracture appearances of irradiated A 533, grade B, class 1 steel specimens over the temperature range investigated are shown in relation to the fracture toughness curve in Fig. 3.7. An increasingly tougher appearance is evident with increasing test temperature. The most pronounced increase in shear lips and fracture toughness is observed between 145 and 175°F.

Tensile specimens and compact tension specimens irradiated to 8×10^{19} neutrons/cm^2 ($E > 1$ MeV) are

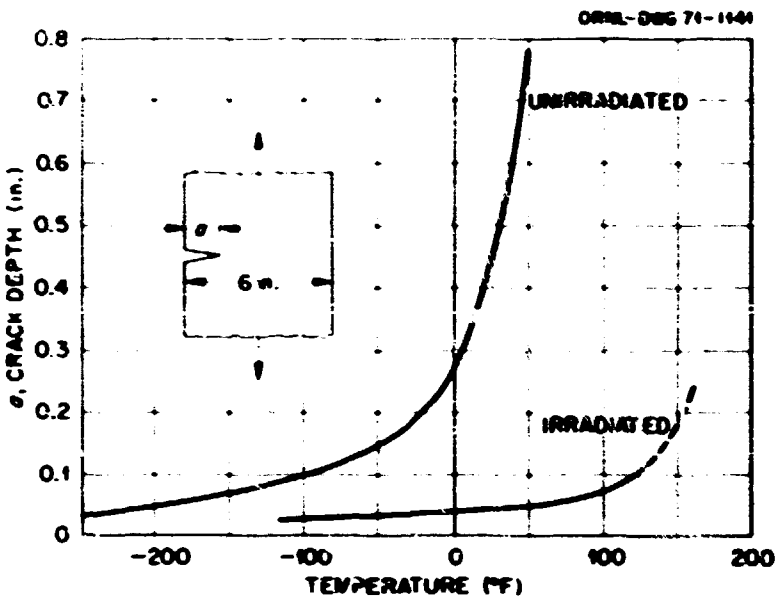

Fig. 3.6. Critical flaw size as a function of temperature in a simple structure of irradiated and unirradiated A 533, grade B, class 1 steel. The indicated shift is of significance because the effects of irradiation on both the yield strength and the fracture toughness were considered in the analysis.

9. P. C. Paris and G. C. Sih, "Stress Analysis of Cracks," *ASTM STP 381 – Fracture Toughness Testing and Its Applications*, p. 44, American Society for Testing and Materials, 1964.

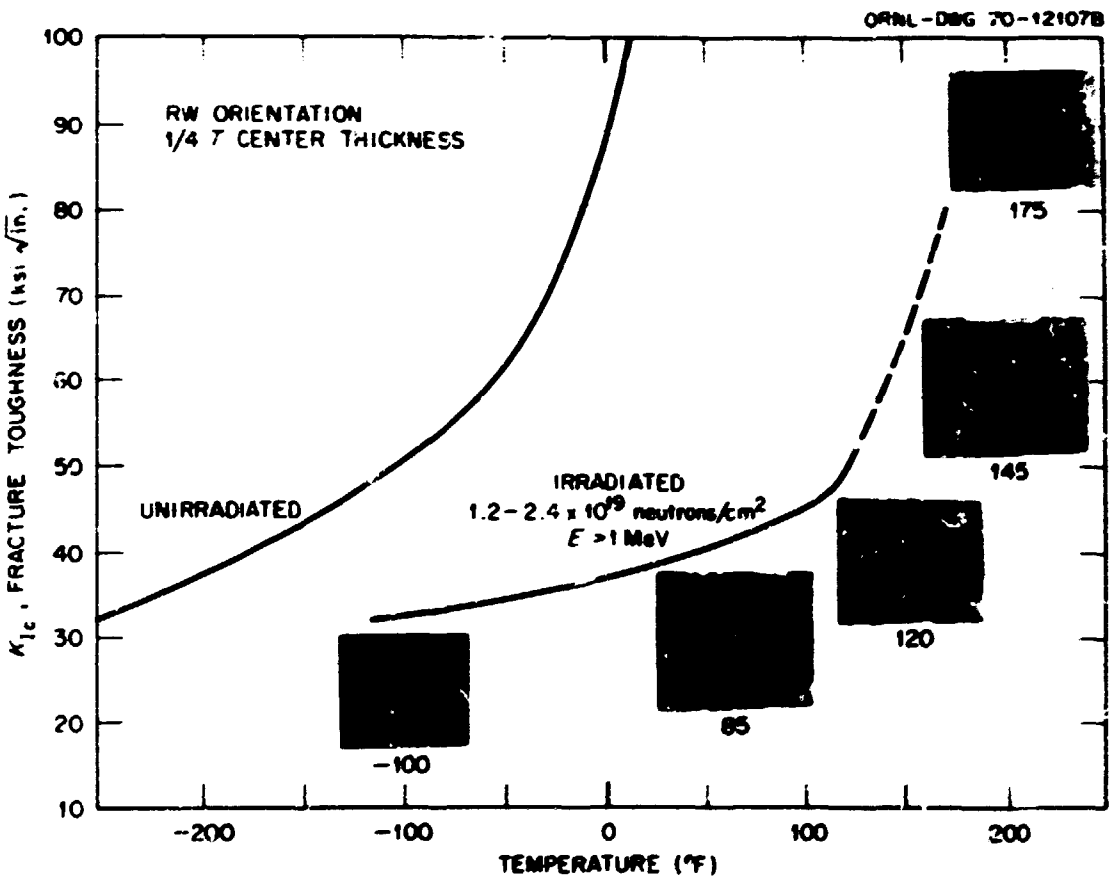

Fig. 3.7. Fracture surfaces from 1-in.-thick specimens of irradiated ASTM A 533, grade B, class 1, pressure vessel steel related to toughness characteristics.

currently in various stages of testing and preparation for testing. Tensile specimens will be tested between −100 and 500°F prior to testing of the fracture toughness specimens.

Fatigue-crack preparation in compact tension specimens

In linear elastic fracture toughness determinations, the critical stress intensity, K_{Ic}, is that for fracture initiation from a sharp fatigue crack. Hence the preparation of a fatigue crack in the fracture specimens is necessary preliminary to actual toughness determinations. Consideration of the loading conditions during such fatigue-crack preparation provides an opportunity to obtain information on fatigue-crack behavior. However, these loading conditions were not intended to provide pure propagation data, such as the relationship of crack growth rate per cycle, da/dn, to cyclic stress intensity, ΔK, developed by Paris.[10] Nevertheless, this information does offer some insight into the practical situation of crack initiation, stalling, and reinitiation (incubation), as well as propagation.

The details of the fatigue cracking were previously described.[5] The effective crack growth for initiation and propagation in the base material and weldment approached pure crack propagation rates, with a distinct propensity for hindrance. Fatigue-crack propagation in irradiated base material specimens has provided an opportunity for a cursory assessment of the irradiation effect on fatigue. The comparisons in Table 3.6 suggest doubling of the effective propagation rate by irradiation. However, this observation must presently be considered as preliminary, because a different crack-monitoring system was used in the hot cell on the irradiated specimens than on the unirradiated ones.

Table 3.6. Irradiation influence on effective fatigue-crack propagation in 1-in.-thick compact tension specimens of ASTM A 533, grade B, class 1 steel from HSST plate 02

Fatigue step	Unirradiated specimens		Irradiated specimens[a]	
	ΔK (ksi $\sqrt{\text{in.}}$)	Crack rate (in./cycle)	ΔK (ksi $\sqrt{\text{in.}}$)	Crack rate (in./cycle)
		$\times 10^{-6}$		$\times 10^{-6}$
1[b]	26.1	1.22	26.1	2.44
2	22.2	1.73	21.7	2.71
3	18.0	1.97	17.2	1.06
4	13.3	0.31	12.7	0.62

[a]Dose: 1.5×10^{19} to 2.5×10^{19} neutrons/cm^2.
[b]From machined notch.

Fractographic evaluation of irradiation embrittlement in pressure vessel steels

Pressure vessel steels normally exhibit a rapid increase in impact energy over a narrow temperature range. This transition in toughness is associated with a fracture mechanism transition from cleavage to plastic dimpling (shear or glide-plane decohesion). Typically, irradiation embrittlement (1) causes an increase in the temperature at which the impact energy begins to rise, (2) often causes the energy to increase more slowly with temperature, and (3) often causes the upper shelf energy level (high-temperature fracture energy) to be reduced. In addition, there is a marked variability in the character and extent of the neutron embrittlement response among pressure vessel steels, as has been demonstrated by Steele and Hawthorne at NRL.[11,12]

The relations between fracture mechanism and irradiation embrittlement for several materials were previously reported.[13,14] This study showed that for unirradiated ASTM A 302, grade B, 6-in. reference plate the percentage of plastic dimpling correlated well with the increased impact energy in a Charpy V-notch specimen and that 100% plastic dimpling fracture was essential to the full development of upper shelf energy absorption. The fracture surface examination of two irradiated A 543 materials from NRL demonstrated essentially the same fracture mechanism versus impact

10. H. H. Johnson and P. C. Paris, "Subcritical Flaw Growth," *Engineering Fracture Mechanics*, 1(1): 3–45 (1968).
11. L. E. Steele, *The Influence of Composition on the Fracture Toughness of Commercial Nuclear Vessel Welds*, NRL Report 7095, Naval Research Laboratory, June 23, 1970.
12. U. Potapovs and J. R. Hawthorne, "The Effect of Residual Elements on the Response of Selected Pressure Vessel Steels and Weldments to Irradiation at 550°F," *Nucl. Appl.*, 6(1): 27–46 (January 1969).
13. C. L. Hellerich and C. W. Hunter, *Fractography of Irradiated and Unirradiated Pressure Vessel Steel Impact Specimens*, USAEC Report BNWL-S-2298, Pacific Northwest Laboratory, Feb. 1, 1969.
14. C. W. Hunter, J. A. Williams, and C. L. Hellerich, "Irradiation Effect on the Fracture of Heavy-Section Pressure Vessel Steels," pp. 77–90, *Heavy-Section Steel Technology Program Semiann. Progr. Rept. Aug. 31, 1969*, USAEC Report ORNL-4512, Oak Ridge National Laboratory.

energy behavior.[15,16] The striking difference in energy behavior for the two irradiated A 543 materials was that the base plate exhibited a normal transition to a reasonably high upper shelf energy level while the weld metal exhibited a very slow energy increase with temperature and an apparent upper shelf energy absorption of only 41 ft-lb above 400°F.[15] The fracture surface of the weld metal indicated that a large amount of cleavage fracture was still occurring at the apparent upper shelf; this observation is consistent with the dependence of transition and upper shelf energy behavior on the development of plastic dimpling fracture. These observations supported the conclusion that irradiation embrittlement resulted primarily from a loss of the metallurgical ability of the material to undergo the cleavage-to-plastic dimpling transition, rather than the occurrence of low-energy ductile fracture.[14]

The recent examination of fracture surfaces of A 533, grade B, class 2 Charpy V-notch impact specimens from NRL[17] provided an example of the extent to which irradiation may reduce the energy absorption ability of plastic dimpling fracture. The irradiation effect on the impact energy behavior is shown in Fig. 3.8. Irradiation

15. L. E. Steele, J. R. Hawthorne, C. Z. Serpan, Jr., and R. A. Gray, Jr., *Irradiation Effects on Reactor Structural Materials, QPR August 1–October 31, 1966*, NRL Memorandum Report 1731, Naval Research Laboratory, Nov. 15, 1966.

16. L. E. Steele, J. R. Hawthorne, C. Z. Serpan, Jr., and Uldis Potapovs, *Irradiation Effects on Reactor Structural Materials, QPR February 1–April 30, 1968*, NRL Memorandum Report 1872, Naval Research Laboratory, May 15, 1968.

17. L. E. Steele, Naval Research Laboratory, letter communication, Feb. 2, 1970.

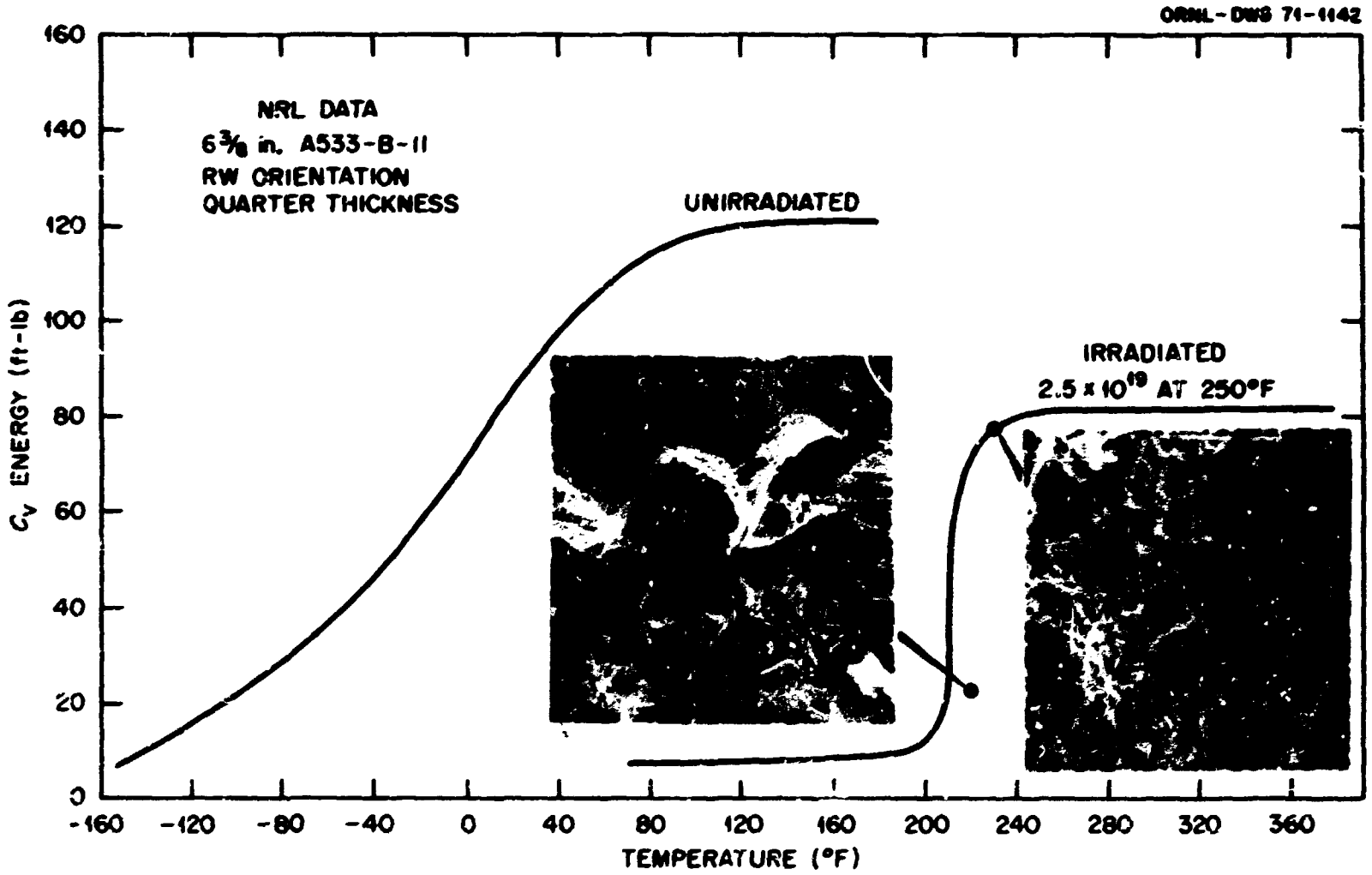

Fig. 3.8. Irradiation effect on the Charpy V-notch impact energy and relation to fracture mechanism of A 533, grade B, class 2 steel. The fracture data are from NRL (ref. 17). The irradiated fracture at 220°F and 22 ft-lb contained a total of 30% plastic dimpling fracture with the dimpling predominantly at the edges of the specimen and cleavage primarily in the center, as shown. The fracture at 230°F and 77 ft-lb was 100% plastic dimpling. The sharp transition from cleavage to dimpling indicates the control that fracture mechanism has over the impact energy and that cleavage fracture is the principal mechanism of irradiation embrittlement. The reduction in upper shelf energy from 120 to 80 ft-lb reveals the significance of irradiation reduced from plastic fracture resistance.

produced a large shift in the transition temperatures, but nevertheless the material still exhibited an abrupt energy transition behavior and attained a reasonably high upper shelf energy level of 80 ft-lb. The two fracture surfaces shown in Fig. 3.8 again demonstrate the correlation of cleavage fracture with low energy levels and plastic dimpling with the upper shelf. However, the facts that 100% plastic dimpling fracture and a genuine upper shelf energy behavior are attained in the irradiated condition and that the irradiated upper shelf is reduced to 80 ft-lb, whereas the unirradiated upper shelf is 120 ft-lb, proves the existence of reduced plastic fracture energy due to irradiation. The decreased plastic fracture energy probably results from decreased strain hardening.

With respect to practical application to vessel fracture resistance, it must be noted that the irradiation-reduced plastic fracture shelf of 80 ft-lb does not comprise a particularly serious threat and that cleavage fracture (rather than reduced plastic fracture energy) was the mechanism through which irradiation produced the sizable shift in transition temperature. For impact tests, fracture mechanics tests and structures, factors that promote cleavage fracture to higher temperatures must receive the most serious attention.

Radiation Hardening and Embrittlement in ASTM A 533, Grade B, Class 1 Steel

R. G. Berggren W. J. Stelzman T. N. Jones

Impact and tensile data were obtained with irradiated samples of weld metal from a submerged-arc weldment made in HSST plate 01 (subplate 51B) and an electroslag weldment (HSST plate 53) made in ASME SA 302, grade B (Code Case 1339), steel plate identified as PVRC 315 (General Electric). The weldment and specimens were described previously, and tensile and Charpy V-notch properties of the unirradiated specimens were presented.[18,19]

Application of the specimen orientation scheme in the weldment presented a problem, since the weld orientation would not be easily apparent. Therefore the three principal directions were modified for the weld only and designated *L*, the direction of the weld center line; *W*, the width direction perpendicular to the weld center line and parallel to the weld surface; and *T*, the thickness direction perpendicular to the surface of the weld. Application of these symbols to specimen orientation remained unchanged. The first symbol indicates the normal to the fracture plane and the second symbol, the direction of fracture propagation. The symbol for the normal to the fracture plane is sufficient to define the specimen orientation in uniaxial tensile tests. The base plate orientation symbol for the heat-affected zone was retained, since the original rolling direction of the base plate may still be an influential factor in data comparison.

Data from irradiated and unirradiated miniature (0.178-in. gage diameter and 1.250-in. gage length) tensile specimens of submerged-arc and electroslag weld metal are presented in Table 3.7. The tensile data from the quarter thickness level of base plate (plate 01K, R orientation) were obtained previously. A comparison of tensile data for unirradiated specimens indicates that the yield stress is 9% lower and the elongations are 12% higher for the submerged-arc weld metal than for the base plate, the tensile properties of the submerged-arc weldment are not significantly different from those of the electroslag weldment, and the electroslag weld metal exhibits 9% lower yield stress and 10% higher elongations than the base plate at equivalent plate depths. After irradiation at 150°F to similar fluences, the submerged-arc weld metal showed a 6% larger increase in yield stress and a 26% larger decrease in elongation than the base plate. The electroslag-weld metal showed a 5% larger increase in yield stress and a 17% smaller decrease in elongation than the submerged-arc weld metal but showed an equal increase in yield stress and a 9% larger decrease in elongation than the base plate or the submerged-arc weldment, respectively. In both weldments, the work hardening portion of the load-elongation curve was absent, as indicated by either a constant load after yielding, followed by a drop in load, or a continuous drop in load after yielding. Irradiation at 450°F to similar fluences indicated that the increase in yield stress was 26% greater and the decrease in elongation was 4 to 10% greater for the submerged-arc weld metal than for the base plate. After a 550°F irradiation to similar fluences, the increase in yield stress was the same for the electroslag weld metal and base plate but 20% greater for the submerged-arc weld metal. The decrease in elongation was the same for both welds but 5% smaller for the base plate. Therefore,

---

18. D. A. Canonico, "Characterization of Heavy-Section Steel Weldments," pp. 29–35, *Heavy-Section Steel Technology Program Semiann. Progr. Rept. Feb. 28, 1969*, USAEC Report ORNL-4463, Oak Ridge National Laboratory.

19. D. A. Canonico, "Characterization of Heavy Section Steel Weldments," pp. 10–13, *Heavy-Section Steel Technology Program Semiann. Progr. Rept. Aug. 31, 1969*, USAEC Report ORNL-4512, Oak Ridge National Laboratory.

Table 3.7. Tensile properties of heavy-section steel weldments at room temperature

Fluence, $E > 1$ MeV (neutrons/cm^2)	Irradiation temperature (°F)	Strength properties (ksi)			Elongation (%)		A_{LY}, radiation sensitivity[c]
		Upper yield	Lower yield	Ultimate tensile[a]	Uniform	Total[b]	
$\times 10^{18}$							
		Base plate from HSST plate 01K, ¼ *T*, *R* orientation					
0		69.5	68.3	89.8	9.8	19.5	
7.5	158	105.5	101.8	102.9	4.7	13.3	12.2
8.8	450	95.5	93.8	108.3	8.9	15.9	8.3
11.8	550	90.2	87.6	106.5	9.5	16.8	5.6
		Submerged-arc weldment from HSST plate 51, ⅜ and ⅝ *T*, W orientation					
0		64.2	62.4	79.7	11.4	21.9	
5.8	150	97.9	93.1	93.1		11.2	12.8
7.1	150	101.0	96.6	96.6		9.2	12.8
7.1	458	101.5	99.9	108.7	8.9	17.6	14.1
8.5	458	103.3	101.7	110.5	9.2	17.1	13.5
12.3	560	89.9	88.7	102.0	11.5	18.7	7.5
12.5	548	93.8	92.5	105.7	10.5	17.7	8.5
		Electroslag weldment from HSST plate 53, ¼ and ¾ *T*, W orientation					
0		63.5	61.9	80.8	11.0	21.4	
8.4	140	95.4	92.6	92.6		12.6	10.6
10.3	140	98.0	95.4	95.4		10.8	10.4
10.4	140	100.6	96.9	96.9		11.8	10.9
10.0	547		77.7	95.4	10.5	18.2	5.0
12.5	547	80.2	79.4	95.6	9.6	17.3	4.9
12.5	546	81.4	80.6	96.8	10.7	17.9	5.3
12.3	543	79.6	78.6	94.8	10.7	18.6	4.8

[a]Ultimate tensile strength is here defined as the maximum load *after* the yield point divided by the original cross-sectional area.

[b]Length to diameter ratio: 7.

[c]From equation $\Delta\sigma_{LY} = A_{LY}(\phi/10^{18})^{1/2}$, where ϕ is the fluence in neutrons/cm^2 ($E > 1$ MeV), $\Delta\sigma_{LY}$ is the change in lower yield strength.

the tensile properties of the submerged-arc weldment show greater sensitivity to radiation damage than those of either the base plate during comparable 150, 450, and 550°F irradiations or the electroslag weldment during comparable 150 and 550°F irradiations.

Irradiated Charpy V-notch data from transverse (WL) specimens of submerged-arc weld metal taken from the $^1/_{12}$ *T* level and electroslag weld metal taken from the ¼ and ¾ *T* levels are presented in Table 3.8. The impact properties are essentially uniform throughout the depth of both weldments;[18,19] therefore comparison of weld impact properties will be made independently of weld depth references. The submerged-arc weldment and base-plate impact properties after 130 and 450°F irradiations were compared above.

Irradiation of submerged-arc weld-metal and base-plate specimens at 565°F to similar fluences resulted in a 24 ft-lb lower shelf energy, a 15°F higher transition temperature, and a 70°F greater transition temperature shift for the weld metal than for the base plate. Therefore, the submerged-arc weldment impact properties show greater sensitivity to radiation damage than those of the base plate during comparable 130, 450, and 550°F irradiations.

Table 3.8. Charpy V-notch properties of irradiated heavy-section steel weldments

Fluence, $E > 1$ MeV (neutrons/cm^2)	Irradiation temperature (°F)	*DBTT*[a] (°F)	Change in *DBTT* (°F)	Shelf energy (ft-lb)	A_{cv}, radiation sensitivity index[b]
x 10^{18}					
Base plate from HSST plate 01K, ¼ *T*, RW orientation					
0		0		120	
6.2	155	180	180	100	72
7.1	450	175	175	100	66
9.4	560	105	105	100	34
Submerged-arc weldment from HSST plate 5i, ¼ *T*, WL orientation					
0		–65		115	
6.5	130	130	195	109	7[illegible]
7.9	455	290	265	75	95
11.5	565	120	185	76	54
Electroslag weldment from HSST plate 53, ¼ and ¾ *T*, WL orientation					
0		–25		85	
9.5	130	135	160	66	52
11.2	555	50	75	85	22

[a]Ductile-to-brittle transition temperature at 30 ft-lb energy.

[b]From equation $\Delta DBTT = A_{cv} (\phi/10^{18})^{1/2}$, where ϕ is the fluence in neutrons/cm^2 ($E > 1$ MeV) and $\Delta DBTT$ is the change in transition temperature in °F.

Comparison of the electroslag and submerged-arc weldment impact data indicates that the unirradiated electroslag weld metal has a higher transition temperature and a lower shelf energy than the unirradiated submerged-arc weld metal. Irradiation of the weldments at 130°F results in a higher transition temperature, lower increase in transition temperature, and a greater drop in shelf energy for the electroslag weld metal than for the submerged-arc weld metal. After a 560°F irradiation, a lower transition temperature, a lower increase in transition temperature, and a higher shelf energy are indicated for the electroslag weld metal.

A comparison of the impact data for the electroslag weldment and the base plate indicates that the unirradiated electroslag weld metal exhibits a lower transition temperature and lower shelf energy than the unirradiated base plate. Irradiation data at 130°F indicate a lower transition temperature, smaller increase in transition temperature, and a lower shelf energy for the electroslag weld metal. After a 560°F irradiation, a lower transition temperature, a smaller shift in transition temperature, and a smaller drop in shelf energy were indicated for the electroslag weld.

Therefore the impact data for the electroslag and submerged-arc weldments and the base plate indicate that the submerged-arc weld metal is superior in toughness in the unirradiated condition but is more sensitive to irradiation damage than the electroslag weld metal during comparable 130 and 560°F irradiations. The electroslag weld metal has a better transition temperature but a poorer shelf energy than the base plate in the unirradiated condition but is less sensitive to radiation damage after comparable 130 and 560°F irradiations.

4. Pressure Vessel Investigations

Emphasis during this reporting period has been placed upon the simulated service tests activity, although effort was continued under the complex stress state studies and the specific safety research studies. Activities reported include the development of a fatiguing procedure for flaw sharpening of the simulated service test specimens, evaluation of the acoustic emission data obtained during the testing of the second large tensile specimen at approximately 210°F at Southwest Research Institute, testing of the third large tensile specimen and a one-sixth-scale model at 50°F at Southwest Research Institute, completion of a parametric study for investigating geometry effects of the SwRI large tensile specimen, and continued expediting of procurement of six intermediate test vessels from Taylor Forge Company.

Development of Hydraulic Fatiguing Procedure for Flaw Sharpening of Specimens

R. W. Derby A. A. Abbatiello
K. K. Klindt

High priority has been given to developing a method of growing a fatigue crack in a notch without resorting to cyclic loading of a complete structure. The advantages in time, money, and control of having such a method are obvious when the problems involved in cyclic loading a pressure vessel with a 6-in. wall and an inside diameter of only 27 in. are contemplated.

The basic procedure used was somewhat similar to one used by Westinghouse.[1] A mathematical analysis validated the feasibility of the procedure and provided useful guidance in the design and operation of the device.

The idea is simple: a notch is filled with hydraulic oil, sealed off with an O-ring, and subjected to cyclic loading at high pressure. In effect, the hydraulic oil acts like a wedge that is continually pushed into the notch and then removed. Although simple in concept the procedure presented certain problems. First, it was necessary to seal the notch, but sealing was complicated because of the high pressure involved and the awkward seal area. It was found that an elastomer O-ring approximately 13 in. in circumference in an oblong continuous groove with minor and major extremity dimensions of ½ and 6½ in., respectively, and backed by a slotted plate was quite effective. The initial preload on the seal was effected by the six high-strength steel studs shown in Fig. 4.1. An SwRI tensile specimen is shown in the sealing assembly in Fig. 4.1. It is currently planned to use the device to sharpen the cracks in the fifth and sixth 6-in.-thick specimens.

The second problem was the design of the cyclic pressurizing equipment. To achieve the high pressures required a pump with a small stroke or displacement must be used. The small-displacement stroke imposes a virtually gas-free requirement on the system to insure that the pumping strokes will be effective. This requirement was met by first evacuating the system, then disconnecting the vacuum pump, and finally releasing oil into the system.

A third problem was the necessity for matching the volume of oil in the system with the displacement of the pump and the compressibility of the hydraulic fluid to insure that the pressure rise per stroke was acceptable. Solution of this problem was complicated because the expansion of the tubes, valves, and specimen due to pressure loading also had to be considered. An adjustable-volume loop, shown in Fig. 4.2, was devised to

1. W. J. Clark, Jr., and L. J. Ceschini, "Fatigue Precracking of Spinburst Toughness Specimens," *Exp. Mech.*, 9(3): 123–128 (March 1967).

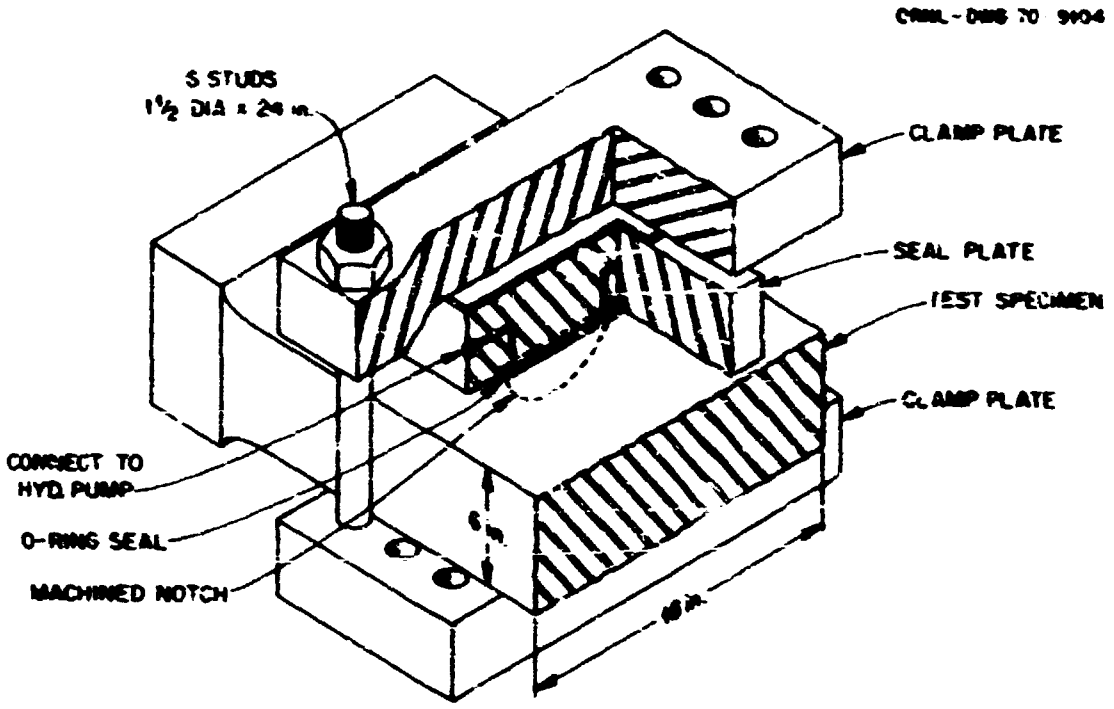

Fig. 4.1. Sealing and clamping arrangement for local fatigue device.

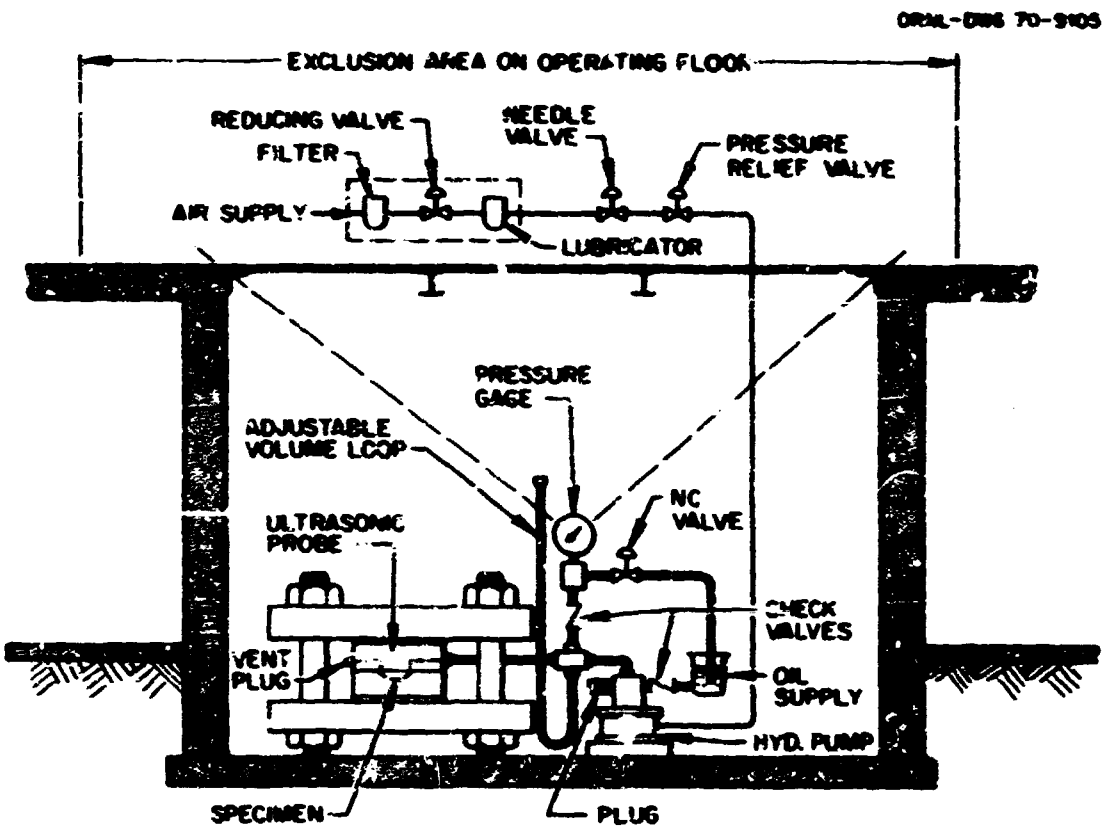

Fig. 4.2. Apparatus for crack starting by using variable volume for pressure control.

solve this problem. The correct balance was expedited by careful calculation of the system volume and by a careful determination of the fluid compressibility. A mixture of three parts motor oil with one part kerosene, which provided good lubricity and yet prevented a very high increase in viscosity at high pressures, was used for the pressurizing fluid.

An interesting detail shown in Fig. 4.2 is the check valve located just below the pressure gage. The purpose of this valve was to keep the pressure gage from experiencing large pressure changes and shock with each piston stroke. However, the check valve allowed the reading of maximum pressures only and obscured observation of the continuous pressure state of the

system. On some runs it was observed after several hours of running that the system failed to bring the fluid up to pressure on each cycle. Hence the check valve was replaced with a needle valve, which was closed after the system was found to function normally. The closing of this valve removed fluid from the system; consequently, an additional loop whose volume was the same as that of the gage was added to the system. As finally designed the system had the capability of a pressure stroke from 0 to 17,000 psi and a rate of 40 strokes per minute.

After designing and developing the hydraulic system the next problem was detection of growth of the fatigue crack. An ultrasonic detection system was devised for this purpose. A special support device for an ultrasonic transducer, which allows both angular and rectilinear motion and permits the positioning of the transducer in a precise and reproducible location, was designed. The rectilinear motion of the support is controlled by a small screw that has features similar to those of a micrometer (see Fig. 4.3).

In a validation run of the equipment, after approximately 13,000 cycles, the reflectoscope began to indicate possible advancement of the crack. By 20,000 cycles the fatigue crack appeared to be close to 0.10 in. deep, and at 26,000 cycles, about 0.19 to 0.27 in. deep. The test piece was removed and dissected, and a photomicrograph (Fig. 4.4) was made of the deepest point in the crack. Figure 4.4 shows that the crack was very close to 0.20 in. deep.

At this time there appears to be no barrier to successful application of the procedure to both the 6-in.-thick tensile test specimens and the 6-in.-thick intermediate test vessels.

ORNL DWG 70-10987

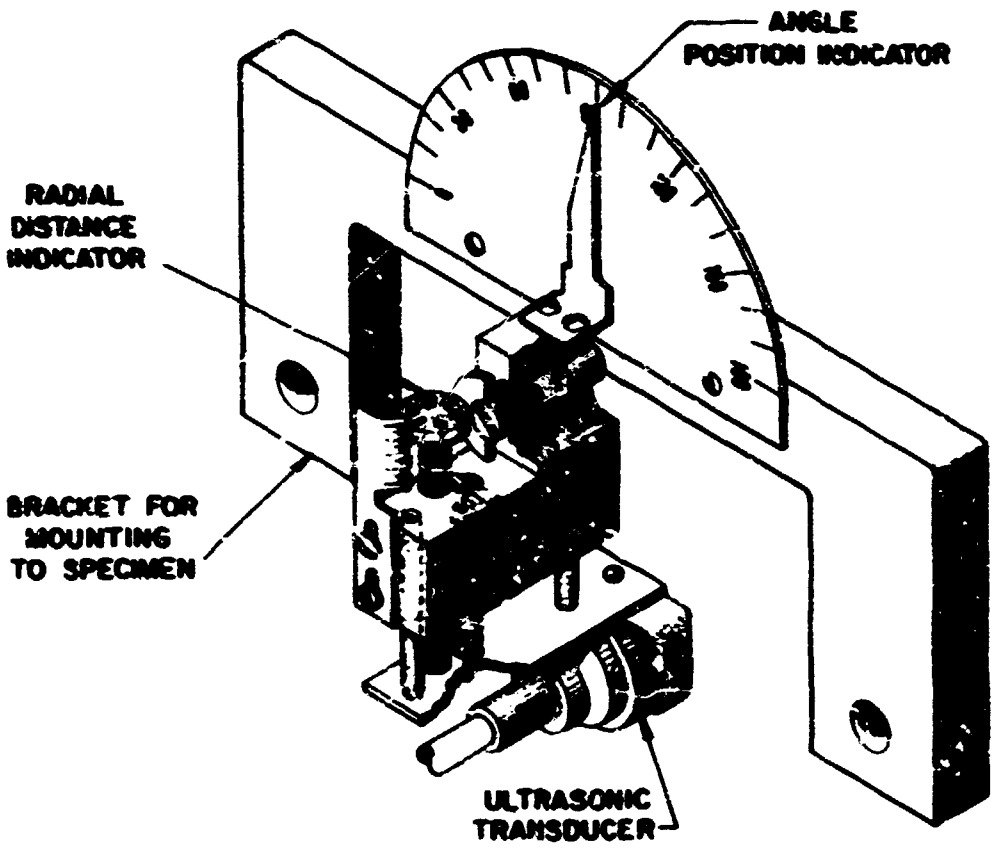

Fig. 4.3. Ultrasonic probe mount.

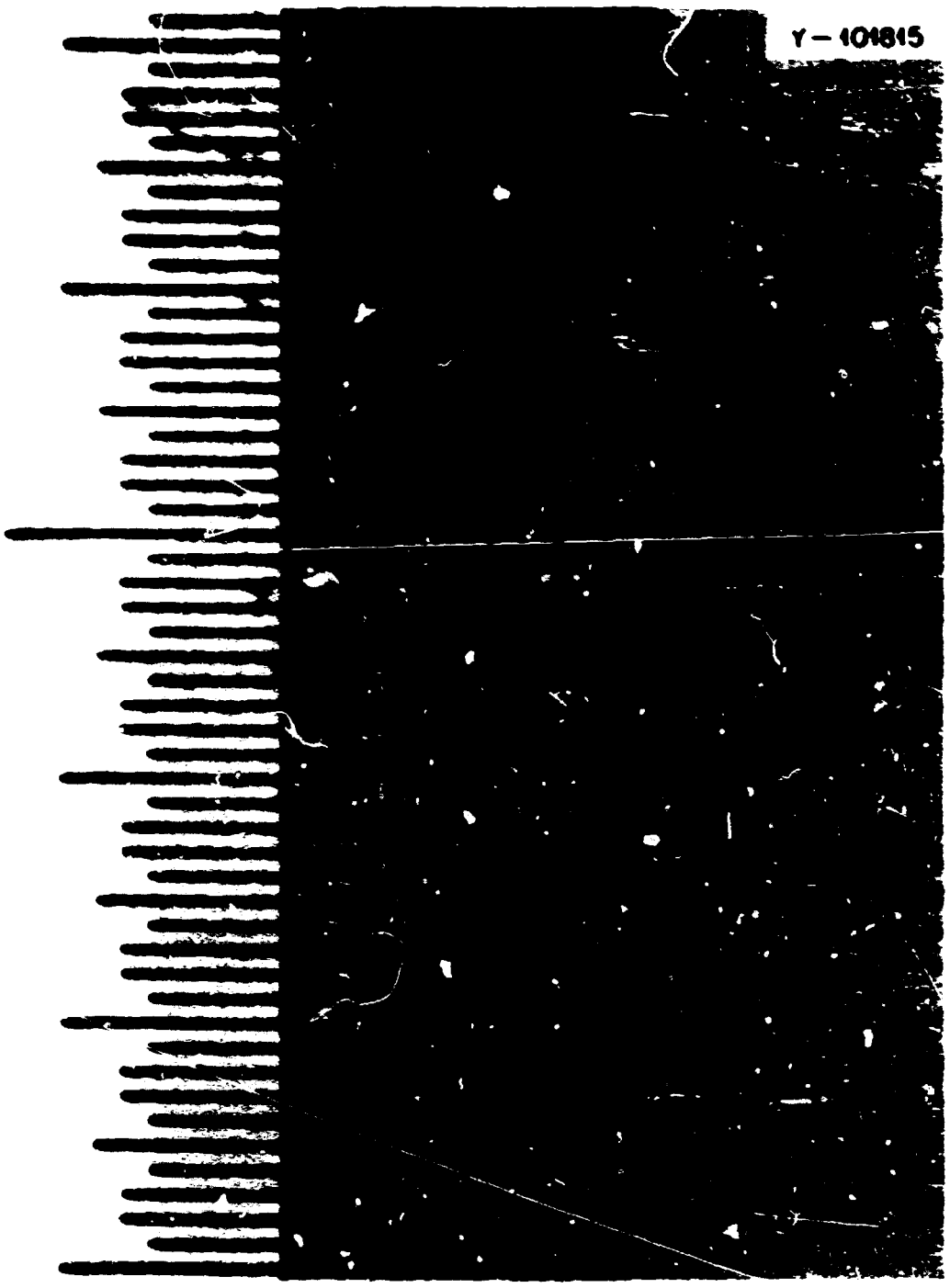

Fig. 4.4. Photomicrograph of fatigue crack in test piece. Scale is graduated in units of 0.01 in.

Acoustic Emission Analysis of the Second Large Tensile Specimen at Southwest Research Institute[2]

W. D. Jolly
Pacific Northwest Laboratory

The Pacific Northwest Laboratory (PNL) participated in the second heavy-section steel tensile test on March 13, 1970, at Southwest Research Institute in support of the Edison Electric Institute's (EEI) acoustic emission system evaluation project. The purpose of PNL participation was to obtain additional acoustic emission data from crack initiation and propagation in heavy-section pressure vessel steel. This opportunity was also used to field test acoustic emission processing electronics of the same design as used in the EEI acoustic emission system.

The second heavy-section steel tensile test at SwRI was performed on specimen 03G2000 at 205 to 215°F. The test section of the specimen, shown in Fig. 4.5, was 24 in. long, 18 in. wide, and 6 in. thick. The specimen was loaded in tension parallel to the 24-in. dimension. A semielliptical slot with a 0.015-in. root radius was

2. This work was sponsored by the Edison Electric Institute under Project AP-73 with Southwest Research Institute in cooperation with the HSST Program.

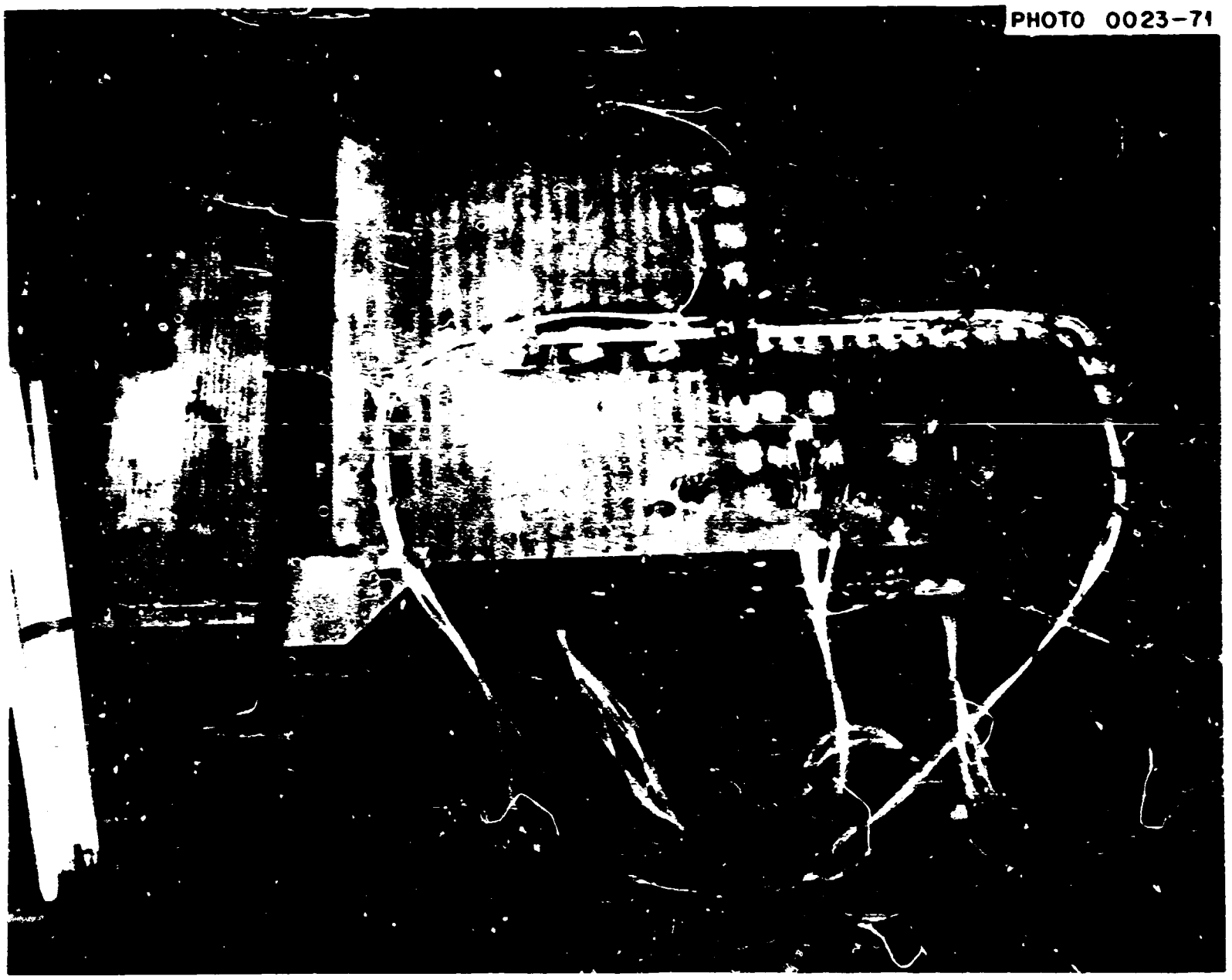

Fig. 4.5. Second large tensile test specimen of 6 × 18-in. cross section. The center slot is semicircular (3-in. radius) with a 0.015-in. root radius.

machined perpendicular to the direction of tension. The specimen was fully instrumented with strain gages and preheated before installation in the tensile facility. It was gripped by the stepped section at either end, as shown in Fig. 4.6, which is a side view of the specimen installed and ready for loading: After initial cycling in 1 × 10^6-lb increments up to 3 × 10^6 lb to balance the stress across the specimen, the loading schedule was, in millions of pounds, 3, 4, 4.4, 5, 5.5, 6, 6.5, 6.6, 6.7, 6.8, 6.9, 7.0, 7.1, 7.2, 7.3, 7.4, etc.

Acoustic emission data were recorded from two experimental doughnut-type sensors mounted approximately in a plane with the semielliptical slot on the 6-in. thickness of the specimen, and the signals were processed by both the counting technique and the amplitude integration technique. Both rate and total were recorded from each type of signal processing, and an extended-range total emission output was also recorded from the amplitude integration system to accommodate anticipated high-level acoustic emission during crack extension.

Analysis of the acoustic emission data, recorded as the load was increased incrementally from 3 × 10^6 to 7.4 × 10^6 lb, indicated that initial yield at the root of the semielliptical slot began at approximately 4.2 × 10^6 lb total load and continued to about 4.8 × 10^6 lb. The first major crack extension began at about 5.7 × 10^6 lb and the second at about 7.1 × 10^6 lb.

This interpretation of the acoustic emission data from the second test is necessarily subject to correction, since

Fig. 4.6. Second large tensile test specimen installed in Southwest Research Institute's 15 × 10^5-lb tensile machine.

it is based on the limited data from the first test and past experience with similar materials. Data from several tests of the same type are needed to refine the placement of events, such as initial yield and crack extension.

Acoustic emission instrumentation

Acoustic emissions were detected by two sensors, one on each side of the test specimen, approximately in a plane with the semielliptical slot, as illustrated in Fig. 4.7. The sensors were attached to the specimen with a flexible strain-gage epoxy to prevent unbalancing when the specimen began to stretch. The sensors were of an experimental Lockheed type having a low output impedance and high sensitivity to shear and surface wave components of acoustic emission. Narrow bandwidth preamplifiers were coupled to the sensors as shown in Fig. 4.7. The preamplifier passband was 530 to 830 kHz, with a voltage gain of 300 in that passband. The preamplifiers were the same type as those supplied with the EEI prototype acoustic emission system but were adjusted for a lower passband.

The amplified acoustic emission signals were connected to the signal conditioner and signal processing unit by 40-ft coaxial cables. Additional gain and filtering were provided by the signal conditioner.

Two different techniques for acoustic emission signal processing were used: ring count and count rate, in which the output is a digital recorder is proportional to the product of emission pulse height and repetition

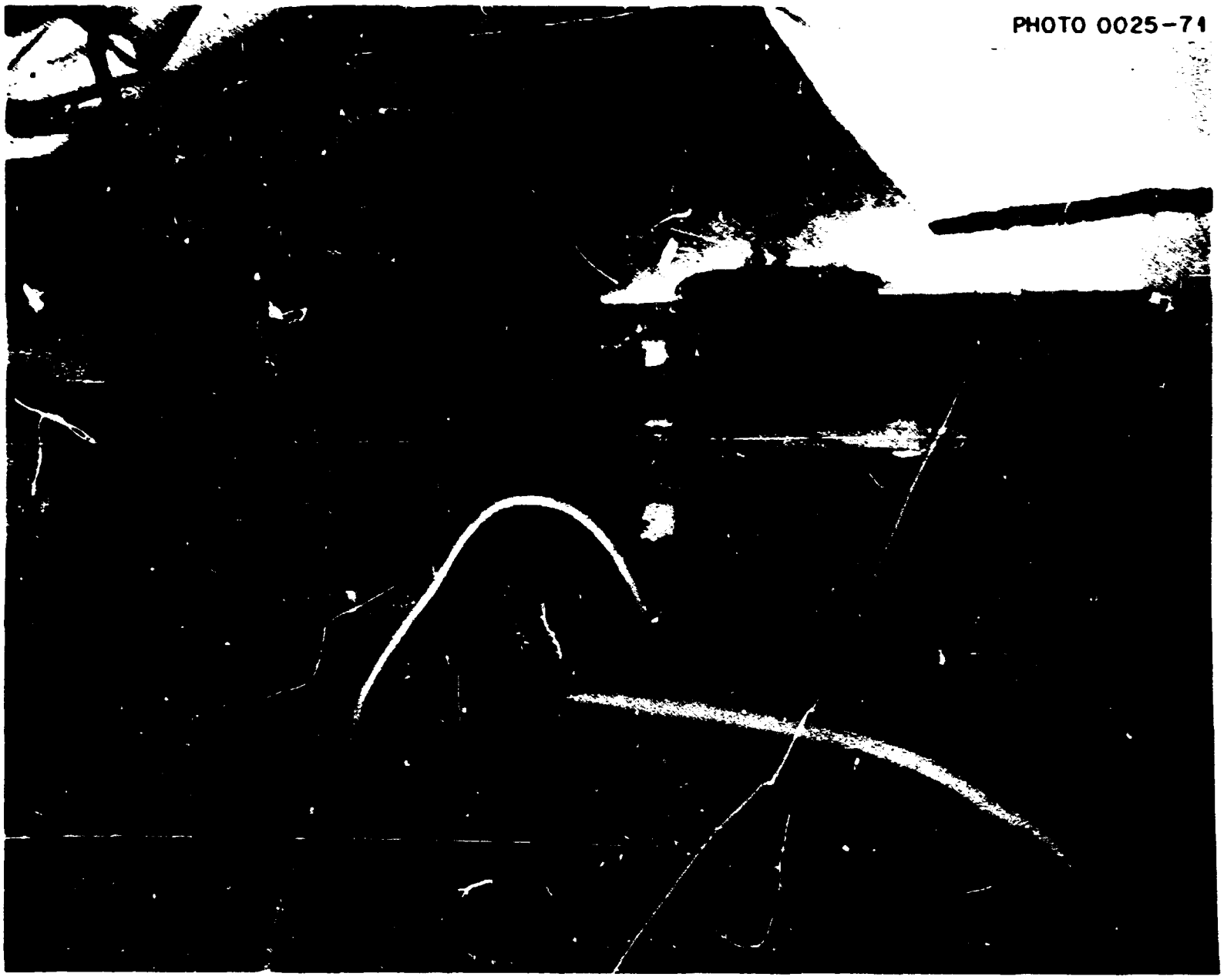

Fig. 4.7. Acoustic emission sensor attached to the edge of the second large tensile test specimen near the center.

rate, and (2) total emission and emission rate, in which the output to a chart recorder is proportional to the product of emission pulse amplitude, pulse length, and repetition rate. The latter technique is used for signal processing in the EEI prototype acoustic emission system. This type of signal processing is accomplished by integrating the amplitude of all signals that exceed a preset noise level. The unit of total emission is the volt-second. To put this unit in perspective, an individual acoustic emission may contribute from 5×10^{-5} to 1×10^{-2} V-sec to the total emission. The emission rate is obtained in the signal processor by differentiating the total emission with respect to time. The time interval may be chosen to provide the desired amount of smoothing on the emission rate output. In addition, the total emission may be manually differentiated with respect to a test variable, such as load or strain.

The significant difference between the count technique and the integrated amplitude technique is the inclusion of acoustic emission amplitude as a variable in the integrated amplitude method. The total count output is proportional to the total time the emission signals exceed a preset level. By using a count-reset time of 10^{-4} sec, an individual emission pulse may contribute from 1 to 40 counts to the total count.

The acoustic emission instrumentation, shown in Fig. 4.8, was installed for the second test. Four chart recorders were used to record gross section strain, total

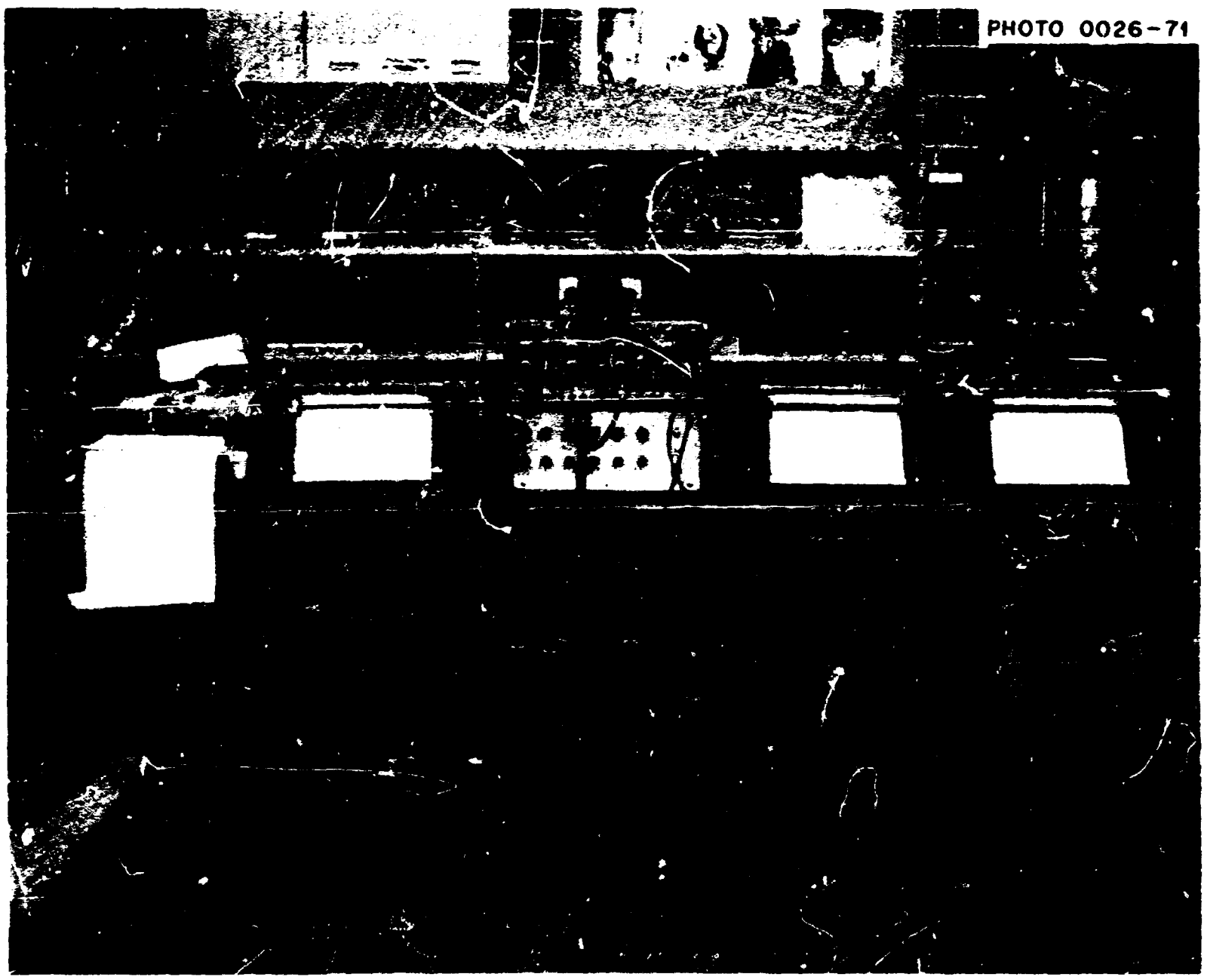

Fig. 4.8. Pacific Northwest Laboratory acoustic emission monitoring instrumentation for the second large tensile test.

count, count rate, total emission, emission rate, extended-range total emission, and extended-range emission rate. Three of the chart recorders were dual channel. The signal conditioner and signal processor unit, located between the chart recorders, were developed by PNL for general acoustic emission monitoring in the field.

Analysis of acoustic emissions

Acoustic emission data recorded during the incremental loading of the specimens by the count and integrated amplitude techniques followed essentially the same patterns of variation with increasing load. The graphs presented in Fig. 4.9 were compiled from the total emission output by using the integrated amplitude method. In the lower graph, the acoustic emission rate in V-sec/10^6 lb is plotted against total load from 3×10^6 to 7.4×10^6 lb. This chart represents acoustic emissions recorded only during loading increments and excludes emissions that occurred under constant load or load reduction. Each data point represents the increase in total emission during a load increment of 0.2×10^6 lb. The first significant event indicated on this graph is initial yield, at about 4.3×10^6 lb. Past experience has shown that initial yield is indicated by a reduction of emission rate during load increase. The emission rate increases more rapidly during the period of plastic deformation following initial yield. The formation of microcracks in the root of the semielliptical slot may also contribute to emission rate in the load range from

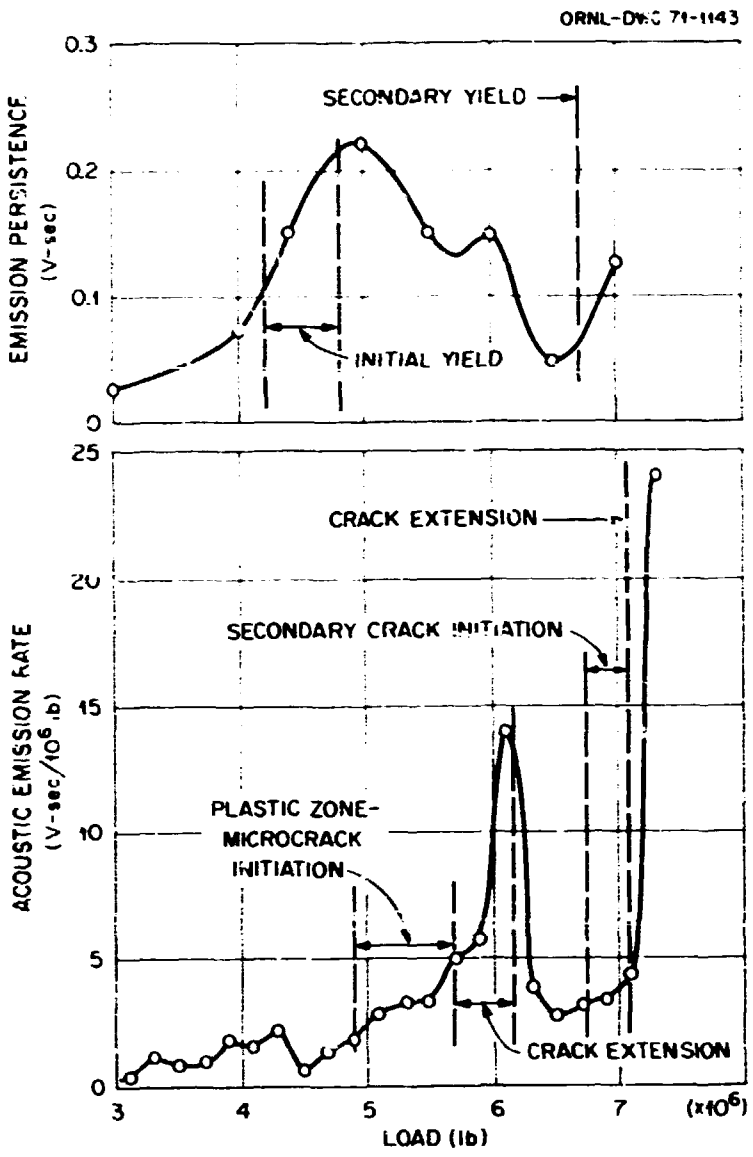

Fig. 4.9. Interpretation of acoustic emission data from the second large tensile test.

4.8 X 10^6 to 5.7 X 10^6 lb. The first major crack extension occurred between 5.7 X 10^6 and 6.1 X 10^6 lb, as indicated by the sharp increase in emission rate. The low emission rate between 6.3 X 10^6 and 6.7 X 10^6 lb may indicate blunting of the crack tip. A second major crack extension is indicated by the sharp increase of emission rate above 7.1 X 10^6 lb.

An additional parameter was considered in the interpretation of the emission rate data. The upper graph of Fig. 4.9 represents emission persistence versus load. Persistence is believed to represent the dissipation of potential energy around the semielliptical slot due to localized yield following a load increment. This graph indicates that initial yielding may have begun at about 4.2 X 10^6 lb and continued to about 4.8 X 10^6 lb. The decrease in persistence above 5 X 10^6 lb is consistent with the plastic deformation zone, since residual stress at the end of a load increment should be negligible in the plastic zone. The increase in persistence above 6.5 X 10^6 lb is interpreted as yielding preceding the second major crack extension.

Emission persistence can best be understood by reference to Fig. 4.10, which presents a typical emission rate recording in the load region of initial yield. Persistence is defined as the total emission in volt-seconds during the first minute of constant load following a load increase. This quantity may be obtained either by integrating the emission rate as shown in Fig. 4.10 or, more directly, by reading the increase in total emission during the first minute

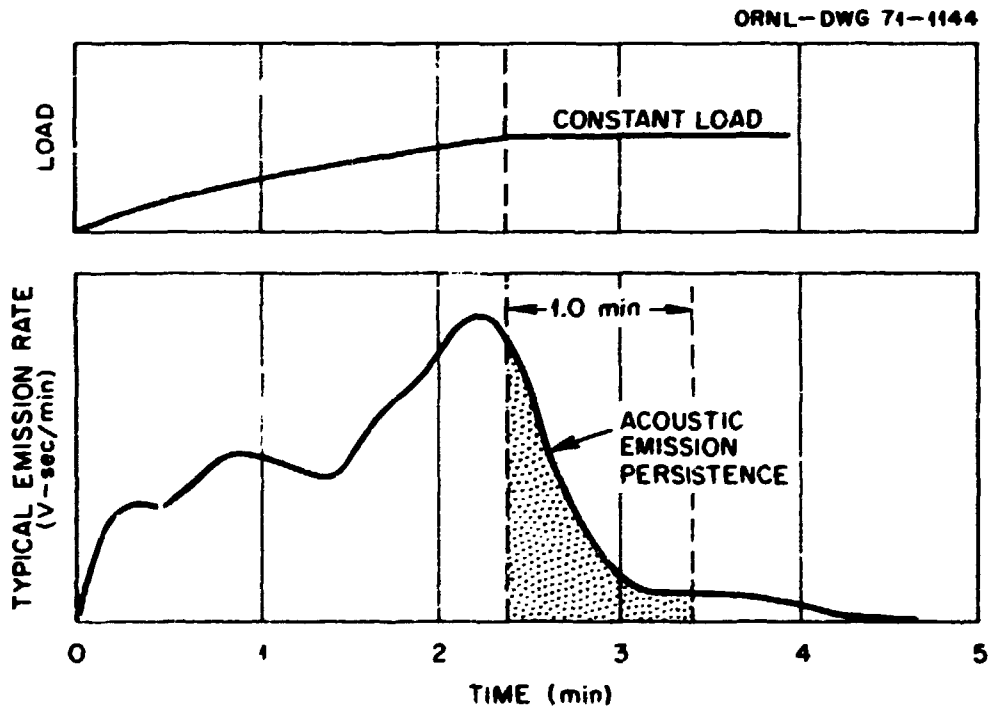

Fig. 4.10. Acoustic emission persistence – The integral of emission rate for the first minute following a load increment.

following a load increment. The interval of 1 min is arbitrary, but in most cases the emission rate decays to a small value in less than 1 min.

Conclusions

The interpretation of acoustic emission data from the second test is based on the limited data obtained on the first test and past experience with similar materials under different conditions. Data from several tests of the same type correlated with detailed stress-strain history and posttest analysis are needed to refine the placement of significant events, such as initial yield or plastic zone. The data presented do, however, present a reasonably complete history of major events during the second test.

Signal detection, conditioning, and processing instrumentation of the same design as used in the EEI acoustic emission system proved satisfactory for acoustic emission monitoring on heavy-section steel at 205 to 215°F. The data obtained from this test are valuable additions to the background information necessary for the evaluation of the EEI system.

Testing of the Third 6-in.-Thick Flawed Tensile Specimen, A One-Sixth-Scale Model, and Parametric Study Specimens[3]

S. C. Grigory G. W. Deel
Southwest Research Institute

Third large tensile specimen and one-sixth-scale model

Summary of test results. Two tensile specimens tested at 220°F were reported on extensively in the last progress report.[4] The third test was conducted at 50°F with only minor changes in preparations for the test and in specimen geometry.

The first two specimens contained semielliptical unsharpened notches and were obtained from HSST plate 03. The third specimen contained a semicircular notch sharpened by a fatigue crack and was obtained from HSST plate 01. The change from a semielliptical to a semicircular notch was made for economic reasons.

The specimens tested at 220°F required a maximum load of about 7.5×10^6 lb to fail and were necked at the net section. The third specimen failed at a load slightly over 5.3×10^6 lb after yielding slightly in the gross section. As may be seen in Fig. 4.11, considerable shear occurred on the fracture face of the specimen tested at 220°F, but the specimen tested at 50°F showed only a slight amount of shear on the top, or notched, surface.

A detailed presentation of data from this and subsequent tests will be made in a summary report at the end of this series of six tests.

A one-sixth-scale model containing a semicircular notch sharpened with a fatigue crack was tested at 50°F to model the test of specimen 01M6602. This model required a maximum load of 223 kips to fail and otherwise behaved much like the models tested at 220°F. Some crack growth was observed before the ultimate load was reached. The fracture surface of the model specimen is shown in Fig. 4.12. As may be seen, the fatigue crack did not propagate uniformly around the notch tip as desired. This is believed to have been the result of misalignment of the fatigue machine that occurred some time during the lengthy test.

All one-sixth-scale model specimens were machined from the center 8 in. of HSST plate 03. Hardness tests on the ends of the specimen varied from R_B 87 to 91 on each specimen.

Future tests. Three additional tests of 6-in.-thick tensile specimens are scheduled prior to November 1, 1970. The next test will be conducted at 100°F, and the other two test temperatures are yet to be determined.

Notch sharpening. A fatigue crack was generated at the root of the semicircular notch of specimen 01M6602 by subjecting it to a three-point bending load, as shown in Fig. 4.13. The specimen is supported on two pins with a center-to-center span of 42 in. A load of 187,000 lb was applied repeatedly at the midplane of the specimen on the unnotched side, and a pin was used to transmit the load from the jack to the specimen.

A total of 35,000 cycles was applied to the specimen to produce the fatigue crack shown in Fig. 4.14. Fatigue cracks were noted in the root of the notch at about one-third its depth at about 15,000 cycles. The cracks joined in the base of the notch after about 20,000 cycles but did not propagate to the surface until 35,000 cycles had been applied.

In order to test the notch-sharpening procedure, a one-sixth-scale model specimen was notched, and the notch was sharpened by exactly the same loading mode

---

3. This work is being carried out under UCCND Subcontract 3202 between Union Carbide Corporation and Southwest Research Institute.

4. S. C. Grigory, G. W. Deel, and R. Sherman, "Tests of Large Tensile Specimens," pp. 138–143, *Heavy-Section Steel Technology Program Semiann. Progr. Rept. Feb. 28, 1970*, USAEC Report ORNL-4590, Oak Ridge National Laboratory.

Fig. 4.11. Six-inch-thick tensile specimens 03G2000 (220°F) and 01M6602 after test.

Fig. 4.12. Fracture face of one-sixth-scale model of the third large tensile specimen. Test temperature was 50°F.

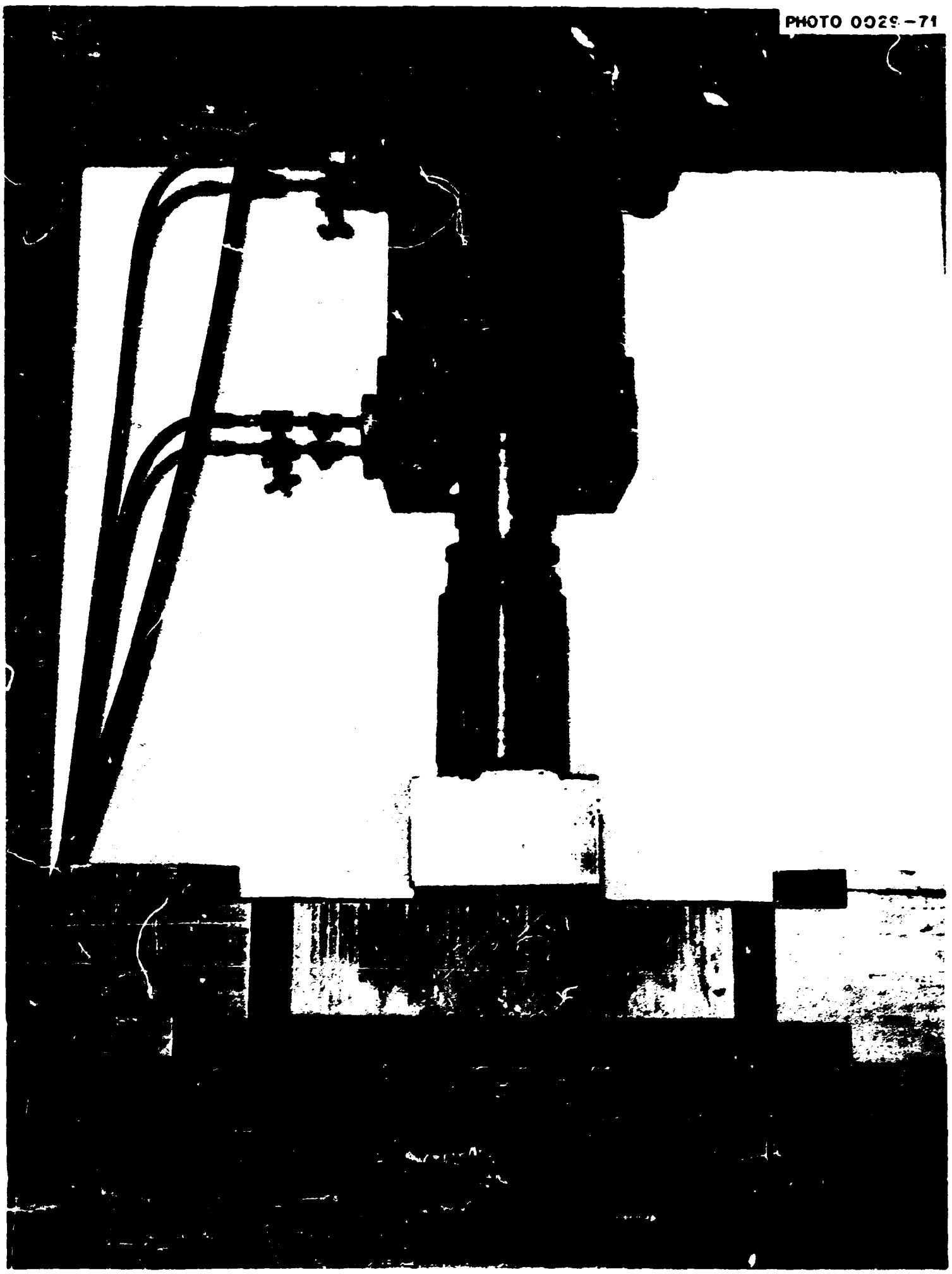

Fig. 4.13. Six-inch flawed tensile specimen 01M6602 during notch sharpening by fatigue.

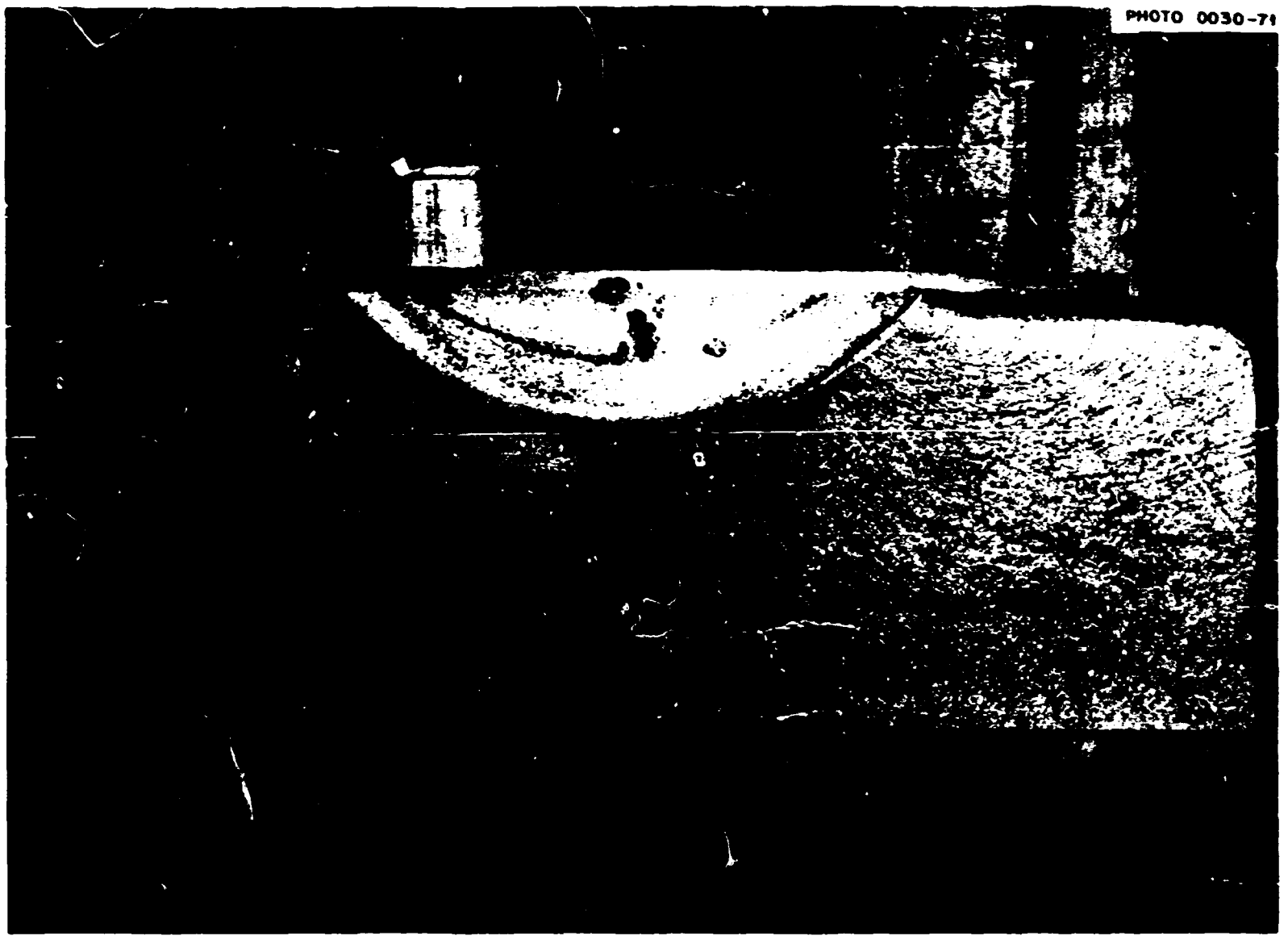

Fig. 4.14. Fracture face of specimen 01M6602. The machined notch and the fatigue crack are clearly visible.

as that described above. The load was determined by multiplying the prototype load by $\sqrt{6/36}$ to take into account the scale factor and the notch size effect so that the resulting load of 12,750 lb would produce a fatigue crack in approximately the same number of cycles as the load of 187,000 lb applied to the full-size specimen.

A fatigue crack was noted in the root of the notch at the surface of the specimen at about 15,000 cycles, and it had grown the full length of the notch by 20,000 cycles. An additional 5000 cycles was applied to be sure the crack was of sufficient depth at the base of the notch. This specimen was not tested but was cooled and broken open for inspection of the shape and depth of the fatigue crack. Also a valid tensile test of the small specimen might not have been possible, since high residual stresses were no doubt produced at the crack tip – a problem experienced with the stress-corrosion cracking procedures.

The dimensions of the machined notches in the full-size and the one-sixth-scale models are shown in Fig. 4.15. The notch in the 6-in.-thick specimen was produced by electric-discharge machining at ORNL, and the notch in the 1-in. specimen was machined with a cutting wheel.

Another one-sixth-scale model was notched, sharpened by fatigue, and tested at 50°F to model the test of specimen 01M6602. The fatigue load was 5200 lb ($^1/_{36}$ X 187,000) for the first 1 X 10^6 cycles, and no fatigue crack was produced. A fatigue crack was finally obtained by increasing the load to 8150 lb and cycling for an additional 163,000 cycles for a total of 1.163 X 10^6 cycles.

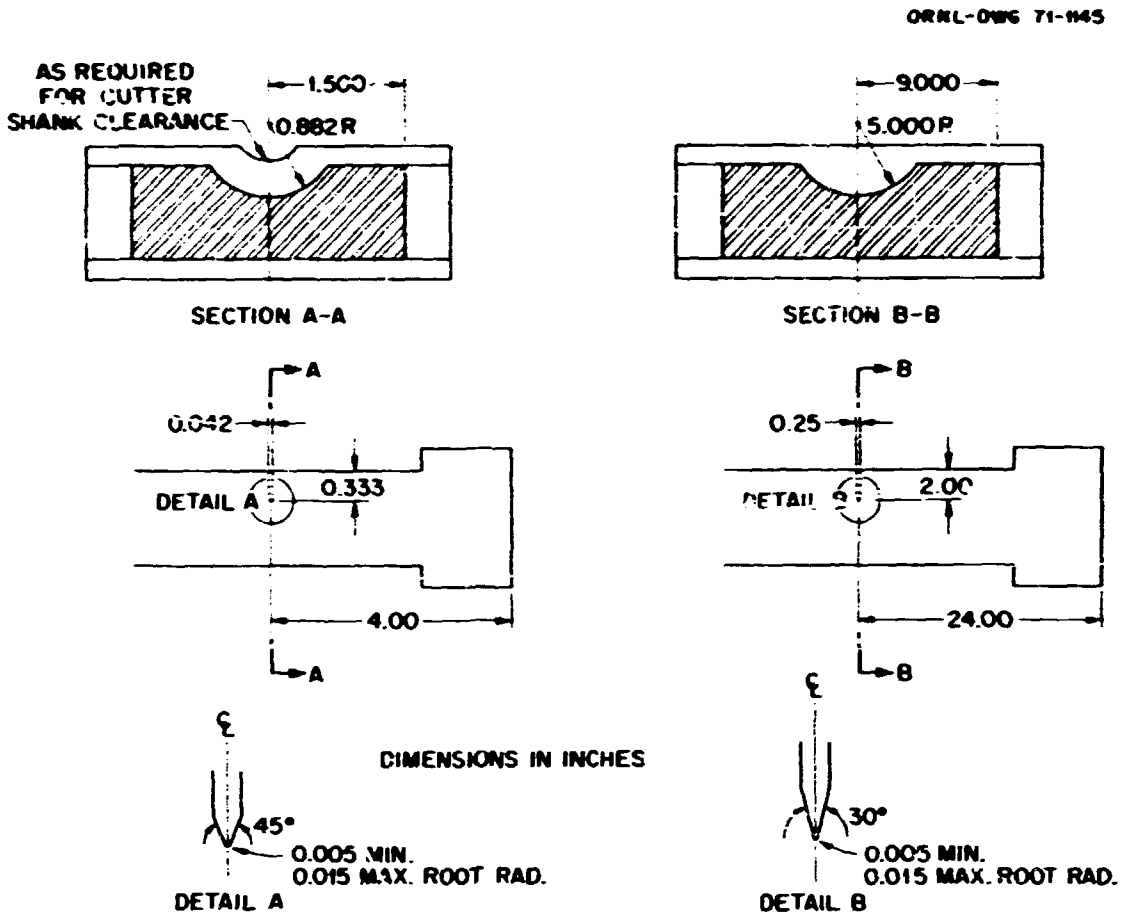

Fig. 4.15. Notch details for one-sixth-scale and full-size test specimens.

Parametric study of tensile specimens of rectangular cross section

The rectangular cross section of the large tensile specimens has caused some questions to be raised on the effects of the ratio of width, depth, and length parameters on strain at maximum load. To study these effects a series of five tensile specimens, whose parametric ratios are given in Table 4.1, was tested, and the results were compared with those for the 6- and 1-in.-thick tensile specimens being tested for the HSST program.

Figure 4.16 shows the instrumentation initially planned for the test series. Because of the good correlation observed between crack-opening displacement and gross strain displacement with gage length displacement in the first two large tensile tests, only gage length displacement was obtained during the testing of the model parametric specimens. In addition to the strain gages shown, a square grid having a 0.100-in. spacing to about 0.0001-in. tolerance was scribed on one face and side of each specimen. The grid pattern was intended to provide for observation of any asymmetric or anomalous strain pattern that might develop. To permit this observation it was intended to interrupt each test as soon as maximum load was reached.

Table 4.1. Dimensional parameters of 0.5-in.-thick specimens for model parametric study of SwRI tensile test

Specimen	Width-to-thickness ratio	Gage length-to-width ratio	Flaw
03ED-2000	10	1	No
03EE-2000	3	2.667	No
03ED-2001[a]	10	1	Semielliptical[b]
03ED-2002	3	1.333	No
03ED-2003[a]	3	1.333	Semielliptical[b]

[a]Specimen is one-twelfth-scale model of the 6-in.-thick SwRI tensile specimen.

[b]A semielliptical flaw, minor-to-major diameter ratio of 0.72 and depth of 0.167 in., was placed perpendicular to the load direction at midlength and midwidth.

Data were recorded manually for specimen 03ED-2000 and automatically on a B & F strain-gage data recorder for other specimens. In retrospect the use of the B & F recorder proved to be a disadvantage due to its limitation of recording strains to about 6%. The gage length displacements were obtained by means of mounting the gage on posts that were rigidly attached

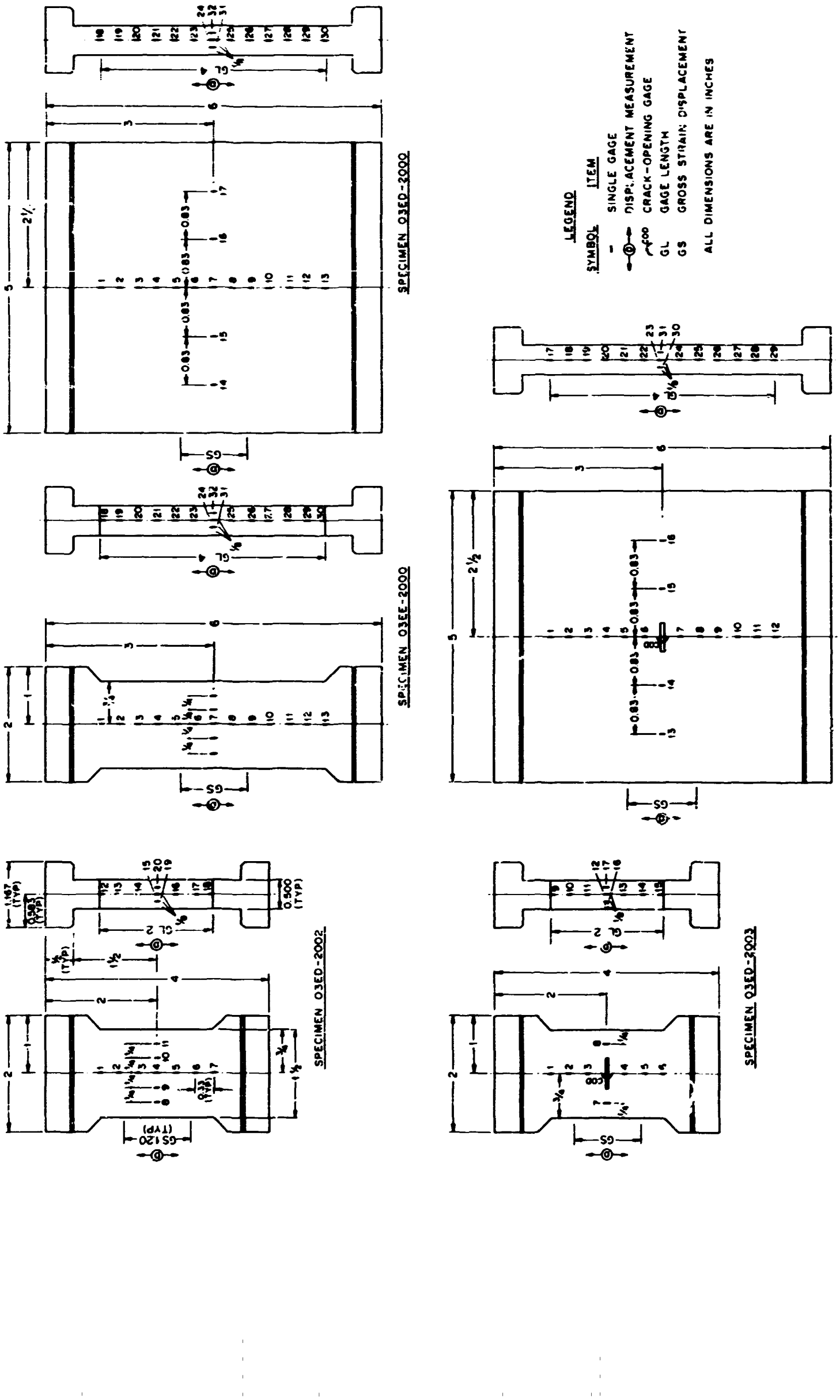

Fig. 4.16. Instrumentation of specimens for SwRI model parametric test.

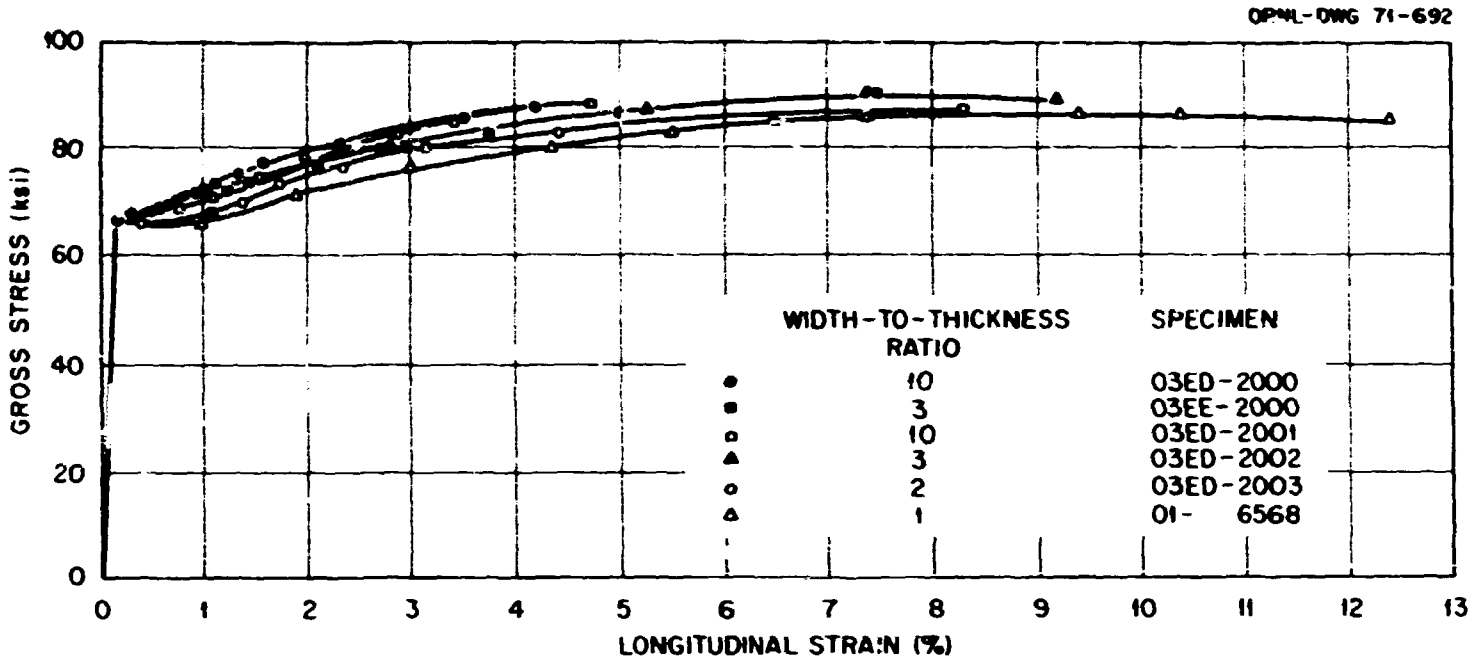

Fig. 4.17. Gross stress versus longitudinal strain for SwRI model parametric tests.

by tack welding to the specimen side at the grip end. It was assumed that with this method and location the grips would not yield and thereby influence the readings. This assumption unfortunately subsequently proved to be fallacious in the testing of specimen 03ED-2001 because of the pronounced curvature that developed on the sides early in the uniform strain regime.

Table 4.2 presents the load deflections, stresses, and strains at maximum load in the model parametric tests in comparison with the results of the second full-scale tensile test and the second one-sixth-scale model test. Figure 4.17 shows a composite of the conventional engineering stress-strain curves for each of the five model parametric specimens and for specimen 01-6568, a conventional, round tensile specimen.

Procurement of Intermediate Test Vessels

C. E. Childress

Six intermediate test vessels are being obtained from the Taylor Forge Company of Paola, Kansas. The vessels will be fabricated from forge components essentially as shown in Fig. 4.18, except that one will be provided with a 9-in.-ID nozzle, and, among the vessels, certain parameters, such as weld type and weld location, will be selectively varied. Further, each vessel will be provided with artificially induced flaws of varying size, configuration, and location. Each vessel will serve as a test specimen for demonstrating capability to predict safe behavior of thick-walled pressure vessels containing flaws of known dimensions under frangible, transitional, and tough loading regimes. Each particular vessel will serve to provide a determination of critical flaw size for a specific set of test parameters.

Fabrication of the vessel components has been sublet to two forging manufacturers: National Forging Company and Lenape Forging Company. Lenape is making the hemispherical heads and the flat-head closure covers. National Forge is making the shell courses, closure flanges, and a weld test plate to be used for qualification of Taylor Forge welders. All components are being fabricated from ASTM A 508, class 2, materials.

Materials for the hemispherical heads were obtained from a billet with a 32-in.-square cross section, made from a single melt, heat Q2A18. The ladle analysis for heat Q2A18 follows:

	Ladle analysis (wt %)
C	0.19
Mn	0.78
P	0.008
S	0.022
Si	0.23
Cr	0.39
Ni	0.82
Mo	0.63
V	0.003

The billet was cut into six sections that measured 32 X 14 X 45 in. long, and each weighed about 5400 lb.

Table 4.2. Results of parametric study of rectangular tensile specimens

Specimen	Gage length[a] (in.)	Specimen width (in.)	Gross area ($in.^2$)	Net area ($in.^2$)	Elastic limit load (kips)	Elastic limit stress (ksi)		Ultimate load (lb)	Ultimate stress (ksi)		Deflection[b] at ultimate (in.)	Average strain[b] at ultimate (%)
						Gross	Net		Gross	Net		
Full-scale specimen No. 2[c]	24	18	108	97.82	6000	55.5	68.4	7550	69.9	77.5	0.92	3.83
One-sixth-scale model No. 2[c]	4	3	3.00	2.659	175	58.4	65.7	230.6	78.6	88.9	0.240	6.00
03ED-2000	5	5	2.50		170	68.0		222.5	89.0			4.2[d]
03ED-2001	5	5	2.50	2.429	170	68.0	70.0	222.5	89.0	91.6		4.8[d]
03ED-2002	2	1.5	0.750		50	66.6		67.5	90.0		0.15	7.5[e]
03ED-2003	2	1.5	0.750	0.679	45	60.0	66.3	65.0	86.6	95.7	0.15	7.5[f]
03EE-2000	4	1.5	0.750		50	66.6		67.5	90.0		0.30	7.5

[a]Effective gage length was actual gage length, including ends of specimen.

[b]Deflection is total over actual gage length and includes slight elastic strain from heavy end sections. Average strain is deflection at ultimate divided by effective gage length.

[c]Test temperature, 215°F; all other tests at room temperature.

[d]Average of strain-gage readings on the side of the specimen.

[e]Specimen 03ED-2002 was necked more than other specimens.

[f]Crack growth occurred in the notched specimens.

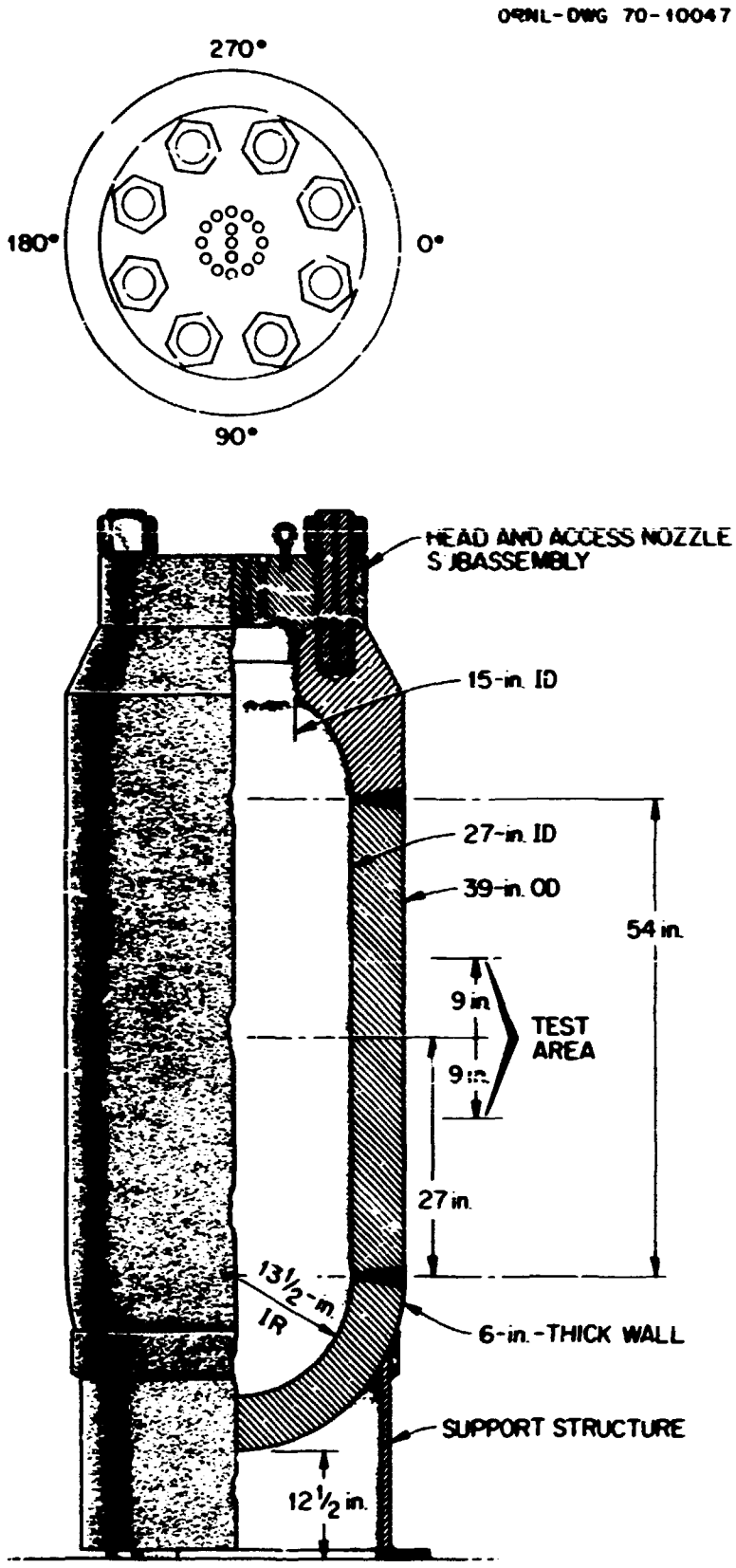

Fig. 4.18. Essential features of intermediate test vessels V-1, V-2, V-3, V-4, and V-6.

Each piece was then placed in a furnace and heated to about 1950°F. The first operation consisted of forging the section of billet into a square configuration. The part was then rounded by working opposite corners. On completion of this operation, the part was cylindrical, with a nominal diameter of 24 in., and was 48 in. long. The temperature of the part upon completion of preliminary forming was 1740°F. (Lenape advised that their minimum forging temperature was 1650°F.) Each of the six pieces was forged into a cylindrical configuration before the next operation began.

The cylindrical parts were then reheated to about 2050°F, removed from the furnace, and placed upright in a specially prepared, preheated, and lubricated die, as shown in the top view of Fig. 4.19. The cylindrically shaped steel was then pressed into the die, but the mass was slightly less than enough to completely fill the die; that is, the steel did not fill the die to the sidewalls. Lenape advised that they had tried to provide such an amount of steel, since the next operation would force the steel to the sidewalls and facilitate machining of the inner surface. Following this operation (each required about 5 min), the pieces were again returned to the furnace for reheating. Each piece was reheated to about 2040°F, removed from the furnace, and reinserted in

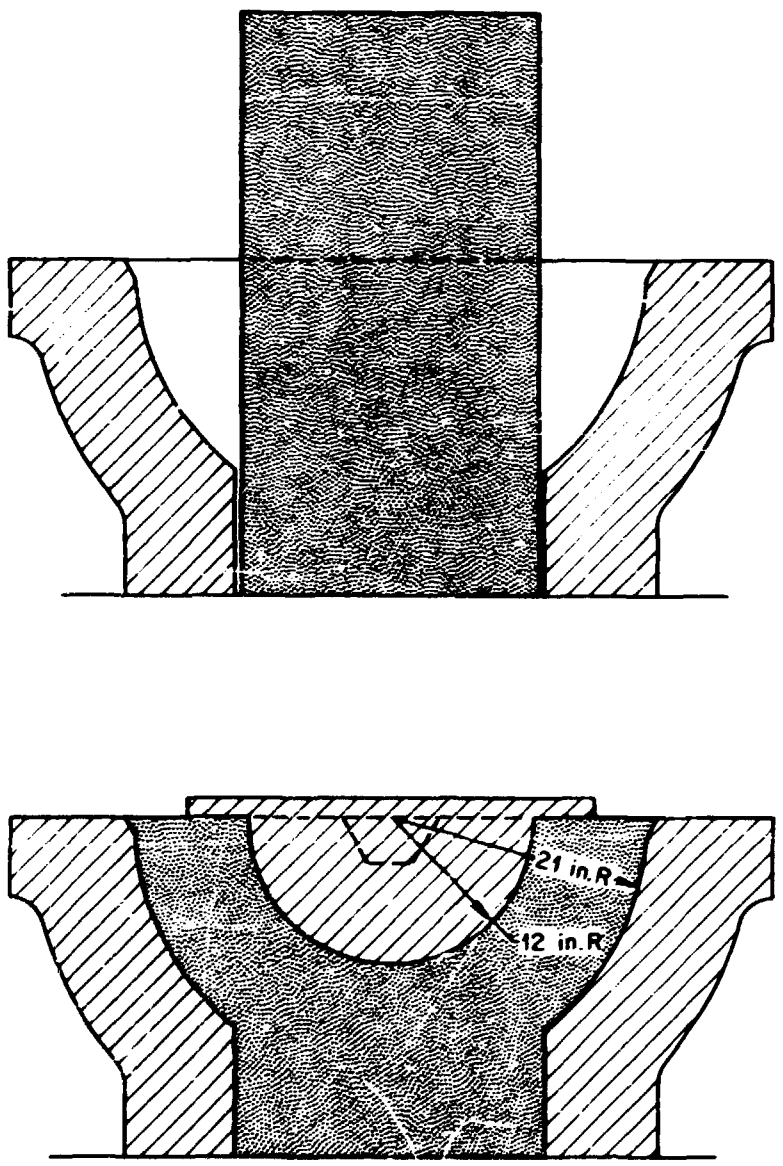

Fig. 4.19. Procedure for forging hemispherical heads of intermediate test vessels.

the preheated, lubricated die. Next, a blunt-ended tapered die was placed over the center of the mold and pressed about 6 in. into the steel. A second die having a radius of 12 in. was then placed over the tapered hole (see bottom view of Fig. 4.19) and pressed deeper into the mass of steel. This operation forced the hot steel to the sidewalls of the die. Forging in this manner was designed to permit the use of a minimum amount of steel and to eliminate much unnecessary machining on the inner surface of the heads.

Lenape advised that they had hoped that the upset ratio would be about 1.75:1 to the top of the die, and then the center would be worked so that the upset ratio in the center would be 4:1. The upset ratio of 1.75:1 to the top of the die was not achieved; however, Lenape advised that they would determine the ratio and advise the HSST staff of their findings.

Figure 4.20 shows a preliminary forging operation in process. Figures 4.21 and 4.22, respectively, show a hemispherical head immediately before and after final forming. After final forming, the configuration of the forging was essentially as shown in Fig. 4.23. It should be noted that some of the forgings contain surface imperfections that may extend through the metal designated for clean-up machining and into the finished head. In this case, repair welding will be necessary.

Upon completion of the forging operations, the parts made by Lenape will be subjected to normalizing, austenitizing, quenching, and tempering heat treatments in accordance with Lenape Procedure HT-12 Rev. 1. This procedure requires that each part be (1) normalized at 1650 ± 25°F and cooled in air, (2) austenitized at 1560 ± 25°F, (3) quenched in agitated water, and (4) tempered at 1225°F min and cooled in

Fig. 4.20. Preliminary forging operation in the forming of the intermediate test vessel hemispherical heads.

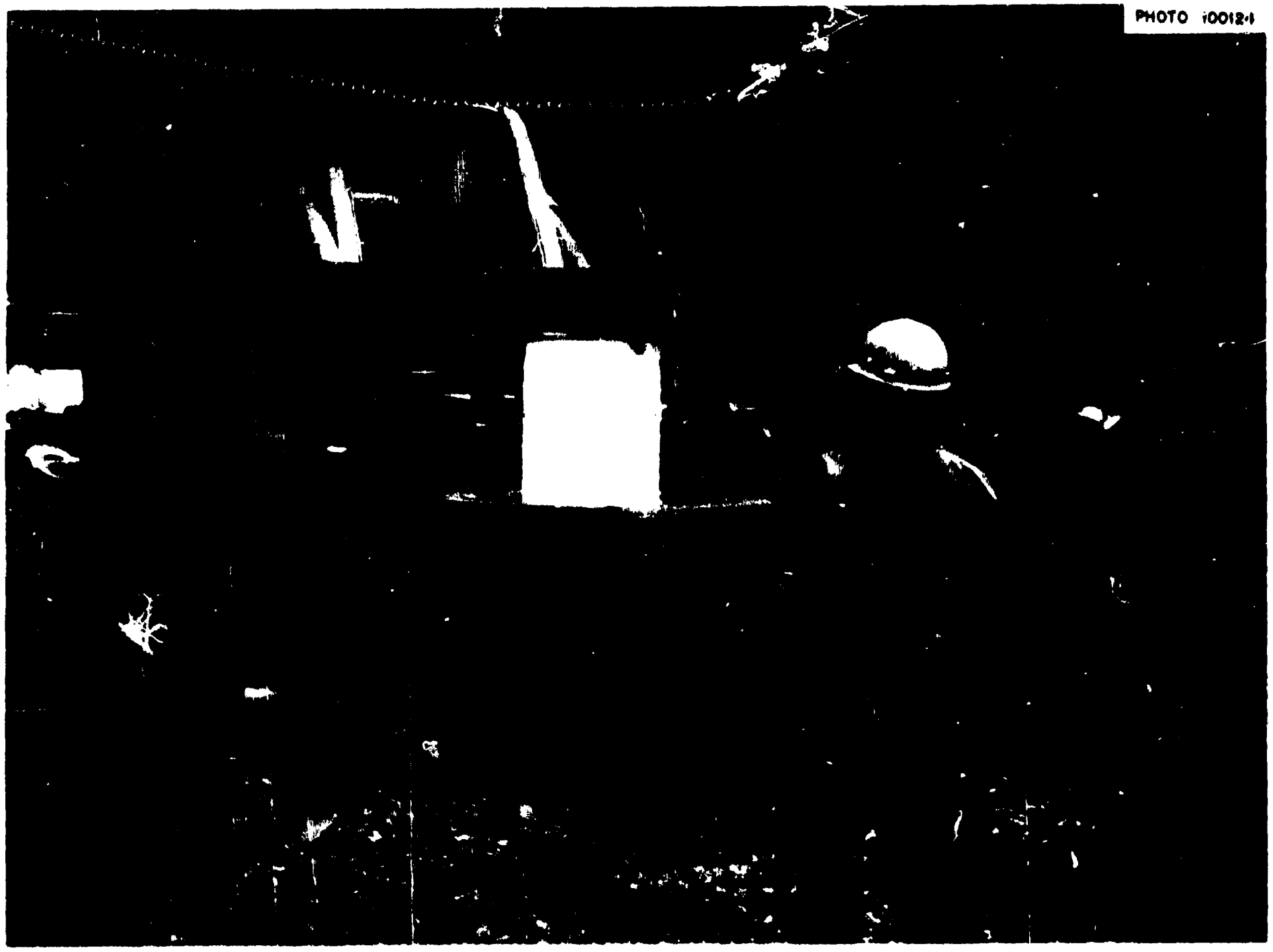

Fig. 4.21. Beginning of final forging operation on the hemispherical heads of the intermediate test vessels.

Fig. 4.22. Completion of final forging operation on the hemispherical heads of the intermediate test vessels.

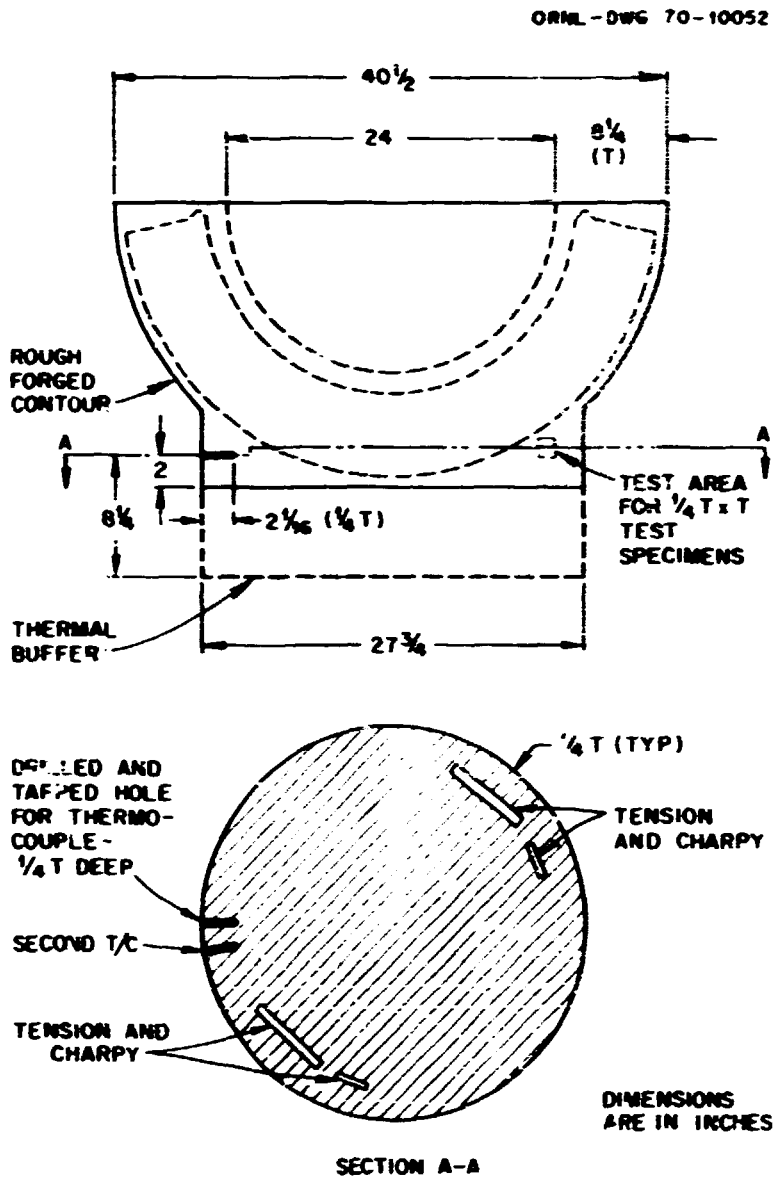

Fig. 4.23. Completed rough forging of a hemispherical head for the intermediate test vessels.

air. All parts must be held at temperature for 1 hr per inch of metal thickness. Lenape has advised that the hemispherical heads will be stress relieved at 1125 ± 25°F for 24 hr.

The test specimens for determining mechanical properties of the forgings will be heat treated by Lenape by using their Data Trak programmed testing procedure. Accordingly, it was necessary to equip one forging with a thermocouple during quenching to determine the cooling rate to which test specimens would be subjected. A stainless steel-sheathed Chromel-Alumel thermocouple was installed in one head at the $\frac{1}{4}\ T \times T$ position, as shown in Fig. 4.23.

The instrumented part was austenitized and quenched, and the resulting cooling curve is shown as curve A in Fig. 4.24. Based on past experience, the cooling rate thus obtained was considered to be too fast. Lenape elected to instrument a second head and this time installed two thermocouples (see Fig. 4.23). The cooling rate obtained from the second quench was somewhat slower than the first, as shown by curve B in Fig. 4.24. Both thermocouples recorded essentially the same values during this quench.

Lenape has advised that each of the hemispherical heads will be equipped with embedded thermocouples during the tempering heat treatment. The heads will be heat treated (three per furnace) and instrumented with stainless steel-sheathed Chromel-Alumel thermocouples, as shown in Fig. 4.25. At this time the results of chemical check analysis and physical properties tests for the hemispherical heads have not been reported.

The 31-in.-diam flat heads were forged from pieces of billet measuring 26 X 26 X 13½ in. long. Each piece was cubed and rounded into a cylindrical configuration on an open-die press and then upset into a 33-in.-OD, 10½-in.-deep die. The upset ratio was 2:1. A rough-finished forging is sketched in Fig. 4.26.

It was also necessary to equip one of the flat heads with an embedded thermocouple during quenching to determine the cooling rate for the test specimens from the flat heads. The location of this thermocouple is shown in Fig. 4.26. The cooling rate obtained for the flat heads is shown as curve C in Fig. 4.25.

The flat heads, too, will be equipped with embedded thermocouples (see Fig. 4.27) during the tempering heat treatment. As noted previously, the parts will be tempered at 1225°F min and held at temperature for 1 hr per inch of metal thickness. Since much of the heat treatment and machining are not completed, the results of check chemical analysis and mechanical properties tests have not been reported.

The National Forge Company will make the shell courses, closure flange, and a weld test plate. The ingot used to make the shell courses (one ingot provided material for three shell sections) weighed about 200,000 lb and was poured simultaneously from two furnace heats, 3V924 and 1V3828. The configuration of the ingot was essentially a truncated cone, 76 in. in diameter at the top ingot end and 65 in. in diameter at the bottom end by 12 ft long, excluding the hot top.

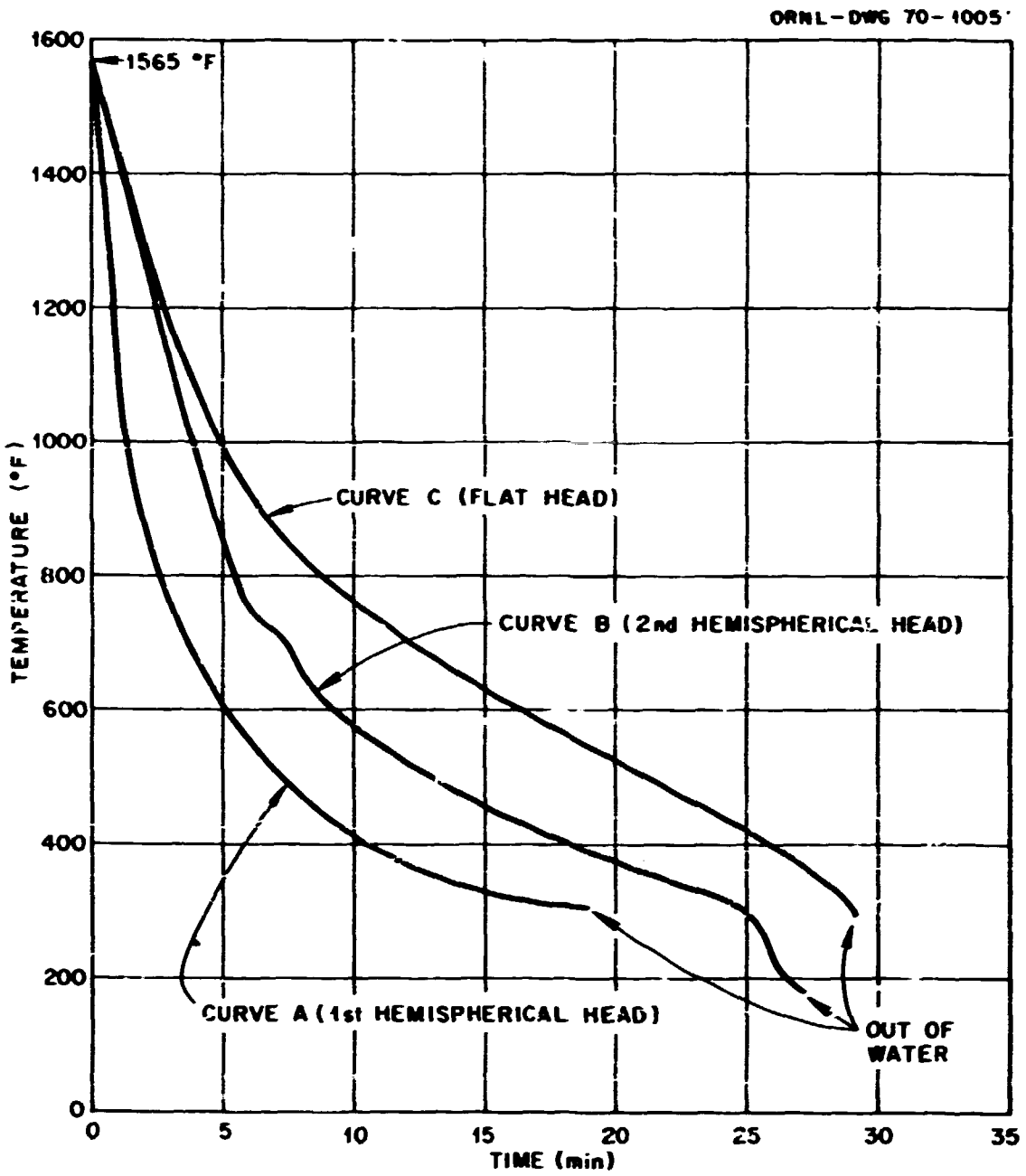

Fig. 4.24. Cooling curves for the hemispherical and flat heads for the intermediate test vessels.

The ladle and check chemical analyses follow:

	Ladle analysis (wt %)	Check analysis (bottom end) (wt %)
C	0.27	0.22
Mn	0.87	0.82
P	0.007	
S	0.012	
Si	0.32	0.32
Ni	0.74	0.73
Cr	0.34	0.33
Mo	0.64	0.60
V	0.64	0.04
Cu	0.13	0.13

The temperature of the ingot upon removal from the soaking pit was 2350°F, as determined by an optical pyrometer reading. Upon removal from the pit the ingot was conveyed to a 3000-ton open die press, which was used for the forging. During the first forging operation the ingot was reduced to a 56-in. octagonal cross section, and the length of the forged section was increased by 4 ft.

The part was then conveyed to the cutting area, where a few surface defects were removed so that the piece would fit into the furnace. Also, a 5-lb chunk was cut from each end of the ingot for check chemical analysis. The results of the analysis from the bottom ingot end are given above. The temperature of the part was then down to about 1600°F, and it was returned to the furnace for reheating.

About 9 hr later the temperature of the piece was about 2350°F, and it was again removed from the

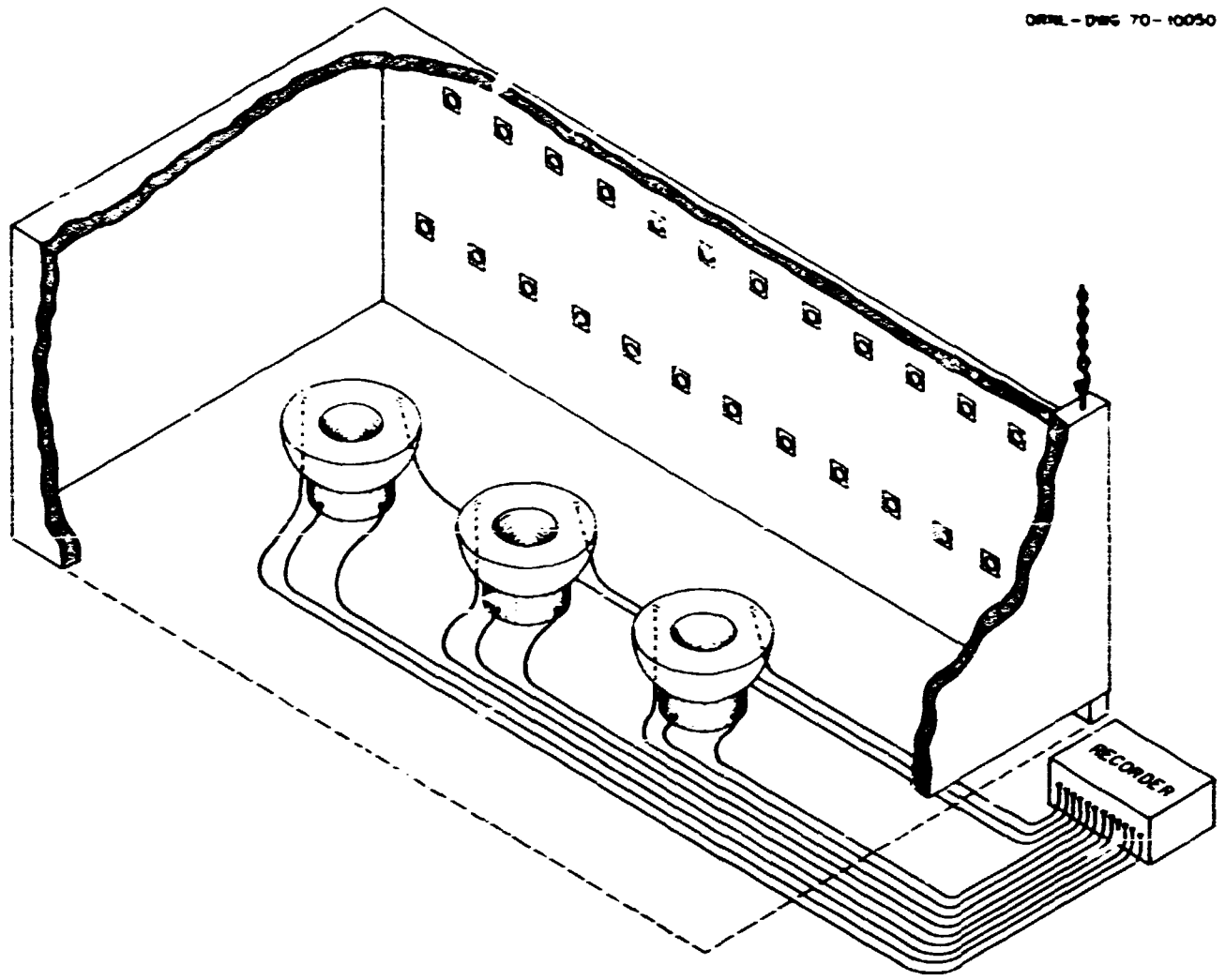

Fig. 4.25. Schematic arrangement and thermocouple location of hemispherical heads in furnace for the tempering heat treatment.

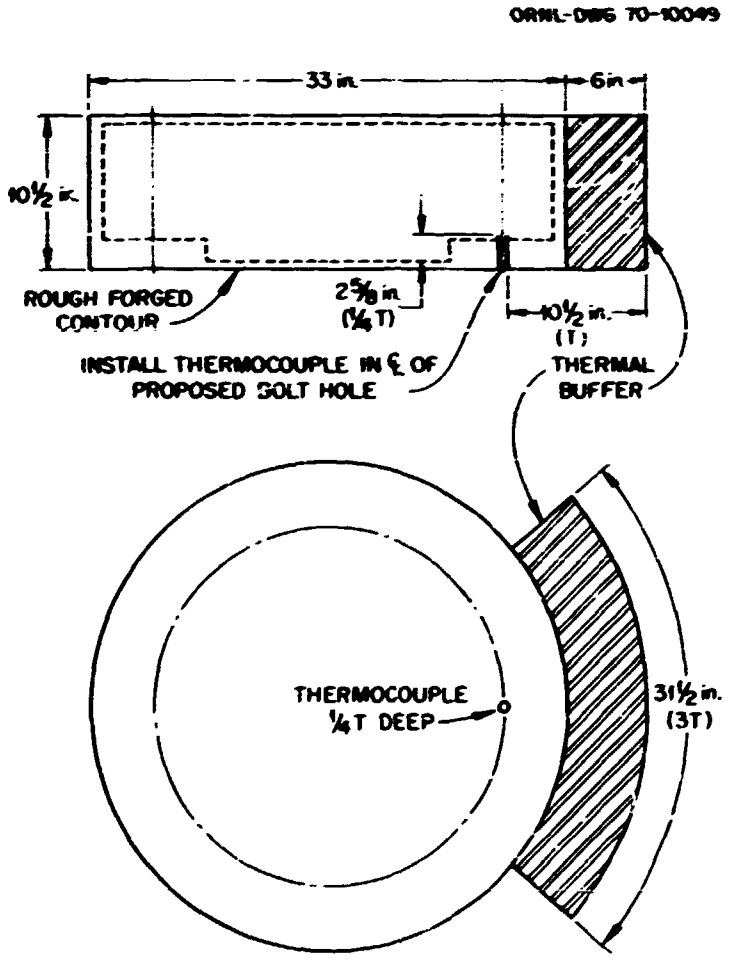

Fig. 4.26. Completed rough forging of a flat head.

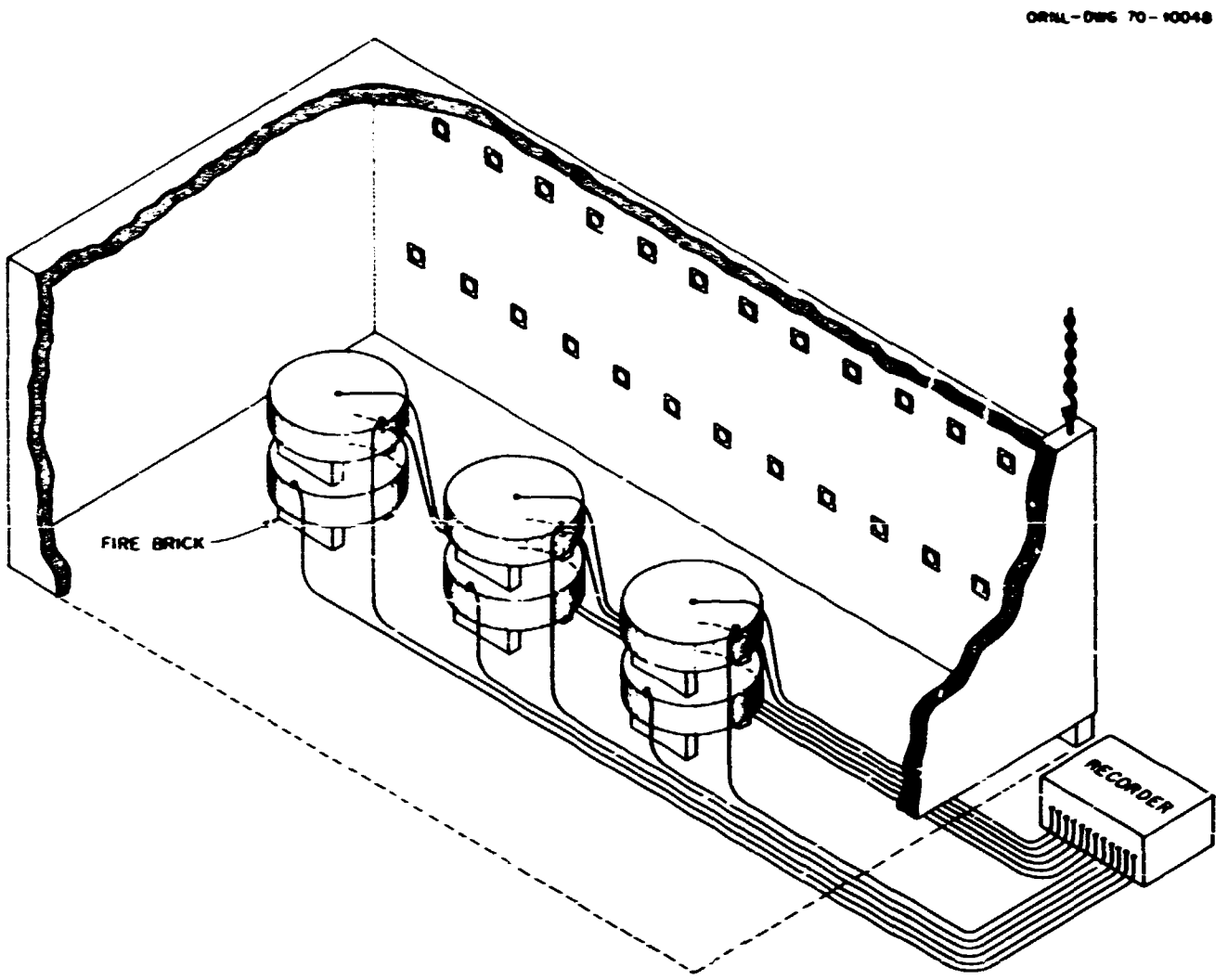

Fig. 4.27. Schematic arrangement and thermocouple location of flat heads in furnace for the tempering heat treatment.

furnace for further forging. After about 2 hr of forging the part was cylindrical, with a usable length of about 27½ ft and a nominal diameter of 41 in. The temperature of the part upon completion of forging was 1440°F. The unusable material from each end was then cut off, and the tip ingot end was identified with a deep-die stamp.

The postforging heat treatment procedure for the part will consist of the following:

"Immediately on removing the two ends, the usable length will be returned to the furnace and 'equalized' at 1180°F for 8 hr. On completion of the 8-hr hold, the forging will be allowed to furnace cool to 500°F and held at this temperature for 22 hr. Following this 22-hr hold, the temperature will be raised at a rate of 90°F/hr to 1180°F and held for 8 hr, then raised at 100°F/hr to 1600°F and held at this temperature for 32 hr. Following the 32-hr hold, the forging will be removed from the furnace and air cooled to 700°F, then returned to the furnace and furnace cooled to 500°F. It then will be held at 500°F for 22 hr. After this 22-hr hold, without cooling further, the temperature will be raised at 90°F/hr to 1240°F and held for 30 hr. The forging will then be furnace cooled to below 500°F, thus completing the post forge heat treatment.

"On completion of post forge heat treatment, the forging will receive a preliminary ultrasonic inspection, after which it will be sawed into three pieces of equal length (a 2-ft prolongation will be left on each piece). Each piece will then be shipped to the NF plant in Irvine, Pa. for machining, final heat treatment, and final ultrasonic inspection."

When forging of the weld test plate made from A 508, class 2, material was completed, it measured 18 X 72 X 6 in. thick. It was then heat treated (data not available at this time) and sawed into four 18-in.-square pieces. These pieces were not subjected to ultrasonic inspection at the mill but will be subjected to all the nondestructive inspection requirements of Section III of the *ASME Code* upon completion of the weld tests.

Fabrication of the closure flanges is in process, but data are not yet available.